UNIVERSITY OF COPENHAGEN

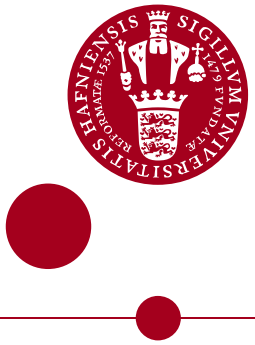

PhD thesis

G. S. Halvorsen

Generalized epidemics in heterogenous networks and homogenous metapopulations

This thesis has been submitted to the PhD School of The Faculty of Science, University of Copenhagen

Supervised by Kim Sneppen

October 10, 2021

"I love deadlines. I like the whooshing sound they make as they fly by."

Douglas Adams

Abstract

Epidemic processes operate on all scales of life – from infectious pathogens to the spread of rumors on social networks. This work is about epidemic spreading in different network substrates. The thesis is apportioned between three related research topics.

The first seeks to estimate the effect of coordinating lockdowns between subnational entities that sustain recurring out-of-phase outbreaks of SARS-CoV-2. The uncoordinated strategy delays longer when given the same disposable resources. This difference is minimal on a metapopulation network with small-world properties. The coordinated strategy is superior if it is only slightly better at reducing transmission.

The second topic explores the dynamics of reactive social behavior on infectious disease outbreaks in a spatially extended system. This model exhibits a critical transition where the disease can no longer spread because reactive behavior changes have depleted the susceptible population around the outbreak. We show that the model can explain the 2014–2016 outbreak of the Ebola virus disease and introduce a statistical measure of spatial heterogeneity.

The final topic concerns the spread of information on a social network. Here we simulate how influencers compete for attention on a social network by new spreading information. The "virality" of information decays over time. Consequently, an influencer must discover new information or appropriate it from other subcultures to retain its subscribers' attention. The collective attention of the network exhibits metastable states in the presence of positive feedback. We consider the model on an assortment of social network topologies and find mutual coexistence between a few dominating influencers on a scale-free social network. Our findings suggest that either fake news or the perception of fake news as ubiquitous is endemic to our society because everyone can become a news outlet (e.g., influencer).

Resumé

Epidemiske processer opererer på alle former for liv – fra smitsomme mikroorganismer til rygtespredning på sociale netværk. Arbejdet beskæftiger sig med epidemisk spredning i forskellige netværks substrater. Afhandlingen er opdelt i tre relaterede forskningsprojekter.

Det første forskningsprojekt forsøger at estimerer effekten af at koordinere nedlukninger mellem forskellige regioner der rammes af SARS-CoV-2. Det påvises af den ukoordinerede nedlukningsstrategi er bedre til at udskyde epidemien, hvis begge strategier undertrykker smittespredning lige meget. Forskellen på de to strategier er minimal på et netværk af koblede metapopulationer der er tæt forbundet. Den koordinerede strategi er bedst hvis den er marginalt bedre til at undertrykke smittespredning.

Det andet forskningsprojekt omhandler effekten af reaktive adfærdsændringer på smittespredning i rummelige systemer. Modellen har en kritisk tilstand hvor sygdommen ikke kan sprede sig, fordi adfærdsændringerne har udtømt den modtagelige befolkning omkring udbruddet. Vi viser at modellen kan forklare Ebola-udbruddet i Vestafrika 2014-2016 og introducerer et statistisk mål for rummelig heterogenitet.

Det sidste projekt beskæftiger sig med informationsspredning i sociale netværk. Vi simulerer hvordan influencers konkurrerer om opmærksomhed. Viraliteten af information aftager over tid. Det er nødvendigt at opdage ny information eller at approprierer det fra andre for at forblive relevant. Netværkets kollektive opmærksomhed opnår en stabil tilstand når vi tilsætter positiv feedback. Modellen simuleres på en række forskellige netværks topologier. Gensidig sameksistens blandt nogle få influencers opstår på et skalafrit netværk. Vores resultater viser at "fake news" eller indtrykket af "fake news" som et allestedsnærværende fænomen er endemisk i en verden hvor alle kan blive en nyhedskilde.

Acknowledgements

Thanks to professor Kim Sneppen who has supervised this work. I have very much enjoyed our collaboration. I also wish to thank professor Lone Simonsen for helping and advising me. Thanks to the assessment committee for evaluating this work.

The Biocomplexity group has offered a uniquely good work environment with helpful and brilliant colleagues. I feel privileged to have been a part of this outstanding group. Thanks to my family and friends for their help and support in times of need.

Publications

This work is based on the following papers in order of appearance. The published and submitted manuscripts are enclosed within the thesis at the end.

1. *Estimating the effect of coordinating lockdowns betweeen recurring SARS CoV-2 outbreaks*
   (submitted to Scientific Reports)

2. *Spatial model of Ebola outbreaks contained by behavior change*
   (submitted to Plos One. Under review but expected to published after minor revisions)

3. *Social contagion in a world with asymmetric influence*
   (Published in Physical Review E)
   DOI: 10.1103/physreve.103.022303

Scientific publications must be concise, and mine are no exceptions to this norm. I have therefore dedicated a chapter to each manuscript to expound on the material therein. Since the pending manuscripts were submitted many months ago, there are discrepancies between them and the work contained within the thesis. The thesis contains the most recent work, so it cannot be assessed solely based on the manuscripts.

Contents

Chapter 1

Introduction

Epidemic processes operate on all scales of life – from infectious pathogens to information spreading and social behavior. The destructive power of contagion is not easy to dispute. The ongoing coronavirus pandemic has brought to the world to halt and caused millions of fatalities. Yet, this catastrophic event began with a few seemingly innocuous cases of influenza-like illness before spreading and replicating around the world. Epidemic processes (e.g., diseases, social behavior) are the thesis's subject matter. We put particular emphasis on the dynamic interplay between diseases and social behavior. The coronavirus pandemic, although not originally intended, has become a significant piece of this work. SARS-CoV-2 has caused great loss of life, inflicted enormous economic damage, and changed human behavior worldwide. It has also changed the study of human behavior itself [11]. We now have access to a wealth of data and natural experiments on social behavior during a pandemic. Here I aim to set the stage for the work carried out in this thesis by providing a lucid and concise introduction to the topic. This chapter contains nothing novel, and the reader may choose to jump ahead to the next chapter. First, I will state more precisely what is meant by generalized epidemic theory.

1.1 Generalized epidemic theory

Epidemic processes extend far beyond contagious diseases and cover a surprisingly diverse range of phenomena. Goffman defines an epidemic process as a time-dependent transition process where exposure to some infectious material causes state changes in members of a population [79]. This definition captures the essence of contagion and serves as a decent starting point, although we will not exclusively consider populations of humans or animals in the following. For a disease to be contagious, it must be able to spread between humans. Certain infectious diseases (e.g., vector-borne diseases such as Malaria and lime disease) can replicate inside a host but cannot spread without a disease vector (e.g., mosquitos and ticks).

A contagion process must be able to spread and self-replicate, i.e., make copies of itself, but such an epidemic process need not involve biological entities. John von Neumann envisioned a way to explore the universe with a self-replicating spacecraft. The eponymous von Neuman probe is a space probe that travels to another planet and uses its resources to build one or more

copies of itself. This process is vaguely analogous to how viruses spread by hijacking host cells to replicate. More recently, the spread of computer viruses has been modeled as epidemics on scale-free networks (the internet's topology) [139]. Computer viruses are self-replicating programs that infect a device by copying itself onto it. The Neuman probe and computer viruses are generalized by von Neumann's theory of self-replicating automata [131]. While computer virus epidemics have not caused havoc comparable to natural epidemics, they are nonetheless responsible for substantial economic damage.

There are also physical processes that mimic contagion. Consider, for example, the nuclear chain reaction: A uranium-235 atom splits into two fission fragments after absorbing a neutron and releases three neutrons and some binding energy in the process. These neutrons induce additional fission events like an infectious material. Intriguingly, the analogy goes further yet. The effective neutron multiplication factor m_f is defined as the average number of neutrons from one fission that causes another fission event. This m_f factor is analogous to the effective reproductive R_e number in infectious disease epidemiology. Nuclear power plants should operate at the endemic state $m_f = 1$ to maintain a stable fission reaction. In contrast, nuclear weapons are designed to have a m_f factor above one, so the number of fission reactions increases exponentially, releasing a large amount of energy.

The hazard posed by self-replicating processes (e.g., epidemics, nuclear fission) is self-evident. Exponential growth occurs when a quantity y increases over time by a rate proportional to y. A growth rate that is proportional to y implies that self-replication is involved. We have seen this for all the processes above. Remarkably, a single lucky SARS-CoV-2 virion can take over the world through exponential growth – a single neutron in a fissile material can unleash destruction on a massive scale. However, while a self-replicating process can grow exponentially, it will not necessarily do so. Consider, for example, Eden Growth used to describe the various growth phenomena, including tumors and bacteria colonies [47]. Here a cluster of cells aggregates on a square lattice by occupying neighboring sites. Only the cells on the colony's edge contribute to aggregation, and the radius grows at a constant rate. The spatial constraints preclude exponential growth. Cluster growth models (e.g., Eden growth and diffusion-limited aggregation) are related to percolation, which itself is connected to epidemic spreading. Percolation describes a range of physical phenomena (e.g., fluid movement through a porous material). The mathematical study of percolation has brought insight into topics in geology, traffic flow, complex networks, and epidemiology.

1.1.1 General epidemic process and percolation

The connection between percolation and disease spreading appears to have been suggested by Frisch and Hammersley but was first formally introduced by Grassberger [65, 84]. Grassberger considered the general epidemic process (GEP), a stochastic multiparticle process that is believed to describe many

spatial growth phenomena, including solitary chemical waves, forest fires, and epidemics. Here the infectious medium spreads to nearest neighbors at some rate β, while sites are removed with a rate γ — unlike Eden Growth, where cells are immortal. GEP does not allow the susceptible medium (e.g., food, people, trees) to be replenished and is thus necessarily non-ergodic. GEP is essentially the *sir* model on a lattice. The epidemic propagates like a solitary wave in an infinite homogenous medium, leaving a depleted area behind it. In a finite medium, the epidemic reaches a maximum size before it inevitably dissipates—the connection to percolation lies in the critical behavior of the growth process. Whether the cluster grows from a single site to deplete the entire system or dies out depends on the ratio β/γ, analogous to a percolation threshold.

1.1.2 Transmission of ideas as an epidemic process

The epidemic process also extends to the spread of ideas, memes, and rumors. In 1964, Goffman and Neville introduced a generalized epidemic theory to describe the transmission of ideas and rumors [80, 81]. Daley and Kendell showed that rumor spreading could be explained by the *sir* model, depending on what mechanisms govern the spreading process [35]. Here a susceptible person (or population) X represents someone who has not yet heard the rumor. An infectious person Y is actively spreading the rumor, and a person Z who is recovered or dead is no longer spreading the rumor. If the rumor spreads by a rate proportional to XY and decays at a rate proportional to Y, we obtain the Kermack-McKendrick Model. Here the decay process $Y \to Z$ represents forgetting. Another possibility is that an active spreader Y stops spreading the rumor if she learns it has lost its novelty. This reaction can occur upon contact with an inactive spreader $Y + Z \to Z$ or another active spreader $Y + Y \to 2Z$. This form of rumor spreading is different from the *sir* model. There is no analogy for this annihilation process in infectious disease epidemiology. Two infected persons never recover or die upon contact with each other. More recently, variations of the *sir* model have been used to understand the spread of news and rumors on social networks [136].

The spread of ideas and rumors applies to a host of phenomena. Belief systems (e.g., religions and political ideologies) are essentially a collection of ideas that spread in a population. Consider a missionary as an infectious agent who seeks to recruit or convert susceptible individuals to a particular faith. Individuals who have left the religion or are ardent followers of another religion may be considered immune, and a person who joins the faith can help spread the word. Religions can have many mutually exclusive competing denominations, just like viruses can mutate into new variants. They can also go extinct by failing to retain their adherents or persuade others to join the faith.

There are some historical analogies between efforts to contain disease outbreaks and political ideologies deemed hostile or undesirable. A Cordon Sanitaire is a restriction on movement into or out of a particular area. Many people have been affected by such regulations during the ongoing coronavirus

pandemic—notably in the city of Wuhan, where unprecedented restrictions were imposed to contain the outbreak. However, the word has also been used metaphorically to describe ideological containment. Bolshevism was likened to infectious disease during the interwar period. The French Minister of Foreign Affairs Stephen Pichon (1857-1933) even compared the spread of Bolshevism to the plagues that had swept over Europe from the east [58]. Western Europe thus sought to establish a Cordon Sanitaire as a bulwark against this encroaching ideology [154]. The United States continued this line against communism during the cold war with the Truman doctrine as a cornerstone of American foreign policy. The Vietnam war was greatly influenced by the domino theory asserting that communism would spread to neighboring states in Mainland Southeast Asia like a domino effect if a government fell to communism.

More generally, the dissemination of culture can be regarded as an epidemic process. Axelrod proposed a model of cultural dissemination where agents on a lattice adopt the cultural traits of their neighbors when they interact [13]. Agents interact with a probability equal to their cultural similarity and adopt random features from each other. This model satisfies Goffman's definition of an epidemic process as a transition process where exposure to some infectious material causes state changes in members of a population. In this sense, everyone is infectious because each person is knowingly or not passing on cultural traits to other members of the population. The theory of epidemics has also been used to model survival, and coexistence between competing languages [162]. Here a population speaks two languages, a majority language a minority language. The population is then divided into a group of majority speakers, a group of minority speakers, and a group of bilingual speakers. The minority language disappears if its associated reproduction number R_0 is below one. Generally speaking, things must reproduce to avoid extinction – this is true not only for populations of biological organisms but also for systems (e.g., languages, ideologies, and religions).

1.1.3 Simple and complex contagions

While many of the examples above are superficially similar to the spread of a contagious disease, the mechanics of the transmission process can be very different for behaviors, ideas, and beliefs. More recently, it has become fancy to distinguish between a simple and complex contagion. Simple contagions need just one source of exposure to induce a state transition. Conversely, a complex contagion process requires multiple sources of exposure [26]. Examples of simple contagions include the spread of information and infectious diseases. This work carried out in this thesis exclusively concerns simple contagions involving the spread of diseases and information (e.g., news, rumors, and memes).

1.2 Mathematical modeling of epidemics

The modeling of infectious diseases appears to have been invented by Daniel Bernoulli, who proposed a model of smallpox in 1766 [20]. The conventional approach to model epidemics is based on compartmental mean-field analysis. Individuals within a homogeneously mixed population belong to mutually exclusive classes (e.g., susceptible or infectious). The origin of such models can be traced back to Ross, Hudson, Kermack, and McKendrick [105, 149–151]. The most famous compartmental model is the *sir* model introduced by Kermack and McKendrick in 1927. A group of infectious individuals I spreads disease to a group of susceptible individuals S, and the number of infected persons grows by a rate β that is proportional to IS. The infectious persons die or recover with immunity at a rate γ proportional to I. The infectious population will grow exponentially until the susceptible population has been sufficiently depleted.

There are many variations of the *sir* model. The choice of model depends on the characteristics of the disease. Some relevant examples are covered below. The susceptible-infectious-susceptible model is used for diseases that do not confer long-lasting immunity after recovery. Influenza is an example of a viral infection that does not confer lasting immunity because of antigenic shift and drift. The emergence of SARS-CoV-2 variants around the world appears to be driven by a large global reservoir. This would suggest that large-scale outbreaks of a novel pathogen make achieving long-lasting immunity more challenging. An infected host will generally not become symptomatic or contagious immediately after exposure to a pathogen. If a pathogen successfully invades a host, it needs to evade the immune system and replicate above some threshold before affecting the host organism. Here a distinction is made between the latency period, i.e., the time elapsed between exposure and infection, and the incubation period, which is the time between exposure and onset of clinical symptoms. A person may become infectious before showing signs of illness, as is the case of SARS CoV-2, which makes containment more difficult. If a disease has a long latency period, it may be appropriate to include an exposed state for susceptibles who have been infected but are not yet contagious.

1.2.1 Contact heterogenity

Human populations are not well mixed. Nonetheless, homogenous mixing models are successful in describing epidemics [7]. To understand how this is possible, let us consider the transmission of an infectious pathogen in a large population. Let us further assume that contact rates vary inside the population. With the benefit of hindsight, we may fit the observations and extract a contact rate that reproduces the epidemic. However, this contact rate will be some average of the different contact rates [178]. R_0, the basic reproduction number is also defined as the mean number of secondary infections caused by an infected person in a susceptible population. Modeling transmission in heterogeneous populations with average quantities may obscure the effect

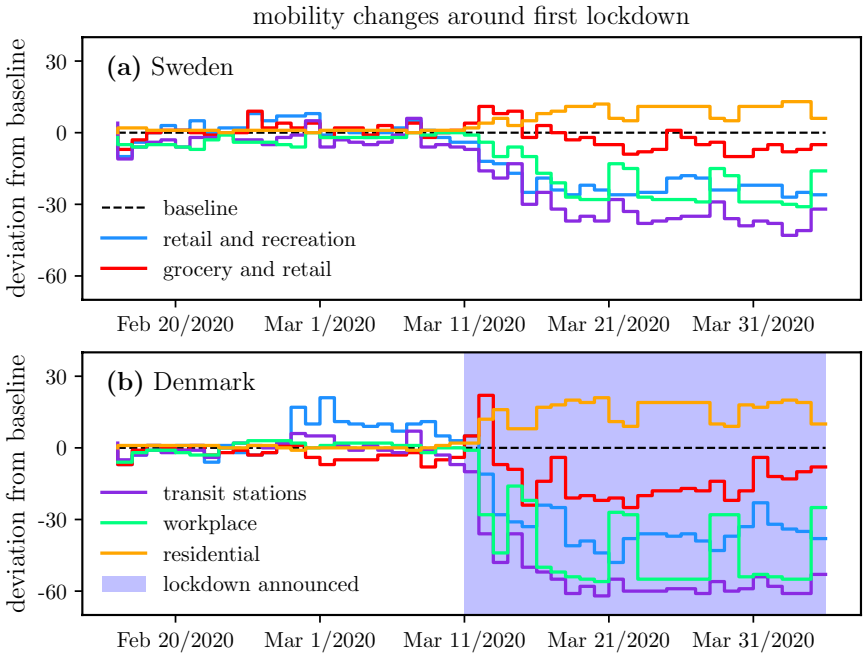

Figure 1.1: **Mobility changes in Denmark and Sweden around the first COVID-19 lockdown**. Data from Google mobility reports.

of individual variation [121]. Superspreading is a phenomenon observed for some diseases (e.g., SARS and EBOV) in which particular individuals cause a disproportionately high number of secondary infections [111, 121]. Knowledge of individual variation can inform public health policy. If a few superspreaders are responsible for sustaining an epidemic, targeting them is more effective than a population-wide effort. A large-scale study by Mossong et al. recorded all the contacts between many participants over a day. Mixing was found to be highly assortative with age [130]. Younger people also appear to have more contacts in general. This study may have influenced the Danish Health Authority's decision to vaccinate adolescents and young adults (16-24) against COVID-19 before adults (25-39).

Heterogeneous mixing models do not assume that transmission or contacts between people occur with equal probability. There are many causes of individual variation. It is convenient to differentiate between sources of variability that are disease-dependant and those that are not [15]. An infected person with a very high pathogen load may more easily transmit the disease. Disease-independent sources of variation are environmental factors (e.g., seasonal effects) and social effects (e.g., social distancing). This thesis is more concerned with social dynamics than environmental factors or the biology of a particular disease. Humans exhibit variable social behavior that affects the risk of receiving or transmitting infection [54]. A person who rarely leaves the confines of his home is unlikely to be infected or infect others. This is precisely the point of social distancing and isolation. To reduce the number of contacts by regulating human behavior.

Governments can impose restrictions on movement (e.g., social distancing measures and quarantines) to put a brake on transmission. We refer

to this as extrinsic behavior change as an external entity enforces it. Recently, we have seen restrictions on movement around the world to control the spread of coronavirus. The word quarantine has an interesting etymology. It appears to be derived from the Venetian word for "forty," referring to the isolation period imposed on ships and visitors during the Black Death [123].

Intrinsic behavior change is when individuals voluntarily change behavior as a response to perceived risk. The local prevalence of HIV/AIDS is associated with an increased demand for contraception [2]. The ongoing coronavirus pandemic has given us precious insight into intrinsic behavior change, which is worth expounding on. Sweden chose not to impose a lockdown during the early stages of the coronavirus pandemic like other countries. Nonetheless, mobility in Sweden decreased suddenly around the first danish lockdown. Scandinavian countries are both culturally and demographically similar and rarely pass radically different policies—the different reactions to SARS-CoV-2 make for an interesting natural experiment. Natural experiments are empirical studies where individuals are exposed to conditions that the researchers do not control. We use natural experiments when it is impractical or unethical to conduct controlled experiments. It would be impracticable to raise or lower the minimum wage for an extended period to study its effect on employment. Google has published data on mobility trends for many countries during the ongoing coronavirus pandemic. This data yields insight into the impact of COVID-19 on human behavior and the effectiveness of restrictions.

Fig. 1.1 show mobility trends across different categories in Denmark and Sweden (e.g., recreation, transit, workplace). Danish Prime Minister Mette Frederiksen announced extensive restrictions on March 11, closing schools, ordering non-essential public employees to work from home, and prohibiting large gatherings. Sweden did not impose similar restrictions. However, citizens were encouraged to practice social distancing. Nonetheless, Denmark and Sweden follow the same trend. Work, public transportation, and recreational activities decline the most. Retail and groceries are less affected as people need to purchase essential consumer goods. Residential mobility increased because people spend more time at home (e.g., working from home). It is not surprising that mobility declines more in Denmark with obligatory restrictions. It is, however, interesting that mobility declines at all in Sweden. The mobility patterns began to change around March 11 in both countries, suggesting that the Danish Government's decision to impose restrictions increased the perceived risk of SARS-CoV-2 in Sweden.

However, it has to be said that behavior changes are not necessarily benign. Fear and panic may adversely affect efforts to contain an epidemic outbreak. A team of health care workers was attacked in Guinea during the 2014 Ebola epidemic in West Africa, and patients are reported to have fled from treatment centers [160]. This form of spontaneous behavior change and its effect on disease transmission is covered in more detail in chapter 3. Here we review some approaches to model contact heterogeneity (e.g., space and network structure). These models will be of use to us later on.

1.2.2 Spatial and network structure

Spatial or geographic spreading is a natural starting point. Proximity to an infected person or animal increases the risk of being infected – but how much depends on the mechanics of how transmission happens. Not all diseases are transmitted by direct contact with the host. Measles particles can remain infectious in the air for up to two hours. So a host can infect others through a residual collection of virus particles in the air or on a surface. Nonetheless, the host and the susceptible individual must have been around the same location within a limited time interval. The global outbreak of severe acute respiratory syndrome coronavirus (SARS) is a notable example of spatial spread. This outbreak has been traced to a superspreading event (SSE) by a man who spent one night in a hotel in Hong Kong on February 21, 2003. Dr. Liu Jianlun was a medical doctor from the Guangdong province, where the virus originated. During his brief stay at Hotel Metropole on the 9th floor, he infected 16 other guests who also stayed on that floor [62].

J. V. Noble modeled the spread of bubonic plague across Europe with a diffusion model [133]. It seems inconceivable that a pandemic can be modeled with simple diffusion. However, the movement of humans and animals (e.g., rats and fleas) was limited in medieval times. Mobility patterns must be very local for a disease to spread by diffusion. It seems unlikely that such a description would be valid in a post-industrial or globalized society. The effect of civil aviation on global epidemics has been studied in many scientific publications [31, 97, 152].

Metapopulation models

Multi-patch (or metapopulation) describes transmission inside and between spatially separated subpopulations (e.g., district, city, municipality). Here the transmission is modeled with a compartmental system of ordinary differential equations (ODE's) for each patch [41, 120]. We obtain a large system

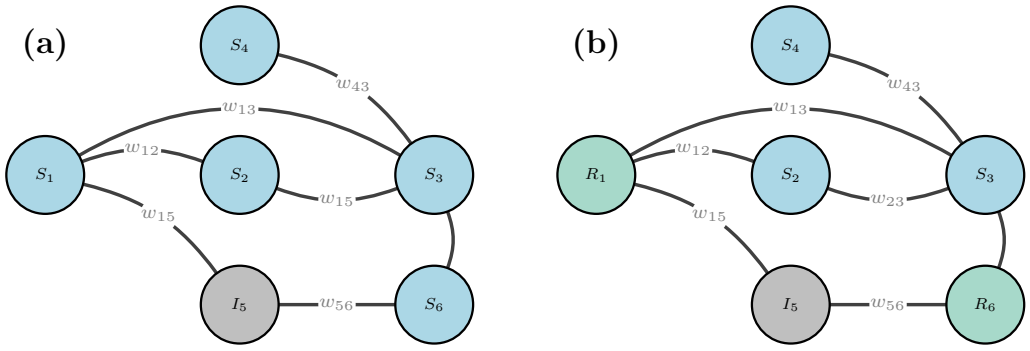

Figure 1.2: **Sketch of a weighted contact network**. (a) shows an infected node in a contact network. (b) shows how immunizing the contacts of the infected node prevents the disease from spreading. Hindering the spread of disease by vaccinating those most likely to be infected is known as ring vaccination. This network is heterogeneous because the nodes can occupy different states. Networks composed of identical nodes are homogenous.

of ODE's if we use many patches. Individuals in one patch can also infect individuals in other patches. However, there is naturally more mixing within a patch than between them. Further, patches can be out of sync with each other as one would expect in a spatially heterogenous epidemic [55]. Multi-patch models have been used to explain and model several epidemiological features [41, 146]. We a metapopulation model in chapter 2 to investigate the effect of coordinating lockdowns between recurring outbreaks of SARS-CoV-2.

Epidemics on networks

Many diseases are spread by direct physical contact, which led us to consider spatial transmission models. However, individuals can be physically close without interacting at all. Residents of a neighborhood or an apartment building live close together but do not necessarily interact with or know each other. Individuals tend to have more direct contact with friends, family members, and colleagues than strangers. Spatial models are oblivious to the intricate social structure of human interaction, but network models can overcome this deficit. Networks are made of nodes that are connected by links. We can take a node to represent a host in one of many mutually exclusive states (e.g., susceptible, infectious, immune). The links between nodes may represent one or more contact events between two hosts.

Networks offer unique flexibility to describe arbitrary levels of contact heterogeneity. Multiple contacts between individuals naturally increase the probability of disease transmission. Furthermore, the likelihood of transmitting a disease also depends on the specific nature of the contact event. For example, the risk of HIV transmission depends on the type of sex. Weighted networks have been proposed to accommodate this lower level of heterogeneity [103, 157]. Networks can be directed or undirected. Undirected networks are made of bidirectional links, representing symmetrical interactions between the hosts. Conversely, directed networks are made of unidirectional links with asymmetrical interactions. Intuitively, there is no reason why a respiratory virus should spread from host P to host Q but not from Q to P if the roles were reversed. However, symmetries are easily broken in the real world. For example, if one of the two hosts wears a mask, that would induce an asymmetry. There are also sexually transmitted diseases (STDs) that are more easily transmitted to a woman than a man during sexual intercourse [129]. Thus, a contact network can be semi-directed and contain both directed and undirected links.

Contact networks have been used to model the spread of sexually transmitted diseases (e.g., HIV/AIDS) [108]. It is naturally difficult to construct a network for infection spread by fleeting contact (e.g., airborne and respiratory droplets) as these events are likely to go unnoticed. However, individuals generally know whom and when they have sexual intercourse, which allows us to construct a temporal contact network and trace contacts.

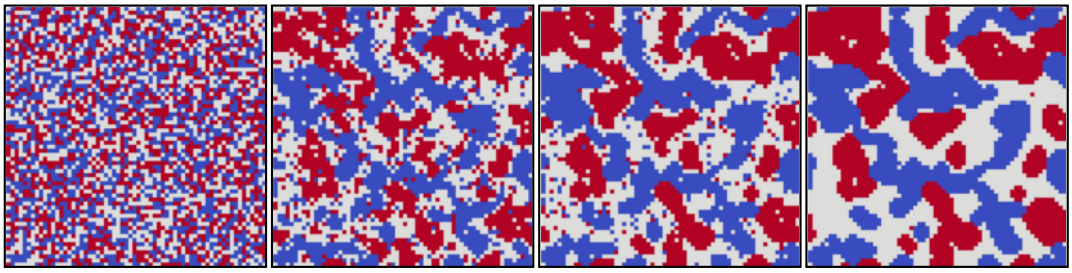

Figure 1.3: **Spontaneous order emerges from in-group preference**. Simulation of the Schelling model with periodic boundary conditions. Individuals will relocate to a random empty site if less than 4 of his 8 neighbors belong to his group.

Individual-based models

Individually-based models are computational models that simulate autonomous agents (e.g., humans, animals) with simple rules. These models have been applied to problems in many fields (e.g., ecology, epidemiology, and social science). Such models have shown that complex dynamics can emerge from simple rules, which traces back to the work of Stanival Ulam, and John von Neumann on cellular automata in the 1940s [131].

In 1971, Thomas Schelling proposed a simple model of racial segregation [153]. This model is very instructive and worth expounding on. Let us consider a $N \times N$ grid. A grid cell can be vacant or contain a person assigned to one of two mutually exclusive groups. Individuals have some preference for members of their group in their neighborhood. The system is then updated by checking the immediate neighborhood of a person. A person who is not content relocates to an empty site that satisfies his preference. The updating can be synchronous or asynchronous. In synchronous updating, the status of each cell on the grid is updated simultaneously—conversely, the asynchronous scheme updates the status of each cell one by one. Schelling discovered that a population with modest in-group preferences would self-organize into a racially segregated state. The Schelling model successfully explains a phenomenon that would otherwise have been impracticable to capture with other modeling approaches (e.g., partial differential equations).

In epidemiology, individual-based models have been used to simulate disease outbreaks of smallpox and coronavirus [1, 147]. Individual-based models capture spatial heterogeneity (e.g., space and network structure) and allow us to specify unique properties of individuals, diseases, and the environment. However, the models can be time-consuming to run and require extensive validation.

We use an individual-based model on a spatial structure to explain the spread of the Ebola virus (EBOV) in chapter 3. We also use them in chapter 4 to model information flow on a social network.

Chapter 2

Estimating the effect of coordinating lockdowns

The ongoing coronavirus pandemic has caused economic and social disruption on a massive scale, plunging the world into a global recession. Governments worldwide have imposed restrictions on travel, movement, and gatherings to curb the spread of the virus, closing educational institutions, nonessential shops (e.g., restaurants and coffeehouses), public places (e.g., libraries), and in some cases, ordering people to shelter in place. Closing entire sectors of society on a global scale to curb the spread of a contagious disease is a novelty. Modeling studies on the global spread of pandemic influenza have considered various interventions such as therapeutic and prophylactic antiviral treatment, vaccination, case isolations, and air travel restrictions, but none so profound as to shut down society [30, 32, 48, 60]. This unexplored topic presents us with a chance to do new research. Here we use a mathematical model to explore the efficacy of different lockdown strategies to stop viral transmission.

2.1 The coronavirus pandemic

The severe acute respiratory syndrome coronavirus 2 (SARS-CoV-2) was discovered in Wuhan, the capital of Hubei Province, in December 2019. SARS-CoV-2 causes coronavirus disease (COVID-19) [117, 183]. On January 23, 2020, the Chinese State Council imposed a Cordon sanitaire, imposing restrictions on movement in Wuhan and elsewhere in the Hubei Province to contain the outbreak. On January 30, 2020, The World Health Organization declared the SARS-CoV-2 outbreak a Public Health Emergency of International Concern (PHEIC) on January Most of Hubei had reopened by March 2020 following the end of local transmission. Wuhan reopened on April 8, 2020 [51]. Nonetheless, the lockdowns failed to prevent SARS-CoV-2 from spreading to other countries despite some of the most draconian restrictions ever seen [33]. The World Health Organization updated the public health emergency to a pandemic on On March 11, 2020. As of October 2021, there have been around 234 million confirmed cases and 4.79 million deaths worldwide, making it the deadliest pandemic since the Spanish flu.

2.1.1 Transmission and symptoms of COVID-19

COVID-19 is generally transmitted through respiratory droplets and airborne particles [85, 119, 172]. These infectious droplets and particles are released when an infected person exhales (e.g., sneezing, breathing, or coughing). The respiratory droplets and aerosols containing the virus then cause infection when inhaled by susceptible humans. Albeit airborne transmission was at first controversial, it has since been established that SARS-CoV-2 can remain in the air for hours [166]. The virus can also survive on surfaces, but this is not believed to be a significant source of infection [115].

There is significant variability in the symptoms experienced by those infected with coronavirus disease (COVID-19). A person infected with SARS-CoV-2 can have various symptoms, ranging from asymptomatic to serious illness. Common symptoms of infection are fever, dry cough, fatigue [175]. Less common symptoms include headache, nasal congestion, loss of taste or smell, sore throat, muscle pain, diarrhea, skin rash, chills, or dizziness. Shortness of breath, persistent pain, high fever, and loss of appetite are symptoms of serious illness [175].

The incidence of asymptomatic infections varies between studies but has been a concerning factor as these carriers can transmit the virus but show no signs of being infectious. [69, 71, 88, 134]. Presymptomatic transmission is also a major problem in containing the spread of coronavirus [9, 161]. The difference between pre - and asymptomatic infection is simply that asymptomatic cases never develop symptoms. Presymptomatic cases become infectious before becoming symptomatic, which occurs for diseases with a shorter latency than the incubation period.

2.1.2 Strategies to control influenza outbreaks

Strategies to control influenza outbreaks have been studied extensively before the emergence of SARS-CoV-2 [8, 30, 32, 48, 56, 57, 60, 122, 128]. In a review of 19 modeling papers on pandemic influenza published between 1999 and 2009, only four considered the effect of combining different interventions on a global scale [30, 32, 48, 60, 114]. One of the studies considered the effects of vaccination, case isolation, and reduced air traffic, and antiviral drugs [60]. This study found vaccination to be the most effective provided it is available, while global air travel had to be almost completely terminated to impact the estimated attack rate.

Only two modeling studies were sanguine about the prospect of containing an influenza outbreak given favorable conditions. One by Ferguson et al. aimed to show how an incipient influenza pandemic could be contained using a combination of pharmaceutical interventions, in particular, the prophylactic use of antiviral drugs and social distancing measures [56]. Another by Longini et al. showed how the prophylactic use of vaccination and antiviral agents together with quarantine measures could contain an influenza strain with a basic reproductive number R_0 up to 2.4 [122].

2.1.3 Responses to the COVID-19 pandemic

The presence of pre - and asymptomatic transmission makes SARS-CoV-2 a very non-trivial containment problem. A study on the effect of travel restrictions found that the Wuhan travel ban in early February 2020 decreased cases imported to other countries from Mainland China by 77% [27]. A 2006 paper on the effect of travel restrictions on pandemic influenza found that it would be necessary to quickly restrict almost all international travel to prevent the new epidemics in other areas [92]. Many travel restrictions during the pandemic have been aimed at symptomatic cases or people traveling from specific regions, while pre - or asymptomatic COVID-19 carriers could slip through the safeguards undetected. While banning all travel could, in theory, prevent this, a single infected person can seed an outbreak in a country previously unaffected.

The United States issued some travel restrictions on passengers inbound from China after declaring COVID-19 a Public Health Emergency on January 31, 2020, which took effect on February 2 [156]. U.S citizens from the Hubei province were subject to a 14-day mandatory quarantine. Asymptomatic U.S citizens from other parts of mainland China were allowed entry, while other foreign nationals who had been to China within 14 days were prohibited from entering the United States [95]. Aside from allowing entry to possible carriers, the coronavirus was already spreading in the United States when the restrictions were implemented [93]. Thus, it would have been necessary to trace and isolate all symptomatic and asymptomatic cases to contain the spread, even if the travel restrictions were completely effective. Only a few countries (e.g., South Korea and Taiwan) managed to control the epidemic early on through mass testing and contact tracing efforts and by imposing mandatory quarantines on **all** travelers entering the country. Neither vaccines nor antiviral drugs were available at the onset of the pandemic. Consequently, many countries resorted to non-pharmaceutical interventions to slow transmission and prevent hospitals from overflowing with patients. However, these interventions have varied significantly both within and between countries. In the United States, the timing and use of interventions varied significantly between individual states. [86]. Some states issued stay-at-home orders while others did not. A modeling study suggests that uncoordinated state policy increased transmission through social and geographic spillover [94]. This study considers the possibility that people's behavior is not solely influenced by their local communities but also by friends and relatives living far away, which may erode adherence to social distancing. Uncoordinated local policies can also mediate geographic spillover to neighboring communities. Another modeling study assessed the impact of local tiered restrictions imposed in England to curb the second wave in autumn 2020 and found them to be less effective than a national lockdown [36]. Denmark imposed harsh local restrictions in 7 municipalities between Nov 5-19, 2020, to eradicate a SARS-CoV-2 variant with several mutations in the spike protein (Cluster 5 variant) [12]. This effort appears to have been successful.

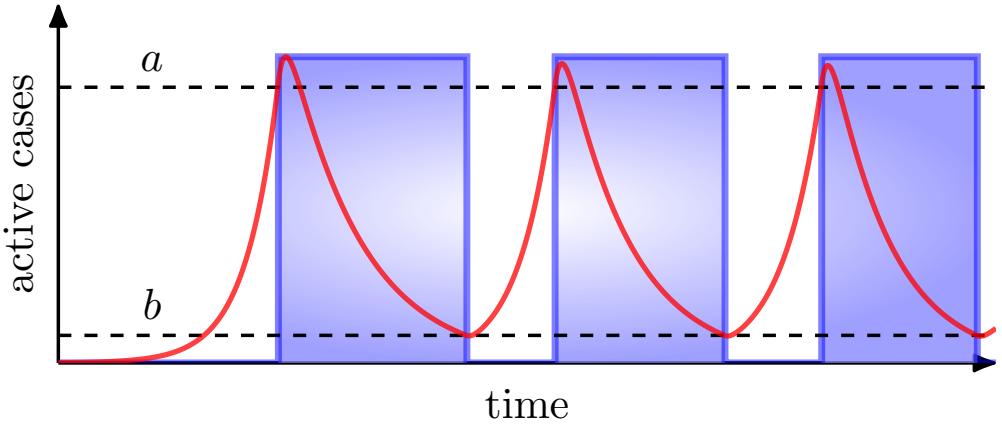

Figure 2.1: **Sketch of the lockdown mechanism**. Uncoordinated lockdown **(UL)** activates when cases in a unit exceeds a. The contact rate β is reduced by a factor of $(1-s)$ while lockdown is activated. The lockdown is annulled when cases drop below b. Synchronized lockdown **CL** activates if cases in just one unit surpass a and is undone when all units have below b cases. The latency period causes the epidemic waves to peak slightly above a.

2.2 Metapopulation model

Here we model epidemic spreading in multiple subnational units that are out of sync with each other. Coupled metapopulations represent distinct administrative units with individual containment policies (e.g., states, counties, or municipalities). From this point, we refer to these simply as **units** for brevity.

2.2.1 Suppression strategies

Two related suppression strategies shall be considered.

Uncoordinated lockdown **(UL)** is activated in a particular unit denoted by subscript i when cases $I_i(t)$ exceed a. Restrictions are lifted when when cases drop below b. Fig. 2.1 delinates the basic concept.

Mathematically, we can write this as a sequence of dynamic boundary conditions. If lockdown is not active then $\beta_i = \beta$ while $a \geq I_i(t)$ until $a < I_i(t)$ at which instant lockdown becomes active and $\beta_i = \beta(1-s_i)$. Then $\beta_i = \beta(1-s_i)$ while $I_i(t) \geq b$ until $I_i(t) < b$ at which point lockdown is no longer active and $\beta_i = \beta$.

Coordinated lockdown **(CL)** follow the same rule but is activated in **all** units if cases in just one of them exceed a and lifted only when cases in **all** them drops below b.

Closing and reopening parameters can vary between units using **UL**. The risk of depleting critical care capacity has been widely used to support lockdown. Substantial variability exists in intensive care bed availability even among wealthy nations [145]. The efficacy of lockdown s_i may also vary depending on the imposed restrictions and the degree of compliance with

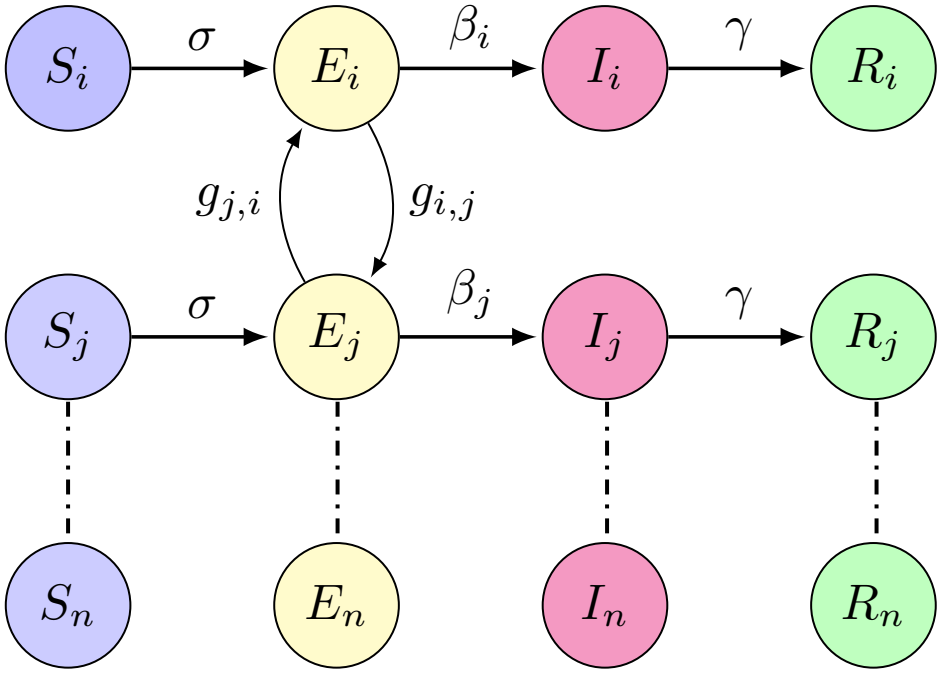

Figure 2.2: Model diagram showing the mutually exclusive states a person can occupy and the transition rates between them. Each row represents the compartmentalized populations in a unit, and each column is the sum population in that state.

them. A study estimating the effect of non-pharmaceutical interventions on COVID-19 transmission in Europe found lockdown to be significantly more effective at reducing transmission than school closure, banning public events, case-based isolation, and encouraging social distancing [61]. Overall, estimates suggest a reduction in transmission by around 60-80 % can be expected [61, 107].

2.2.2 Coupled metapopulations

The transmission within individual units is governed by a susceptible-exposed-infected-recovered model, with a low spillover rate g between them

$$\frac{dS_i}{dt} = -(1 - \sum_j g_{i,j})\beta_i I_i S_i - \sum_i g_{i,j}\beta_i S_i I_j, \tag{2.1}$$

$$\frac{dE_i}{dt} = (1 - \sum_j g_{i,j})\beta_i I_i S_i + \sum_i g_{i,j}\beta_i S_i I_j - \sigma E_i, \tag{2.2}$$

$$\frac{dI_i}{dt} = \sigma E_i - \gamma I_i. \tag{2.3}$$

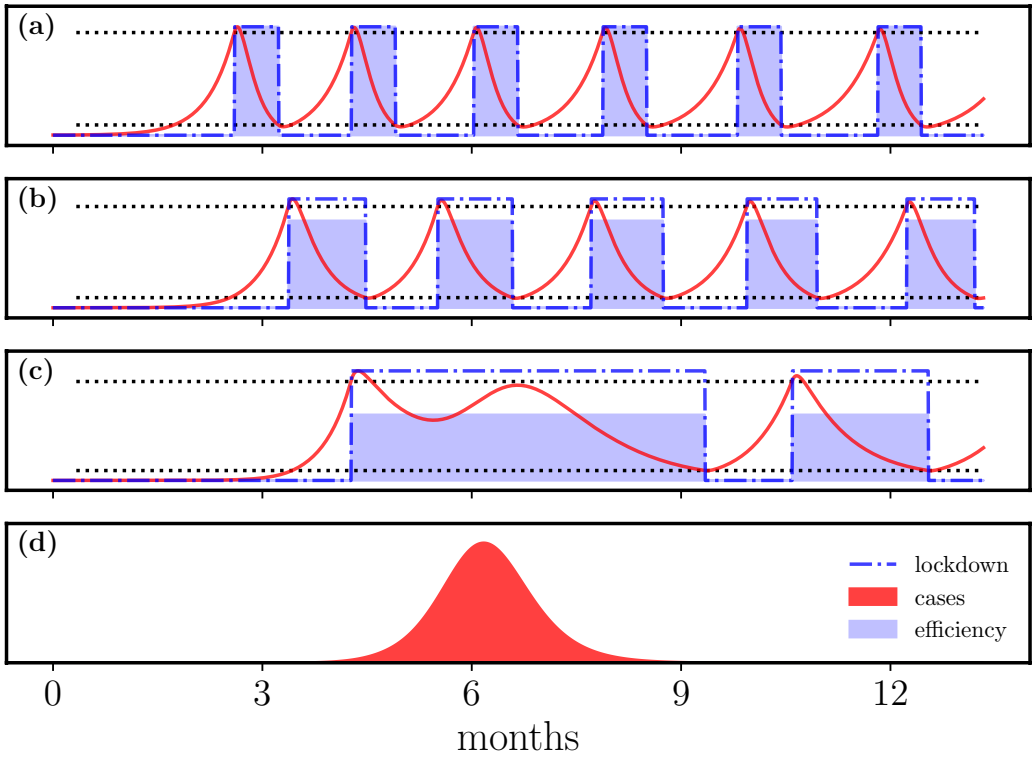

Figure 2.3: **Disease transmission between 4 interconnected units**. Each unit is executing its own suppression policy with decreasing commitment from top to bottom. The top panel (a) does a draconian lockdown that nullifies transmission. (b) is using a hard lockdown with 80% efficiency. (c) is using a soft lockdown with a 60% efficiency. Unit in the bottom panel (d) is not doing lockdown. Spillover from (d) is causing a surge of cases in (c) despite being in lockdown. Initial conditions are $I_a(t_0) = 1$ and the remaining population is susceptible at $t = t_0$. Each unit contains $N = 100.000$ persons. Model parameters: $R_0 = 2.0, \sigma = 1/5$, $\gamma = 1/4$, $g_{ab} = g_{bc} = g_{cd} = 0.01$ and $g_{dc} = 0.04$. Lockdown parameters: $a = 500$, and $b = 50$.

Here the sum is over n units interacting through the coupling matrix $g_{i,j}$, which gives the spillover rate between units. Generally, these spillover rates should be symmetrical, i.e., $g_{i,j} = g_{j,i}$, although slight asymmetries are permissible. The first term in the system above gives the transmission within i. The spillover from i to other units is subtracted from the transmission rate within that unit. This effect is negligible unless spillover rates are abnormally high. The next term gives the transmission from other units to i. Each unit contains the same number of persons N to avoid the proliferation of model parameters. The combined population of all units is nN.

The transmission model blends homogenous mixing inside a metapopulation with heterogeneous mixing between them. The suppression strategies are superimposed as boundary conditions. This continuous model does not permit the eradication of the disease. SARS-CoV-2 quickly spread to so many

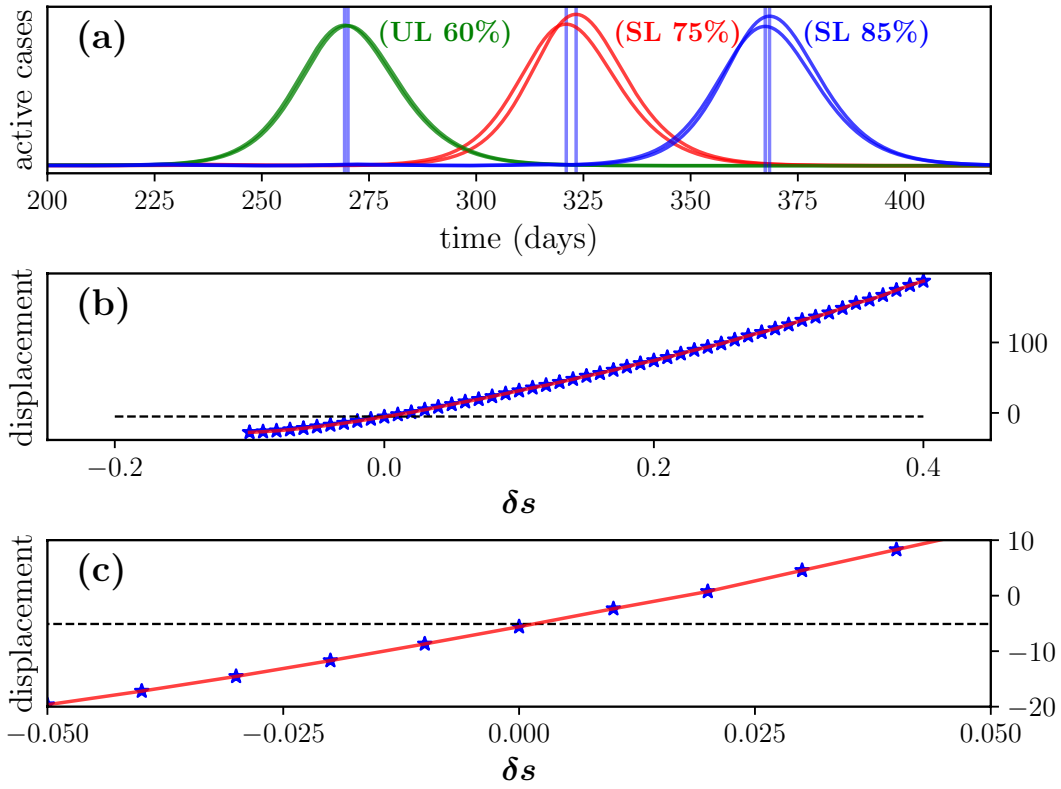

Figure 2.4: **Comparing the two strategies**. (a) show 3 simulations with a limit on lockdown time equal to 160 days. (b) shows the effect of varying s for **CL** on peak seperation. Effectiveness of **UL** is kept constant at $s = 0.6$. (c) shows (b) around parity. Model parameters are $R_0 = 2.38$, $a = 100$, $b = 10$, $\sigma = 1/3.69$, $\gamma = 1/3.48$, with reciprocal couplings $g_{1,2} = g_{2,1} = 0.01$. Each unit contains $N = 100.000$ persons.

countries that any effort to eradicate it with lockdowns was unlikely to succeed after it had spread from Wuhan. A stochastic model would be better suited to investigate the prospect of eradication.

2.3 Exploring the metapopulation model

The possibly large system of ordinary differential equations (ODE's) is solved numerically with the suppression strategies as dynamic boundary conditions. Figure 2.3 shows transmission between $n = 4$ interconnected units using **UL**. The effectiveness of lockdown varies, as shown by the blue filling. The unit in (d) has decided not to enact a lockdown but maintains a strong coupling to (c), which further drives transmission since lockdown here otherwise barely keeps R_0 below the epidemic threshold. Re-directing this coupling to (a) has no effect, and the effect on (b) is negligible. This finding would suggest that border closings are less pertinent if a hard lockdown is in effect. However, if only a soft lockdown is in effect, one should be more cautious about links to a large transmission cluster.

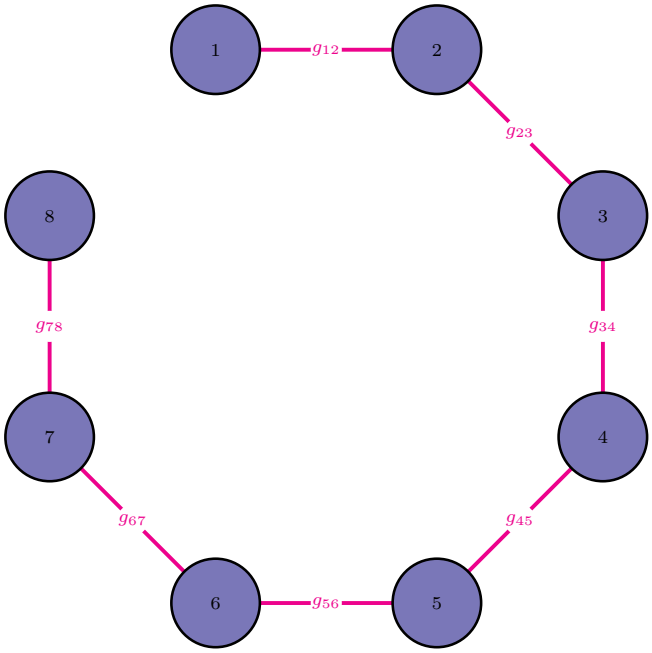

Figure 2.5: **Metapopulation graph with long path length**. The epidemic begins in "1" and must spread between neighboring communities all around the ring to infect "8".

2.3.1 Estimating the model's parameters

The principal objective is to assess which of the two strategies best delay transmission if given the same disposable resources. Each unit is assigned a fixed amount of lockdown time to answer this question. The unit can no longer activate lockdown when this time is spent.

Li et al. estimated the latency period and the infectious period to be 3.69 and 3.48 days, respectively [118]. This analysis estimated the transmission parameters of COVID-19 during the outbreak in Wuhan using maximum likelihood. Here the basic reproduction number was estimated to be $R_0 = 2.38$. New SARS-CoV-2 variants have emerged since the Wuhan outbreak, and there is considerable variation among them in transmissibility. This analysis does include the new variants, but we will discuss the implications of this later.

In this particular numerical experiment, the lockdown threshold should be low to ensure that most of the population is susceptible when lockdown expires or the epidemics dissipate before lockdown time runs out. Threshold parameters are $a = 0.1\%N$ and $b = 0.01\%N$. Each unit has 160 days of lockdown time.

2.3.2 Assessing the effect of coordinating lockdowns

Figure 2.4 shows the output of a simulation with these parameters. The epidemic curve peak afters the unit runs out of lockdown time, so we want the curves to peak as late as possible. (a) shows three individual simulations with different lockdown effects. Unsurprisingly a more effective lockdown

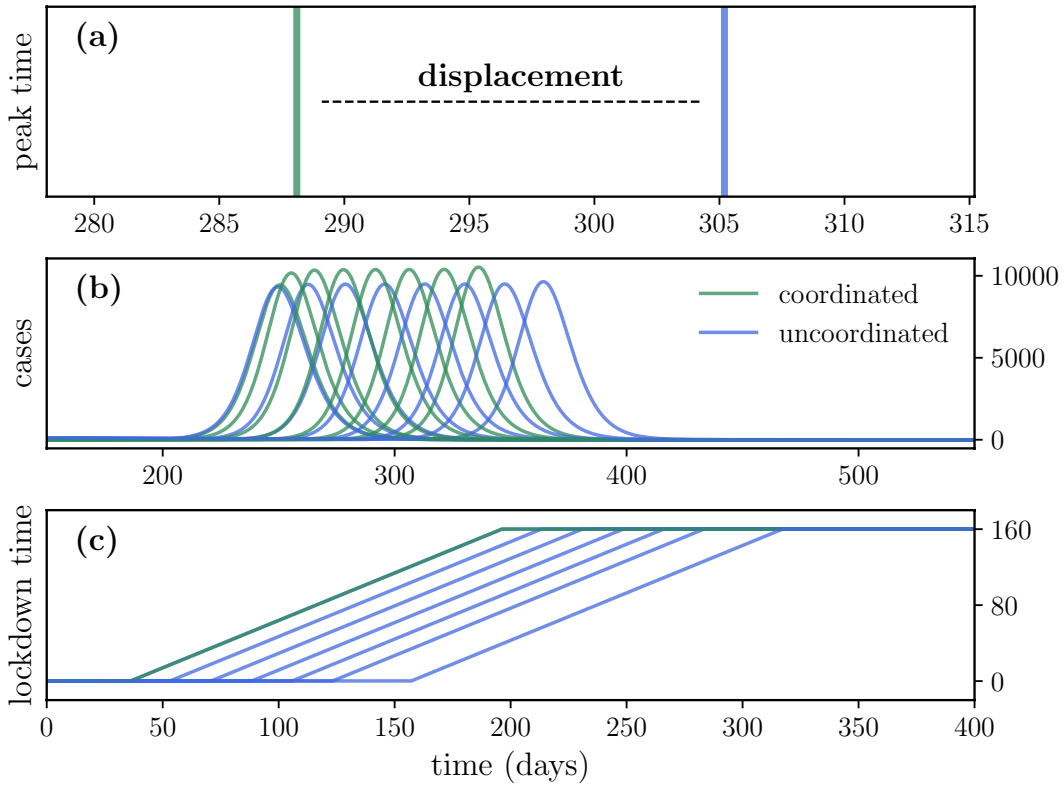

Figure 2.6: **Simulation on graph with long path length**. (a) shows the average peak time for the two strategies. (b) shows the epidemic curves. (c) shows spend lockdown time. Model parameters are $R_0 = 2.38$, $a = 100$, $b = 10$, $\sigma = 1/3.69$, $\gamma = 1/3.48$. Reciprocal couplings have strength $g_ij = 10^{-2}$. Each unit contains $N = 100.000$ persons with 160 days desposible lockdown time.

delays transmission longer with the same resources. (b) shows the effect of varying lockdown efficacy s on the peak separation. **UL** performs slightly better around parity $\delta s = 0$, but this is easily offset by a small difference in s. **CL** is generally believed to be more effective. The peak separation around parity is caused by a phase delay between the units that are coordinating. The phaseshift arises because the epidemic begins in one unit and spreads to the other through spillover. The lockdown is then activated prematurely in the other unit, causing **CL** to run out of lockdown time slightly faster. This phase delay also occurs in **UL**, but here the units activate lockdown individually.

2.3.3 Metapopulation graphs

We can create more favorable conditions **UL** by designing a network of coupled metapopulations with a long path length. Figure 2.5 shows eight poorly connected metapopulations labeled from 1 to 8. The epidemic begins in 1 and must spread through all the remaining units to get to 8. Figure 2.6 shows a simulation with this network. Here the lockdowns are assumed to be equally

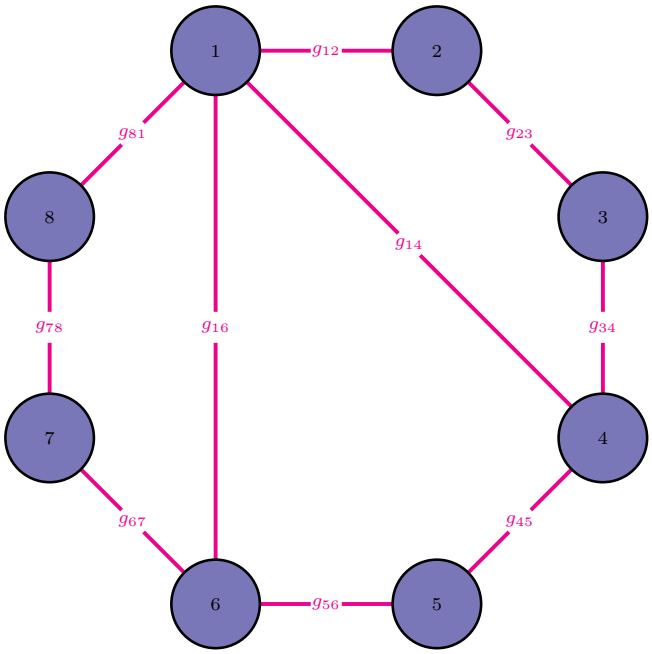

Figure 2.7: **Metapopulation graph with short path length**. Adding a few links to the networks imbues it with small-world properties. The epidemic now spread between units much faster.

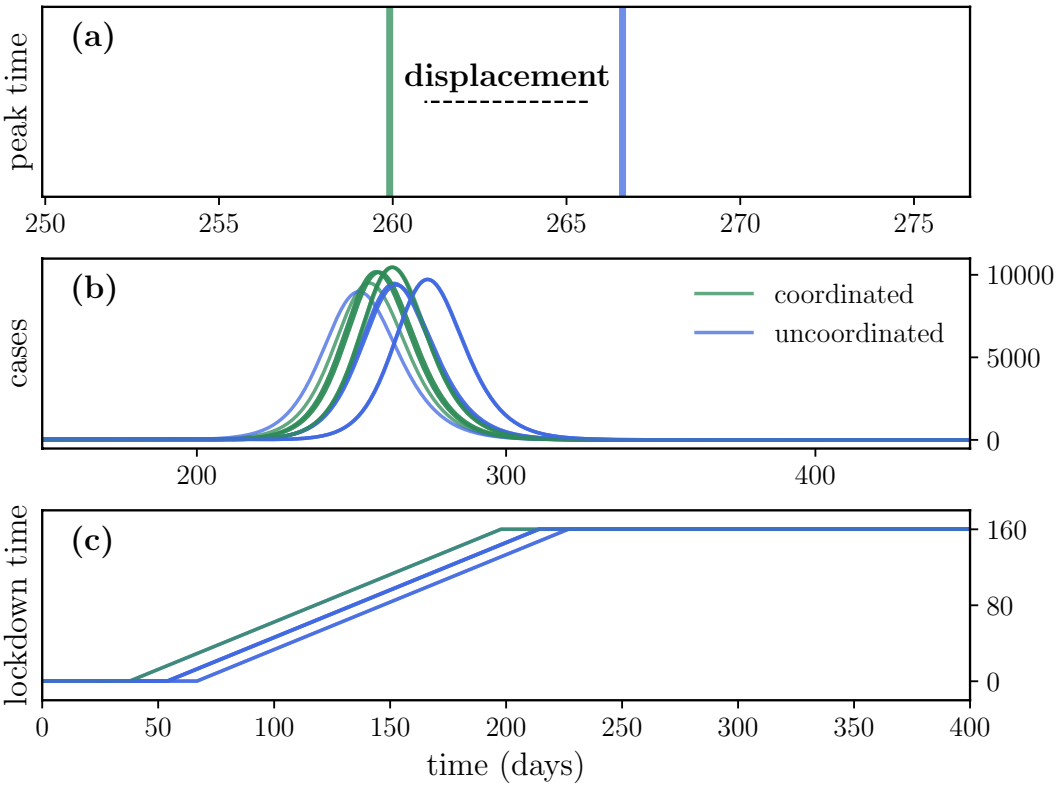

Figure 2.8: **Simulation on graph with short path length**. Adding a few links has significantly reduced the peak separation between the strategies. Model parameters are identical to the previous simulation except for g containing additional entries. The strength of all couplings are $g_{ij} = 10^{-2}$ as before.

effective with $s = 0.6$. Figure 2.6 (a) shows the mean peak separation between the two strategies. Here **UL** performs even better than before as expected. The network in 2.5 was designed to have a long path length and is not a realistic model of a country. Figure 2.7 shows how the distance between nodes is dramatically decreased by adding a few links. Most countries have big cities that are central hubs in a transportation network. The presence of these hubs decreases the mean path length by mediating interactions between less-connected nodes. If the metapopulation network has small-world properties, the mean path length will be proportional to the logarithm of n units. Therefore, adding more metapopulations to the network will not significantly change the result.

Figure 2.8 show a model simulation on this network substrate. The peak separation in (a) is considerably smaller than before, and the local epidemics in (b) are nearly synchronized. We have now considered the model on the different metapopulation networks while assuming parity between the strategies on reducing transmission. Our objective was to assess whether coordinating lockdown was good or bad. The coordinated strategy performs worse on a poorly connected graph because the local epidemics are out of phase, which causes precious lockdown time to be wasted. This disparity was almost eliminated by adding a few connections to the metapopulation graph.

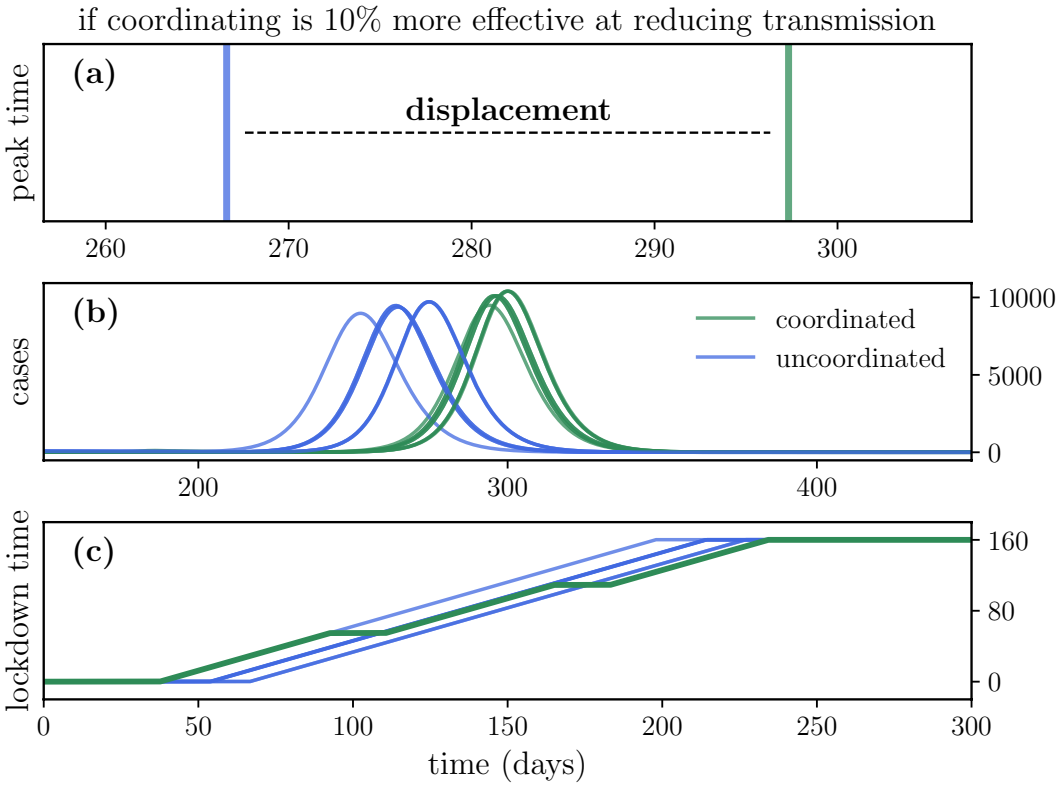

Figure 2.9: **Simulation on metapopulation graph with short path length and** $\delta s = 0.1$. Here the coordinated strategy reduces transmission by 70%, while the uncoordinated lockdown policy reduces transmission by 60%. The other parameters are unchanged.

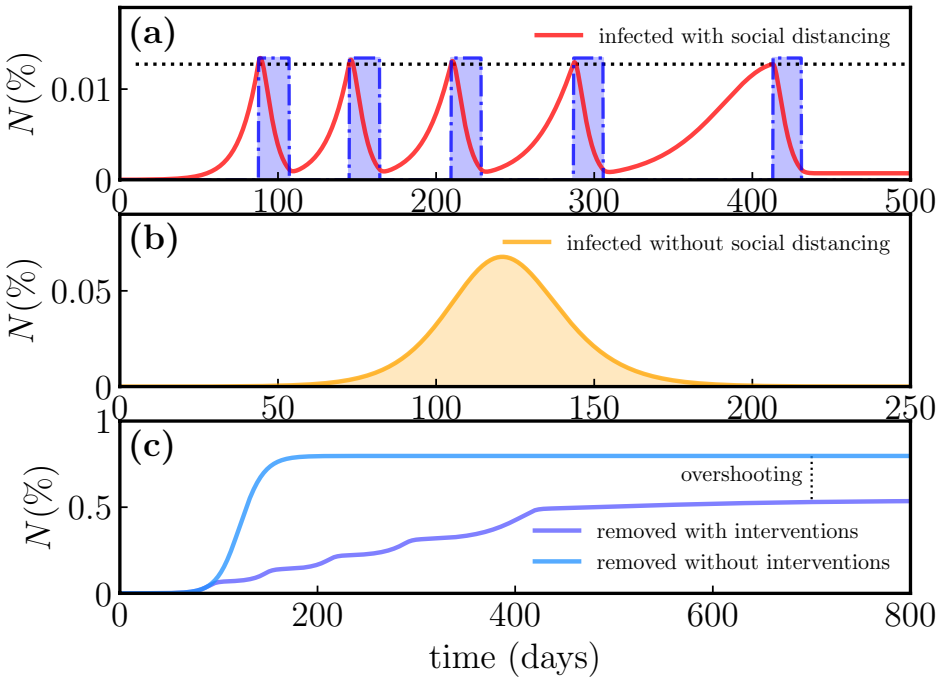

Figure 2.10: **Lockdown decrease the attack rate by decreasing the overshoot**.

Nonetheless, the coordinated "national" policy is conceivably more effective according to some modeling studies. So we need to determine whether a small discrepancy in lockdown efficacy can offset the network-induced displacements that favor **UL**.

Figure 2.9 shows a simulation where **CL** is slightly more effective than **UL**. The simulation is performed on the metapopulation graph with a short path length. Here the coordinated strategy reduces transmission by 70%, while the uncoordinated lockdown policy reduces transmission by 60%. Here **CL** is clearly superior to **UL**. Model simulations show that **CL** had to be slightly less than 2% more effective to get to parity on the metapopulation graph with a short path length; it had to be 5% more effective a the graph with a long path length. Figure 2.9 (c) shows how much disposable lockdown time has been allocated in the different units. **CL** is now effective enough to get cases below the de-activation threshold b. These intermittent lockdowns are responsible for the saw-tooth pattern. A 60% reduction in transmission is barely enough to suppress a disease with a basic reproduction number of 2.38. That is why the blue **UL** curves activate lockdown until they run out of time. This analysis allocated a fixed amount of lockdown time to each subnational entity, and compliance dwindles after lockdown has been activated for this long. The intermittent lockdowns could conceivably replenish compliance by giving people a breathing space to socialize. If so, there could be benefits to a shorter and more effective lockdown.

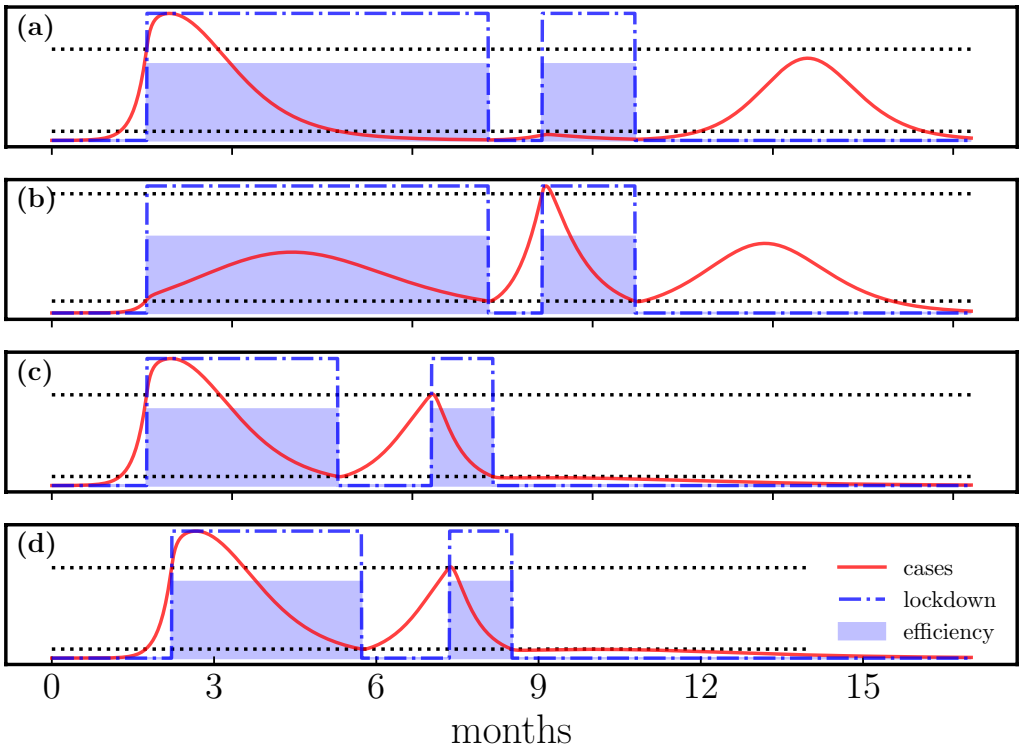

Figure 2.11: **Catastrophic overshooting**. Top panels (a & b) show a simulation with **CL**. The overshoot is not eliminated on the last wave as infection peaks just below a. Bottom panels (c & d) show the simulation with **UL**. Each unit contains $N = 100.000$ persons. Model parameters are $R_0 = 3.0$, $\gamma = 1/4$, $\sigma = 1/5$, and $g_{12} = g_{21} = 0.01$. Lockdown parameters: $a = 2100N$, $b = 210N$, and $s = 0.4$. Failure to eliminate the overshoot can occur for either strategy depending on the input parameters.

Here we digress for a moment to discuss the implication of large disparities in vaccination coverage before moving on to the next topic. The situation has changed with the rapid distribution of SARS-CoV-2 vaccines. There is considerable variation in vaccination coverage between U.S. states. This discrepancy appears to be driven by an unwillingness to be vaccinated rather than a shortage of supplies. Here imposing local restrictions could make more sense to prevent critical care units from overflowing with patients – while a coordinated lockdown policy would force states with high vaccination coverage and low caseload to enact lockdowns as well.

2.3.4 Eliminating the overshoot

The role of control strategies in delaying susceptible depletion has been considered. There are other reasons to impose control strategies than to postpone transmission. Flattening the curve has become a household word in many countries. This strategy aims to impede the spread of SARS-CoV-2 to prevent the healthcare system from being overloaded by patients. Another reason to flatten the curve is to minimize overshoot. The effective reproduction number R_e decreases with susceptible depletion. The epidemic begins to subside

when the effective reproduction number falls below one, and the susceptible population is S_{th}. However, when this occurs, there will be a large number of active cases. This residual infected population causes disease transmission to persist, although the remaining active cases produce less than one new case on average. Consequently, the susceptible population drops below S_{th}. These excess infections are sometimes referred to as overshoot. The overshoot can be significant depending on R_0. Handel et al. proposed control strategies that minimize these excess infections. The optimal strategy seeks to flatten the curve in such a way that the susceptible population never falls below S_{th}. Figure 2.10 show how imposing restrictions results in a lower attack rate, although this strategy is not optimized to minimize overshoot.

There are some caveats worth mentioning if we aim to delay transmission as long as possible. Figure 2.11 shows how a suppression strategy can produce a higher attack rate despite spending a long time in lockdown. The last wave in a & b is barely below the lockdown activation threshold, so the overshoot is not diminished. Units in c & d sustain only two epidemic waves but reduce overshoot on both of them. This catastrophe causes a & b to end up with a higher attack rate despite spending more time in lockdown. Such a catastrophe could happen in the following way. Say a state decides to impose a lockdown to slow transmission until a vaccine becomes available. However, it is hard to predict in advance how long it takes to develop the vaccine, and it is implausible to sustain a lockdown indefinitely, as compliance is bound to fade eventually [82]. We risk this scenario if civil disobedience ensues after a long time in lockdown but before a vaccine is developed and distributed.

2.3.5 Summary and conclusive remarks

Novel infectious diseases outbreaks pose a threat to global public health. Control strategies can blunt the impact, but these efforts to control transmission are only temporary. We have simulated SARS-CoV-2 transmission between coupled metapopulations and imposed different control strategies. The uncoordinated strategy (**UL**) better delays transmission if the strategies reduce transmission by an equal amount. The coordinated lockdown policy (**CL**) had to be 2% more effective at reducing transmission to achieve parity on a metapopulation graph with small-world properties. **CL** had to be 5% more effective on the ring lattice. **CL** is conceivable more effective at reducing transmission, according to some studies. The uncoordinated strategy (**UL**) may be preferable if limited lockdown time is available and the objective is to minimize the overshoot and not to delay transmission. This recommendation comes with the caveat that **UL** should be reasonably effective for this to work.

Coordinated or not, lockdowns are an emergency brake to be used only when other options are unavailable. Containing disease outbreaks early on through enhanced epidemic surveillance and being better prepared for future outbreaks by developing drugs is preferable to locking down society.

Chapter 3

Dynamics of reactive social behavior in spatial epidemics

This chapter considers spatial models of disease spread, emphasizing the effect of local behavior changes on the transmission of Ebola virus disease (EVD). Before addressing those topics, it is necessary to review some basic features of the virus. The virus that causes Ebola virus disease (EVD) was discovered during the outbreak in 1976 in the Democratic Republic of the Congo (DRC). The spread began in a small village called Yambuku, where several villagers fell ill with an unknown hemorrhagic fever [53] The virus appears to have been named after the Ebola river by the virologists who discovered it to avoid stigmatizing Yambuku and its residents [142]. Another Ebola outbreak had occurred months prior in the town Nzara in South Sudan, but it was not recognized as an Ebola outbreak until later [177]. Ebola outbreaks occur sporadically in Sub-Saharan Africa. There have been 24 documented outbreaks between its discovery in 1976, and 2012 [176]. The Ebola virus epidemic in West Africa (2014-2016) was the first occurrence of the disease to be considered an epidemic, causing more loss of life than all previous outbreaks combined. Kivu Ebola epidemic (2018-2020) in the DRC became the second-largest recorded Ebola outbreak, suggesting that widespread transmission is becoming more common.

3.1 The Ebola virus

This introduction is not aimed at ebolaviruses' virology, but a basic taxonomy is not irrelevant. There are currently six known species of the genus Ebolavirus belonging to the family Filoviridae, only four of which are known to cause illness in humans [52, 83, 110]. The Zaire ebolavirus (EBOV) identified in Yambuku is the deadliest, responsible for the Western African Ebola virus epidemic (2014-2016). EBOV has caused most known Ebola outbreaks and fatalities, including the recent Kivu Ebola epidemic (2018-2020) in the DRC [14, 37, 100]. The Sudan ebolavirus (SUDV) was responsible for the first known Ebola outbreak in South Sudan. This species caused other outbreaks in Sub-Saharan Africa (e.g., Congo, Uganda, Sudan) [159, 177]. The Taï Forest ebolavirus (TAFV) was identified in a population of chimpanzees in the the eponymous Tai Forest in Côte d'Ivoire in 1994 [63]. This species has caused one human infection in a scientist who made contact with the chimpanzees

[14, 63]. The Bundibugyo ebolavirus (BDBV) has caused an outbreak of Ebola Virus Disease in the Bundibugyo District of Uganda, where it was discovered in 2007 [165]. It was responsible for another outbreak in DRC in 2012 [98].

3.1.1 Transmission and symptoms of Ebola virus disease

Ebola virus disease (EVD) is transmitted by direct contact with infected human or animal bodily fluids [176]. Ebola is a zoonotic virus, meaning that it jumps from an animal host to a human, after which human-to-human transmission drives onward propagation of the disease. Bats are suspected of being the natural reservoir of the Ebola virus, but other animals (e.g., chimpanzees, gorillas, monkeys) can also have the infection. Consuming an infected animal can cause a zoonotic transmission.

The disease is very lethal, with a case fatality ratio (CFR) of up to 90% for EBOV [176]. Early symptoms may include fever, fatigue, muscle pain, headache, and sore throat, followed by vomiting, diarrhea, rash, internal and external bleeding, signs of impaired kidney and liver function [176]. Someone infected with Ebola is not considered infectious before the onset of symptoms [24]. Thus, a person with symptoms is normally bedridden until death or recovery, reducing the risk of spreading the infection far away after onset. Asymptomatic infection is quite rare, although it is unknown if these cases can transmit the virus [78]. Health care workers and caring family members face the greatest risk of exposure. However, the body of a person who has died from Ebola remains infectious after death. This fact is problematic because burial ceremonies that involve physical contact with the deceased are common in many parts of Africa. We expound on the cultural drivers of Ebola transmission in the following sections. Hewlett et al. has explored the anthropology of Ebola, which is important to understand the spread and containment of the disease [90].

3.1.2 The 2014–2016 Ebola epidemic

The West African Ebola epidemic was the deadliest outbreak of Ebola virus disease reported to this date. On March 23, 2014, local authorities notified the World Health Organization of an Ebola virus outbreak in southern Guinea. The virus quickly spread to neighboring countries, Liberia and Sierra Leone, causing a net count of 28.616 reported infections and 11.310 fatalities before ending in June 2016 [164]. The unprecedented scale of the epidemic resulted from dysfunctional healthcare systems, low trust in government following years of armed conflict, and a slow response to the crisis [141]. Risky cultural practices also compounded the severity of the outbreak, particularly burial rites that involve close contact with deceased Ebola patients.

Fig. 3.1 shows the cumulative number of confirmed or probable cases at the district level in Guinea. The time series began on January 5, 2014, ends on May 8, 2016, and advances in weekly increments. The outbreak originated in Guinea, in the Guéckédou prefecture, and quickly spread to

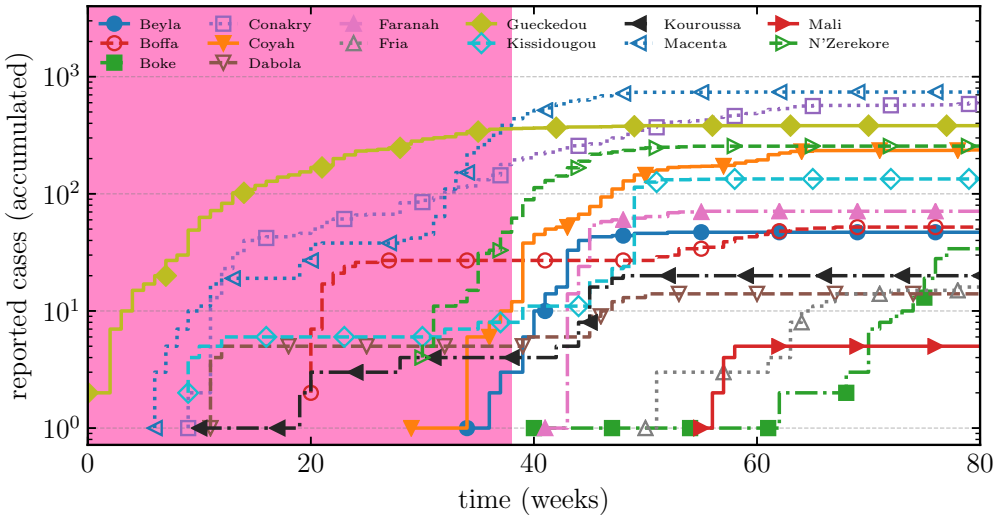

Figure 3.1: **Ebola virus epidemic in Guinea**. Shows the cumulative number of confirmed or probable cases at the district level. The time series begin on January 5, 2014, ends on May 8, 2016, and advances in weekly increments. On August 8, 2014, several months after its beginning, the World Health Organization declared the outbreak in a Public Health Emergency of International Concern. On September 18, 2014, the United Nations established The United Nations Mission for Ebola Emergency Response (UNMEER). The pink shaded region shows the time before the creation of UNMEEER. Guinea was declared free of Ebola by the World Health Organization on June 1. We also show epidemic curves for 14 of 33 Guinean prefectures. The outbreak originated in the Guéckédou prefecture and quickly spread to Conakry, the capital city. Data from the World Health Organization.

Liberia and Sierra Leone. On August 8, 2014, several months after its beginning, the World Health Organization declared the outbreak a Public Health Emergency of International Concern. On September 18, 2014, the United Nations established The United Nations Mission for Ebola Emergency Response (UNMEER). The epidemic was declared to have ended by the World Health Organization on June 9, 2016.

The local outbreaks in Fig. 3.1 tend to saturate long before susceptible depletion. Before the United Nations convened to form UNMEER, many local outbreaks, including the one in the Guéckédou prefecture where the epidemic originated, had already terminated. Naive epidemic theory predicts that onward transmission continues without interventions (e.g., contact tracing, isolation, or immunization) until herd immunity is reached. However, it is unclear whether interventions nor susceptible depletion can explain the abrupt termination of local outbreaks. Despite the large size of the outbreak compared to previous sporadic outbreaks of Ebola virus disease (EVD) in Sub-Saharan Africa, the total number of cases was also small compared to model projections [23].

3.1.3 Mathematical modeling of Ebola

Lagrande et al. proposed a model to explain the dynamics of Ebola using data from the 1995 outbreak in DRC and the 2000 outbreak in Uganda. The model identifies particular settings where Ebola transmission occurs (community, hospitalization, and funerals) estimate how much each of these sources contributes to R_0. This model has become widely used to understand the transmission of Ebola. The contributions from each setting can vary significantly between outbreaks. Lagrande et al. estimates that R_0 was 2.7 (95 % CI 1.9-2.8) for the 1995 DRC outbreak and 2.7 (95 % CI 2.5-4.1) for the 2000 Uganda outbreak. Traditional burials were responsible for most transmission in the DRC, while community transmission accounted for the bulk of transmission in Uganda. A meticulous study on Ebola Transmission in West Africa 2014-2016 found that 25% of cases who reported Ebola reported a funeral exposure [163]. 89% of those reporting a funeral exposure also reported one or more non-funeral exposures. 87% of reported exposure occurred between family members [163]. Modeling studies did consider the possibility of relatively high under-reporting [89, 127].

A myriad of modeling studies has tried to shed light on the 2014-2016 Ebola epidemic [6, 28, 59, 116, 126, 138, 144, 148]. One modeling study of the spatial spread of Ebola virus disease in Liberia (2014) and concluded that Ebola treatment units (ETUs), safe burial procedures, and household protection kits explain the decrease in the incidence [127]. Another computational modeling study of the spread in Guinea found that contact tracing was crucial to eliminating the disease [3]. Here we explore whether awareness-induced behavior changes can explain the dynamics of the disease. Drake et al. found that behavior changes decreased the effective reproductive number in Liberia to almost one and that interventions further brought it down below the epidemic threshold [40]. Another study found that healthcare-seeking behavior doubled throughout the outbreak in Lofa county, Liberia, but this was also linked to increased transmission inside treatment facilities [67]. The RAPID Ebola forecasting challenge compared the performance of eight independent modeling approaches on synthetic data and found that the top-performing models for short-term weekly incidence used reactive behavior changes [168].

3.1.4 Cultural drivers of transmission

There are significant cultural drivers of transmission, as we alluded to beforehand. Burial rites that involve touching the corpse of the deceased are known to drive Ebola transmission [39, 64, 90, 171]. The Kono people in Sierra Leone have a tradition of transporting the deceased's body to bury them in their hometown [137]. This ensuing burial ceremony can then spark a new outbreak.

Previous outbreaks in Uganda and the Democratic Republic of Congo (DRC) have shown that unsafe burial practices linger unless infection-control measures are adapted to local traditions[174]. Nonetheless, the 2014-2016 Ebola epidemic was massive compared to previously known outbreaks. It

is conceivable that an outbreak must reach a certain size before behavior changes occur. Some of the behavior changes we have seen during the ongoing coronavirus pandemic would seem to support this idea. However, the behavior response to COVID-19 has varied significantly both inside and between countries, underscoring that human behavior is complex and difficult to model.

There is some evidence of behavior change. An observational study found that of the cases exposed during funerals, 65% of those giving a response reported having touched the corpse. This proportion declined significantly after October 2014, suggesting that behavior changes had taken place [163]. Some may also have decided to stay away.

Belief in sorcery, spirits, traditional medicine (e.g., herbal therapies), and distrust of western medicine and healthcare workers make it more difficult to control Ebola outbreaks [90]. This problem is not dissimilar to the spread of fake news and conspiracies in some countries during the coronavirus pandemic that drives vaccine hesitancy and low compliance with public health guidelines (e.g., mask use and social distancing). Distrust of foreigners led to attacks on healthcare workers during the 2014-2016 Ebola. A treatment center was attacked by a mob in Liberia who denied the presence of Ebola and freed the patients who would then go on to spread the disease. Lack of trust in the health care system also led some people to care for Ebola patients on their own, which is not recommended [135]. Spiritual Healers who falsely claimed to cure Ebola also exacerbated the outbreak. The spiritual healers also become vectors for spreading the disease if sought out by symptomatic Ebola patients seeking a cure [124].

Local communities often have protocols to contain infectious disease outbreaks [90]. The first documented Ebola outbreak in Yambuku, 1976, was under control when national and international help arrived because the villagers isolated the sick and imposed restrictions on movement between villages [90]. The Ugandan Acholi people had the most comprehensive protocol comprising fifteen behavior changes to control an epidemic outbreak [90]. It is not surprising that local people have devised strategies for containing epidemic outbreaks. After all, infectious diseases have been around long before humans. Social mobilization and community awareness can build on these efforts to control Ebola outbreaks. The effect of this has been a topic of many research papers [50, 73, 112, 140]. Social mobilization was probably important in ending the West African Ebola epidemic [50].

3.2 Transmission models

The behavior changes used to contain Ebola outbreaks (e.g., avoiding direct contact with people who show Ebola symptoms, self-isolating, and not touching the corpse during a funeral or attending the ceremony) can occur spontaneously. We referred to this as intrinsic behavior change to differentiate from the extrinsic behavior changes enforced by government intervention. Estimates of R_0 for Ebola fall in the lower end of the spectrum compared to other infectious diseases (e.g., measles, rubella, smallpox, polio, pertussis).

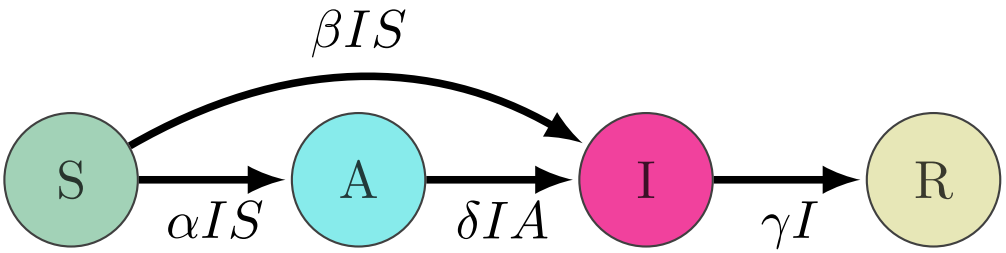

Figure 3.2: Diagram of the compartmental model showing the possible states and transition rates between them. β is the contact rate, and γ is the rate of recovery. Here α is the rate of behavior change, and δ is the contact rate in the aware population.

A review of modeling studies of Ebola virus disease in West Africa found R_0 to be 1.78 [180]. Thus, a small reduction in transmissibility is sufficient to push R_0 below the epidemic threshold [66]. We aim to show that this is plausible.

3.2.1 Mean-field theory

The simplest possible model concerning this reactive behavior change is given by the following system of ordinary differential equations (ODE's). Each equation represents a compartment of susceptible, aware, infectious, or removed agents. Here awareness about the diseases causes people to adopt health-promoting behaviors, thus decreasing the risk of infection.

$$\frac{dS}{dt} = -\beta IS - \alpha IS \tag{3.1}$$

$$\frac{dA}{dt} = \alpha IS - \delta AI, \tag{3.2}$$

$$\frac{dI}{dt} = \beta IS + \delta AI - \gamma I, \tag{3.3}$$

where β is the contact rate, and γ is the rate of removal. α is the rate of behavior change, and δ is the contact rate among aware individuals. Here A is assumed to grow by a proportional rate to I, meaning that only symptomatic persons can spread awareness. Figure 3.3 (a) shows a phase plane of the model. Here each trajectory is obtained by numerical integration. The area under a curve gives the fraction of the susceptible population that is infected over the outbreak. Figure 3.3 (b) shows how the attack rate decreases with α. The epidemic threshold is not affected by α in the mean-field approximation – it appears to follow a power law because doubling α approximately cuts the available susceptible population in half.

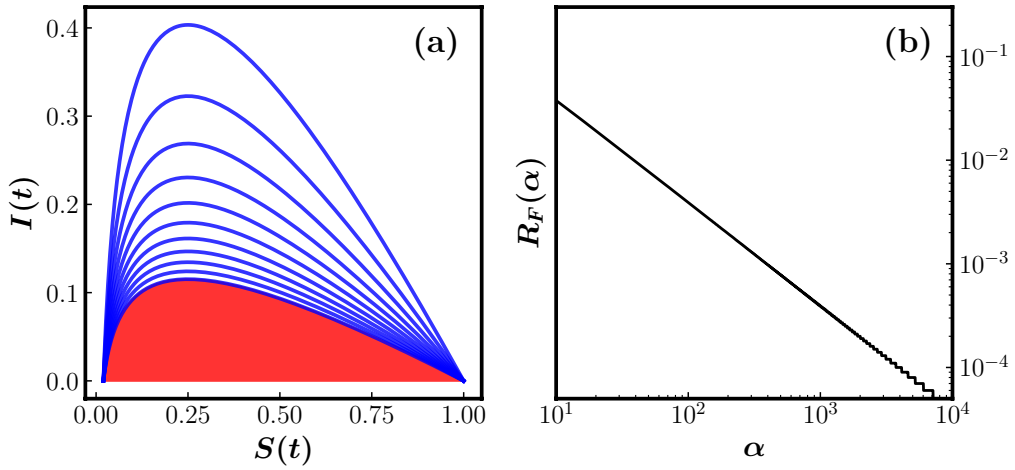

Figure 3.3: (a) Trajectories in the phase plane produced by numerical integration of eq. 3.1-3.3. The parameters are $\beta = 0.4$, $\gamma = 0.1$, and $\delta = 0$. Here α runs between 0 and 1 from top to bottom in increments of 0.1. The attack rate is the area under a curve. (b) shows the **final attack rate** R_F as a function of α.

3.2.2 Spatial model

Spatial heterogeneity was a distinguishing feature of the 2014-16 Ebola epidemic. However, the mean-field model above assumes homogeneous mixing. The 2014-16 Ebola epidemic has been the subject of many spatial modeling studies [42, 106, 109, 127]. A modeling study found that transmission events occurred within a short distance with a median value of 2.51 km. [111].

Funk et al. showed that the impact of behavior change is more pronounced in the presence of spatial structure [68]. The tendency of local Ebola outbreaks to flare up and subside quickly suggests the epidemic could be locally self-organized. To explore this possibility, we will consider a spatial version of the mean-field model. The spatial model is defined on a $L \times L$ lattice where one person occupies each site. A grid cell is either susceptible S, infectious I, aware A or removed R. Grid cells are initialized in the susceptible state with a small number of infected to start the epidemic. Sampling is repeated until all infected sites have been removed. A time step $\Delta t = 1.0$ (unit days) is equal to a sweep of L^2 updates. Do the following to perform an update.

a: Select a random grid cell s_1. If s_1 is infected then proceed to (b). Else proceed to (c).

b: **1)** Select another site s_2. This site is chosen randomly on the lattice with probability p. Else with probability $1 - p$, select s_2 with a probability that decays exponentially with distance from s_1. To be explicit, select a distance d with probability $\propto \exp(-d/\lambda)$ and choose a random point s_2 at this distance.

2) If s_2 is susceptible, it is infected with probability $\beta\Delta t$. Else if s_2 is aware, it is infected with probability $\delta\Delta t$.
3) Select another cell s_3 as above. If s_3 is susceptible, is becomes aware with probability $\alpha\Delta t$.

c: s_1 is removed with probability $\gamma\Delta t$.

There is a tiny probability of selecting identical targets i.e., $s_2 = s_3$. Since the reactions $S \xrightarrow{\beta} I$ and $S \xrightarrow{\alpha} A$ are mutually exclusive, it should be specified what happens in this event. Here we allow the reaction $S \xrightarrow{\beta} I$ to happen first. It is also possible to randomly pick between the two reactions, but the effect is negligible unless α and β are large. Global and local transmission allow for

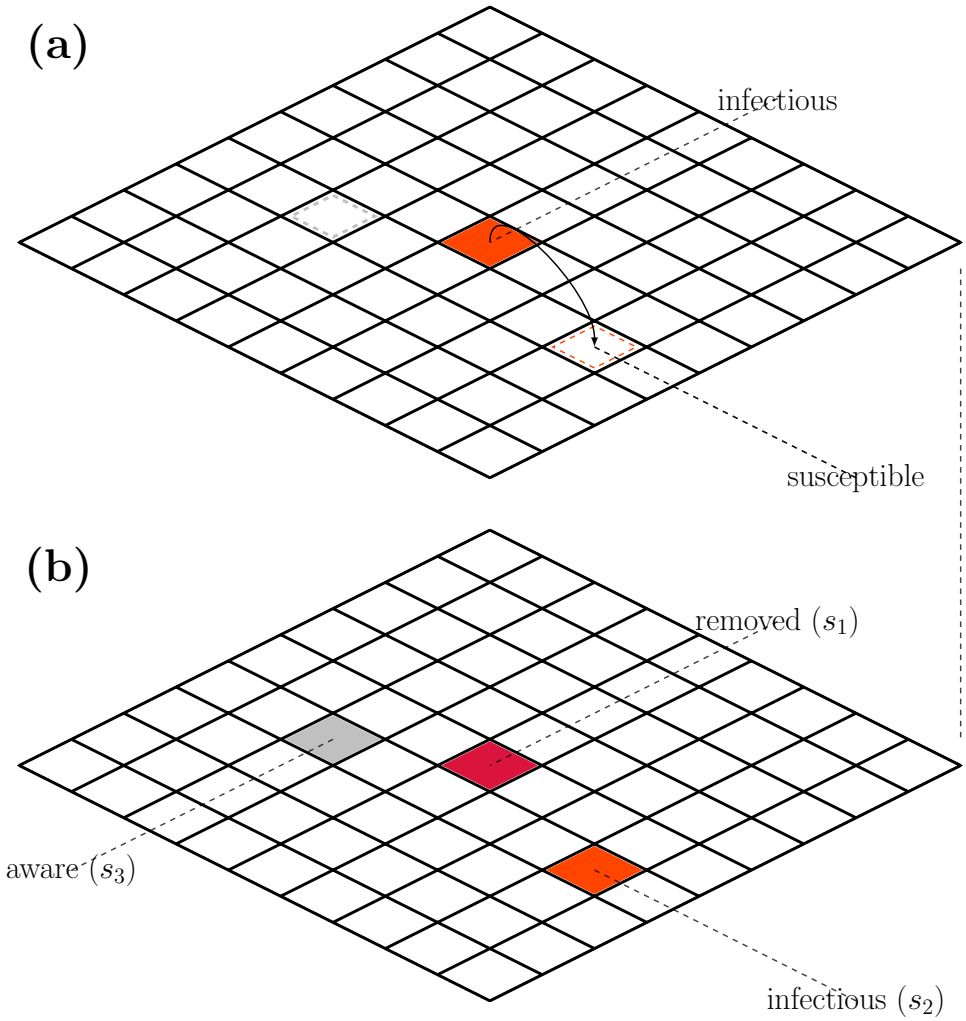

Figure 3.4: Diagram of the spatial model with one infectious person in the center. Each site on the grid contains just one person. (a) the infected person spreads disease and awareness to nearby squares. The transitions occur with probabilities β and α, respectively. The infected cell is removed with probability γ. (b) shows the updated grid.

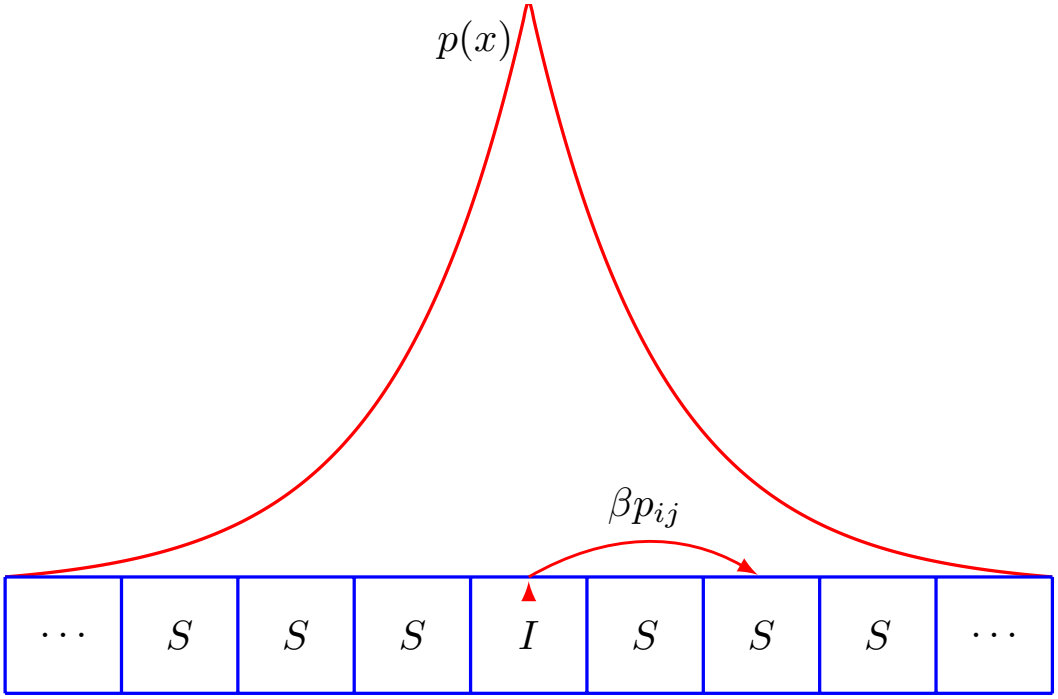

Figure 3.5: **Support figure to analysis of the spatial model**. Here we see the probability density function around an infectious grid cell I in the center of a one-dimensional array. The chance of a grid cell being selected during a single transmission cycle p_{ij} is the integral of $p(x)$ over it. A susceptible cell then has a probability β of being infected.

dispersal on different length scales. The effect of long-distance transmission events on epidemics has been studied by Shaw et al. [158, 179].

3.2.3 Analytical theory of the spatial model

Let us write an analytical theory of the spatial model. Doing so will help us better understand the difference between the mean-field and lattice models. Here we consider the spatial model in one dimension for the sake of simplicity. The effect of awareness spreading is neglected at first.

Consider an infected cell denoted i located somewhere a one-dimensional array of grid cells (sketched in the figure). Each time this cell is selected, it has a probability p_{ij} of selecting a particular element. This probability decays exponentially away from i (see figure 3.6). Susceptible cells are infected with probability β when selected. Further, I has a probability γ of being removed each time it is selected. An infected site will on average survive θ transmission cycles

$$\theta = \gamma^{-1}$$

Note that γ is a distribution that we have approximated by its mean to simplify the analysis. The probability that a susceptible cell j is infected by i over

its entire lifetime is given by $T_{i,j}$

$$T_{i,j} = 1 - \prod^{\theta}(1 - \beta p_{ij}) = 1 - (1 - \beta p_{ij})^{\theta} \tag{3.4}$$

where the probabiliy of a particular site j being selected is

$$p_{i,j} = \int^{(j-i)\pm\frac{1}{2}} p(x)dx. \tag{3.5}$$

Here the limits of integration run between the boundaries of the cell. Consider for example the probability of obtaining the configuraton in figure 3.6 where $i = 0$ and $j = 2$. Thus, integration over $p(x)$ runs from 1.5 to 2.5. $T_{i,j}$ is the probability of i infected a particular cell j over its entire lifetime. Therefore we can write R_0 as a sum over all the nearby cells.

$$R_0 = \sum_{j}^{\text{local}} (1 - (1 - \beta p_{i,j})^{\theta}) \tag{3.6}$$

In the mean-field version, there is no spatial decay away from an infected person, so here we must sum over **all** sites.

Now let us consider the effect of awareness transmission on R_0. Let $U_{i,j}$ be the probability of becoming aware which is identical to Eq. 3.4 with β, and α interchanged.

$$U_{i,j} = 1 - \prod^{\theta}(1 - \alpha p_{i,j}) = 1 - (1 - \alpha p_{i,j})^{\theta} \tag{3.7}$$

Let us imagine that an infected grid cell transmits only awareness until it is removed. Then we re-infect the cell and turn off awareness transmission. The lattice points now occupy a mixed state, being aware with probability $U_{i,j}$ and susceptible with probability $1 - U_{i,j}$. Aware sites are infected with probability δ, and susceptible sites are infected with probability β so we can express R_0 as a sum over nearby lattice points weighted by $U_{i,j}$ and $1 - U_{i,j}$

$$R_0 = \sum_{j}^{\text{local}} (1 - (1 - (U_{i,j}\delta p_{i,j} + (1 - U_{i,j})\beta p_{i,j}))^{\theta}) \tag{3.8}$$

Subject to mean-field interactions, this effect is completely washed out because the entire system absorbs the awareness. Figure 3.3 (b) also show this because α cannot affect R_0 if the attack rate is power law of α. However, in the spatial model, this effect is concentrated on the nearby cells most likely to be infected. Here there will be a critical threshold α_c where the disease cannot spread, which we will show by direct simulation.

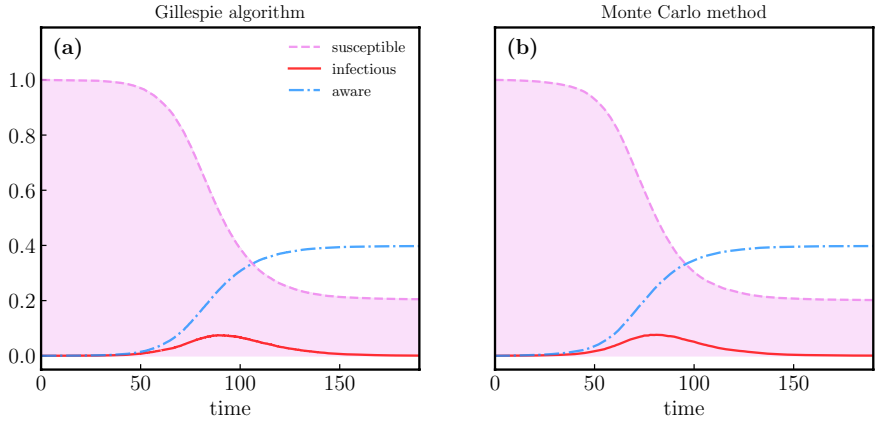

Figure 3.6: **Stochastic simulation of the mean-field model**. (a) is a solution to Eq. 3.1-3.3 generated with the Gillespie algorithm. (b) is a solution generated with the stochastic method we developed above. The transition rates were $\alpha = 0.2$, $\beta = 0.2$, $\gamma = 0.1$, and $\delta = 0$. Each simulation was with $N = 40.000$ agents. Initial conditions were $I(t_0) = 1$. In (b), the random dispersal probability has been set to 1 to obtain random mixing to compare the two methods.

3.2.4 Gillespie's algorithm

Here we evaluate the proposed model by comparing it to the Gillespie algorithm to ensure correctness. The Gillespie algorithm generates a stochastic solution to a system of equations with known reaction rates [74–76].

Consider a well-mixed system of N species which interact through M reactions [76]. The algorithm was originally introduced in chemical kinetics, which explains the residual terminology. However, it has since been applied in many other fields (e.g., computational biology, epidemiology, social systems). In our case, the species are compartmentalized populations (e.g., S, and I), and the reactions correspond to transitions between different states (e.g., $S \rightarrow I$). Let $X_i(t)$ denote the number of persons in i'th compartment at time t. Our objective is to estimate the state vector $\boldsymbol{X}(t) = (X_1(t), \ldots, X_n(t))$ at time t given some initial configuration at time t_0 [76]. Without a comprehensive review of the Gillespie method we write the conditional probability $p(\tau, j \mid \boldsymbol{x}, t)$, given the state vector $\boldsymbol{X}(t) = \boldsymbol{x}$, that one reaction R_j will occur in the time interval $[t, t + dt]$. This probability is given by

$$p(\tau, j \mid \boldsymbol{x}, t) = a_j(\boldsymbol{x}) \exp(\tau \sum_j a_j(\boldsymbol{x})), \tag{3.9}$$

where a_j are the so-called propensity functions [76]. Let us consider the system of equations 3.1-3.3. There are $N = 4$ species and $M = 4$ reactions.

$$S \xrightarrow{a_1} I, \qquad S \xrightarrow{a_2} A, \qquad A \xrightarrow{a_3} I, \qquad I \xrightarrow{a_4} R \tag{3.10}$$

with corresponding propensity functions

$$a_1 = \beta SI/N, \qquad a_2 = \alpha SI/N, \qquad a_3 = \delta AI/N, \qquad a_4 = \gamma I \tag{3.11}$$

The algorithm now consists of the following steps.

1. Initialize the system at time $t = t_0$ and in the state $\boldsymbol{x} = \boldsymbol{x}_0$.
2. Generate a uniform random number u_i on $[0, 1]$ for each reaction. A reaction occurs if
$$u_i < a_i / \sum_j a_j(\boldsymbol{x}) \tag{3.12}$$
3. Here the time increment is, following the conventional approach
$$\tau = \frac{1}{\sum_j a_j(\boldsymbol{x})} \cdot \ln(\frac{1}{u}) \tag{3.13}$$
where u is also a uniform random number between 0 and 1. Generate a τ and update the clock $t \to t + \tau$.
4. Update the state vector. Return to step (1) or end the simulation if no infected remains.

Figure 3.6 show a stochastic solution to Eq. 3.1-3.3 generated by each method. Stochastic effects in the early stage of exponential growth induce significant temporal displacements between successive simulations. Thus, irrespective of the method, there is significant variation between successive simulations. This variation is confined to when the epidemic curve peaks unless it goes extinct early on. The final attack rate is largely fixed within small variations.

3.3 Simulations of the spatial model

Here we explore epidemic spreading with the spatial model. Figure 3.7 shows a simulation of the spatial model on a 128×128 lattice. An infected cell spreads from the center of the grid. However, the growing cluster of infectious sites faces a problem. The effect of susceptible depletion is felt immediately in a spatial environment, which exacerbates intraspecific competition among infected cells. Thus, the effective reproduction number decays much faster than it would in a homogenously mixed system. This effect is compounded by awareness spreading, which immunizes susceptible cells. The aware cells aggregate around the expanding cluster and block transmission much like a barrier. This mechanism is somewhat analogous to ring vaccination because the persons at risk of infection are most likely to change behavior. Here the contact networks of disease and awareness transmission completely overlap; each process uses the same probability density function

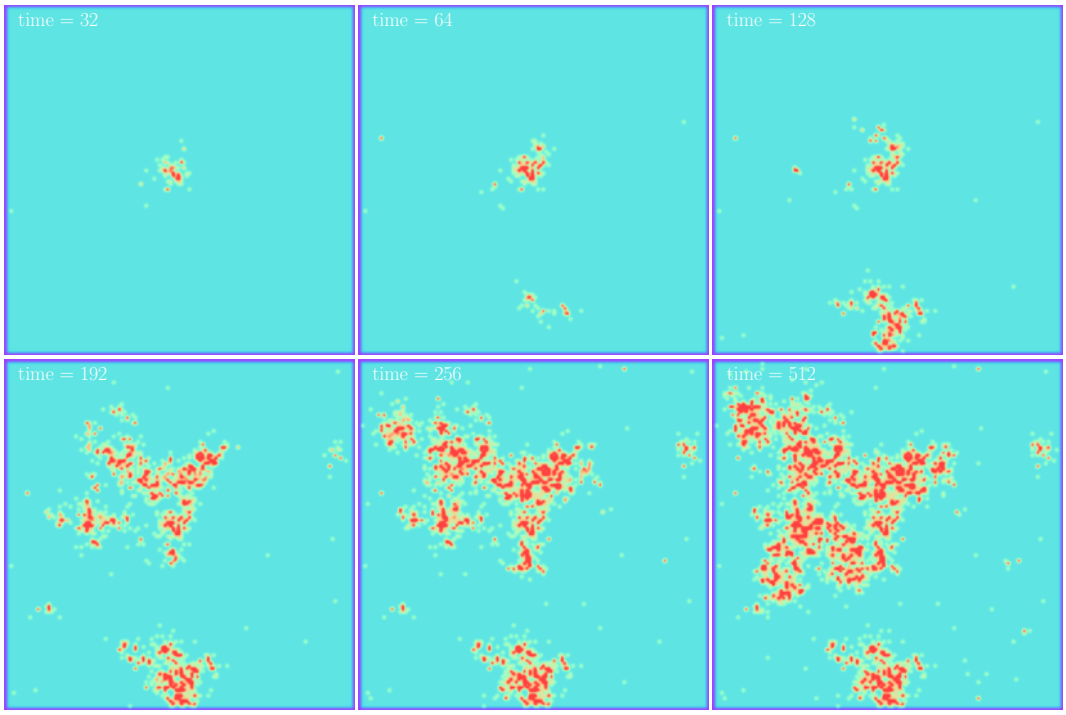

Figure 3.7: **Dynamic simulation of the spatial model on a** 128×128 **grid**. The simulation shows how awareness-induced behavior changes can quash outbreaks in a spatially extended system. Simulation was initialized with one infected person in the center, and the model parameters were $\alpha = 0.48$, $\beta = 0.20$, $\gamma = 0.08$, and $\delta = 0.0$ meaning that awareness confers full immunity. Here the scale parameter of the exponential distribution was $\lambda = 2$ with a $p = 10^{-2}$ chance of global transmission. Color codes: Turquoise cells are susceptible; beige cells are aware, and the red cells are infectious or removed.

with the same scale parameter. The effect of disjointed contact networks on awareness and disease spreading has been studied by Funk et al. [68].

Global transmission events give infected cells a chance to break out from the enclosing barrier by seeding new clusters. These low-probability events can have a big impact on the epidemic, in particular on spatial heterogeneity. The epidemic is a connected cluster of infected cells without global transmission events. Ebola outbreaks have generally been confined to a particular district or province. The Western African Ebola epidemic was a novelty in this respect, comprising many spatially disassociated transmission clusters [44].

Since epidemic spreading is a stochastic phenomenon, it follows that many outbreaks die out early by chance [104]. Figure 3.7 shows this – isolated red cells are the product of global transmission events that are victims of stochastic extinction. The extinction probability is significant if we initialize the system with a single infected node. We will initialize the system with a small cluster of infected sites to prevent unnecessary extinction events.

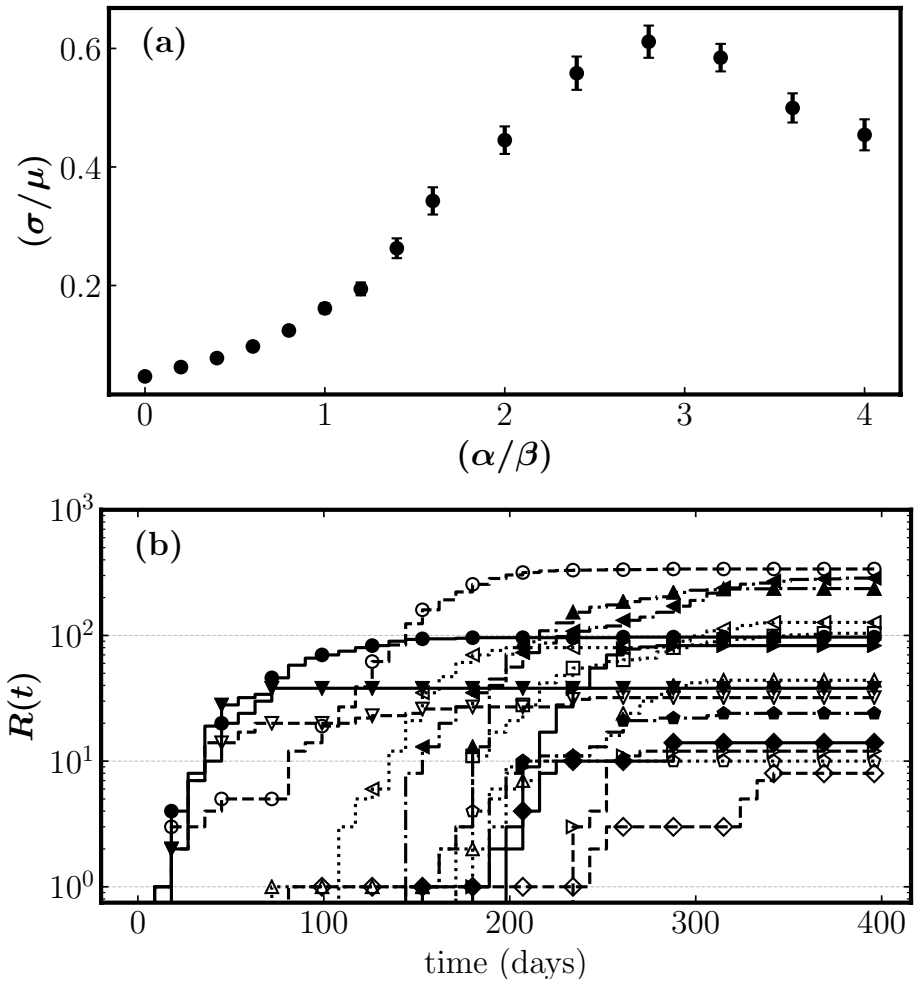

Figure 3.8: (a) shows the coefficient of variation c_v between the subgrids for increasing α. Model parameters: $\beta = 0.25$, $\gamma = 0.10$, $\delta = 0.0$, $p = 0.01$. The scale parameter in the exponential distribution was 2.0. (b) shows cumulative cases $R(t)$ for each subgrid in a simulation around criticality $\alpha = 0.70$ with parameters as above.

3.3.1 Measuring spatial heterogenity

The spatial model exhibits a critical transition from a subcritical state where the disease spreads unabated to a supercritical state where it is contained. This transition occurs as the rate of behavior change α is increased. The boundary between these two domains is particularly interesting. We quantify spatial heterogeneity by partitioning the lattice into equally sized subgrids. We then measure the coefficient of variation c_v between the subgrids.

Figure 3.8 (a) shows the average coefficient of variation c_v between the subgrids for a large number of simulations on a 200×200 system decomposed into 16 blocks of size 50×50. The behavior change rate increases along the horizontal axis while all other parameters are kept fixed. Spatial heterogeneity is low in the subcritical state because the epidemic spreads unabated across the system, which leaves only slight variations between subgrids. Spatial heterogeneity is maximized around criticality. Here the epidemic is made

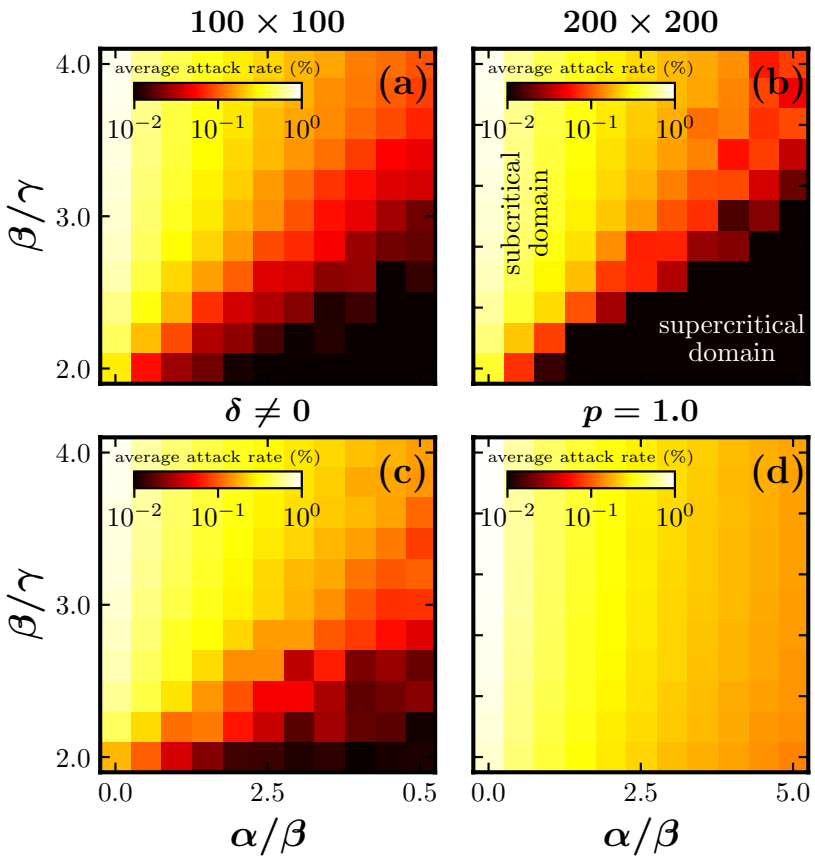

Figure 3.9: Phase diagrams of the spatial model. The color shows the final attack rate (%) for a particular set of parameters. Outbreaks are controlled in the dark domain but spreads unabated in the bright domain. (a) shows the spatial model on a 100×100 grid with $\delta = 0$, $p = 0.01$ and $\lambda = 2.0$. The remaining panels share these parameters except for one feature that is changed. (b) shows simulations on a 200×200 grid. (c) shows $\delta/\gamma = 0.5$. (d) random mixing $p = 1.0$.

up of a collection of spatially disassociated transmission clusters of varying sizes. Some subgrids sustain large outbreaks, and others none at all. Spatial heterogeneity drops in the supercritical state because the epidemic is contained. Most residual heterogeneity comes from the variation between the subgrid where the outbreak starts and the remaining unaffected subgrids.

Figure 3.8 (b) shows the cumulative number of cases (removed cases) in each block around criticality where spatial heterogeneity is maximized. These micro-epidemics share features with the Ebola epidemic in Guinea shown in Fig. 3.1. Local outbreaks are spatiotemporally asynchronous and saturate rapidly. There is significant variability in the duration of the epidemic from stochasticity. The corresponding epidemic curves for a simulation in the subcritical domain have fairly trivial features. Here the micro-epidemics all follow *sir*-like trajectories and saturate at the same level, albeit with slight temporal displacements.

3.3.2 Model's parameter space

Fig. 3.9 shows the parameter space of the spatial model. The attack rate is estimated for a range of parameters by averaging over repeated simulations —β increases along the vertical axis, which increases the attack rate. Conversely, α is increased along the horizontal axis and inhibits transmission. (a) is simulated on a 100×100 with the following set of parameters $\{\delta = 0$, $p = 10^{-2}$ and $\lambda = 2\}$. The remaining panels share these parameters but change one specific feature. (b) is simulated on a 200×200 system. The attack rate is scale-invariant in the subcritical domain as the epidemic invariably grows into a homogeneous cluster spanning the entire lattice. Conversely, the outbreak grows to a finite-sized cluster before containment in the supercritical domain. Thus, increasing the system size decreases the attack rate. This broken scale-invariance explains why the attack rate decreases between (a) and (b) in the supercritical domain. (c) shows the effect of increasing δ above zero, which is small provided that it is not increased above the point where transmission becomes possible in a fully aware population. (d) shows the effect of introducing random mixing in the spatial model. Here there is no supercritical domain, as we have shown in the preceding analysis.

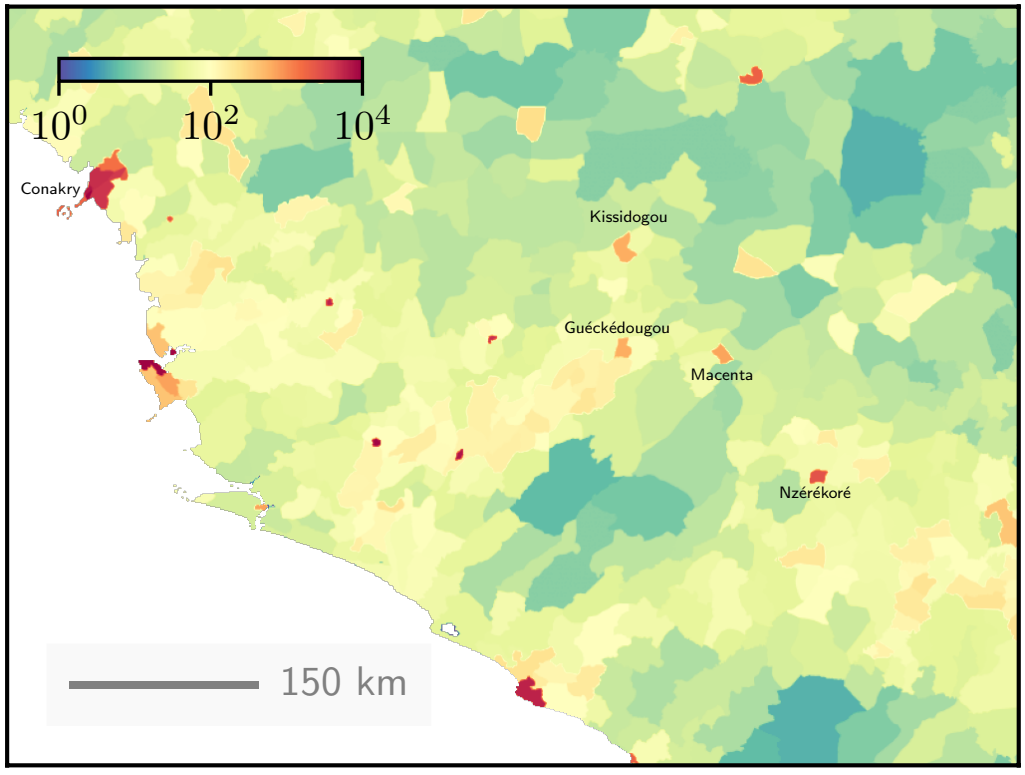

Figure 3.10: **Gridded population density map of West Africa**. Shown are the prefectures in Guinea that experienced the largest outbreaks. The color shows the number of people expected to reside within the cell. The dimensions of a cell are approximately one km^2. Data from SEDAC [101].

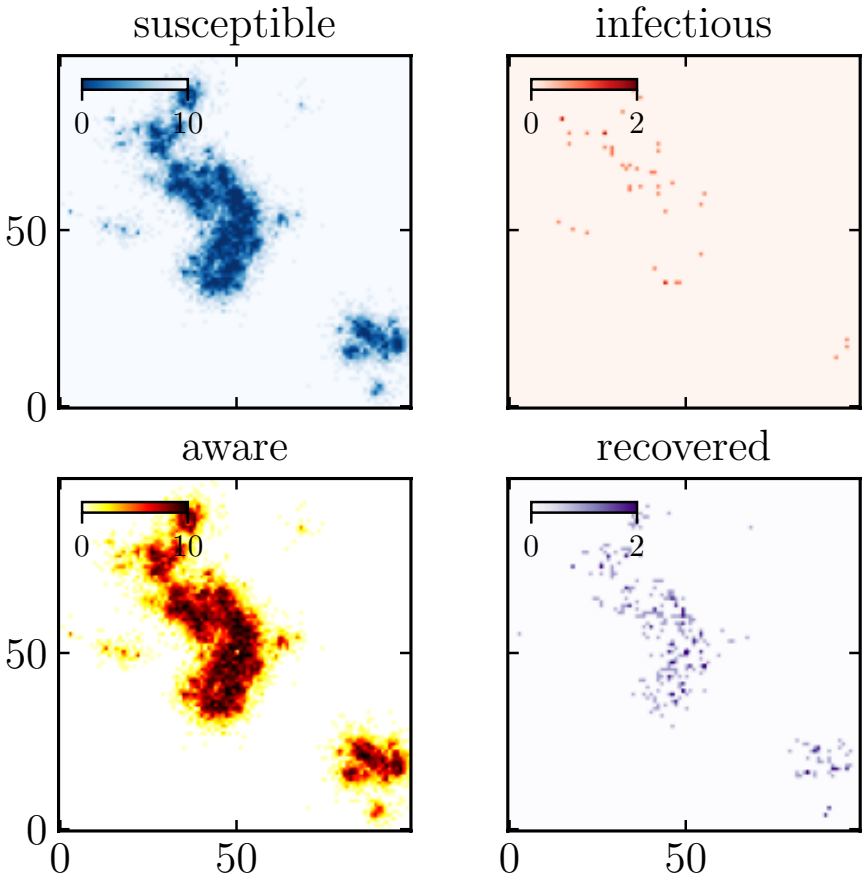

Figure 3.11: Simulation of the model with 10 persons per site.

3.3.3 Effects of population density

The spatial model is simulated on a grid with one idealized person in each grid cell. While this is not realistic, the effect of population density is unlikely to be profound. Hu et al. has estimated how contact rates scales with population density [22, 96]. However, symptomatic Ebola patients are likely to be bedridden during infection. Those most likely of exposure are caring family members, health care personal, or those attending funerals. Accordingly, the rates could be largely independent of population density.

Figure 3.10 shows a gridded population density map of West Africa. While the largest outbreaks in Fig. 3.1 occur in prefectures with somewhat concentrated populations, the difference in the population density cannot explain the variance between them – Macenta sustains a larger outbreak than the much more densely populated Conakry. The largest outbreaks appear to cluster around Guéckédou, where the outbreak originated. We also observe this tendency in simulations of the spatial model because the awareness has not spread around the location where the outbreak originated. The late arrival of international aid may also explain this tendency. Figure 3.11 shows how the spatial model can be extended to accommodate population density.

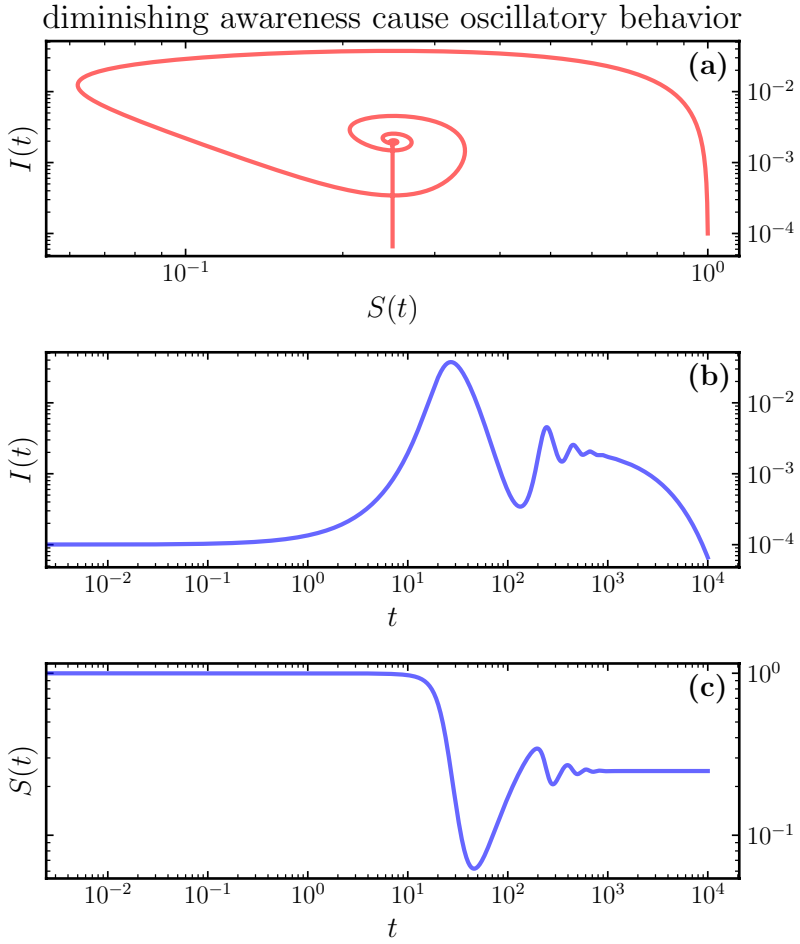

Figure 3.12: Mean-field model with fading. Model parameters are $\alpha = 4$, $\beta = 0.4$, $\gamma = 0.1$, $\delta = 0$, and $\epsilon = 0.004$.

3.3.4 Diminishing awareness

The initial analysis of the mean-field and spatial model assumed behavior changes to be permanent. Furthermore, A becomes an absorbing state if behavior changes confer full immunity. The ongoing SARS-CoV-2 has taught us a great deal about the interplay between human behavior and infectious diseases. For example, one study finds that while lockdown significantly reduces transmission, the impact declines over time, possibly due to lockdown fatigue [82]. It is straightforward to modify the mean-field model to include fading. Here we allow A to fade with a rate ϵ

$$\frac{dS}{dt} = -\beta IS - \alpha IS + \epsilon A, \tag{3.14}$$

$$\frac{dA}{dt} = \alpha IS - \delta AI - \epsilon A, \tag{3.15}$$

Figure 3.12 shows a model simulation with fading, which causes oscillatory behavior [77]. The presence of spatial structure should have a dampening effect on such oscillations, although we do not model this explicitly. There are no infected nearby to spread the disease if a spatially localized outbreak is terminated and the remaining A states become susceptible. It is, therefore, necessary to introduce the disease again, either through a global transmission event or by intrusion from another growing transmission cluster.

3.3.5 Summary and concluding remarks

We have explored the effect of reactive behavior changes on infectious disease outbreaks in a spatially extended system. The spatial model exhibits a critical transition where the disease can no longer spread because reactive behavior changes have depleted the susceptible population around the outbreak. The spatial model we propose describes a disease with the following properties. R_0 is close to the epidemic threshold, transmission is highly localized, and adapting a few behavior changes can significantly reduce the risk of being infected or infecting others. Ebola virus disease is a perfect candidate because it has all of these properties. R_0 was estimated to be 1.2–2.2 during the Ebola outbreak in West Africa [23]. Transmission events occurred within a short distance with a median value of 2.51 km. [111]. Furthermore, behavior changes (e.g., social distancing, funerals, isolation) can reliably reduce transmission.

The model can explain the spatial patterns observed in Guinea's 2014-16 Ebola epidemic, but some assumptions have been made. The rate of behavior change α is not are not derived from data. More data is needed to understand this dynamic interplay between the risk of infection and social behavior. Estimating δ is difficult because humans can exhibit a range of behaviors that produces a spectrum of A states with corresponding contact rates. However, it is possible to identify specific behaviors (e.g., funerals) with a significant effect, and it suffices to show that the disease cannot survive in a fully aware population.

Evidence from the ongoing SARS-CoV-2 pandemic suggests that behavior changes have a significant effect on disease transmission. However, the risk of Ebola infection is likely to induce more drastic behavior changes than COVID-19, given the vast discrepancy in the case fatality ratio. The coronavirus pandemic has also shown us that variations in behavior explain differences between many countries. Many factors influence how people respond, including the risk of infection, age, and compliance with public health guidelines. Nonetheless, the latter will carry more weight in countries with high trust in government. Ebola outbreaks have so far happened in countries where trust in government is low. Here the behavior response is more likely to be a local effect because people respond to community transmission more than recommendations from public health officials. We have shown how such a local behavior response can explain the abrupt termination of local outbreaks, as was observed during the 2014-2016 Ebola epidemic.

Chapter 4

Epidemics on social networks

In this chapter, we return to view communication as an epidemic process. In particular, we consider the spread of aging news and rumors on social networks. Before introducing this work, it is helpful to consider how information transmission systems have evolved throughout history. This non-exhaustive summary will help us motivate and contextualize the research that has been carried out.

4.1 Information transmission systems

The first information transmission systems relied on semaphores (e.g., smoke signals, fire) and messenger pigeons. In ancient China, beacon towers were used to send smoke signals across the Great Wall [38]. This method allowed simple messages to be transmitted quickly across the wall, as the color of the smoke could specify the size of the raiding party. The Ancient Romans used messenger pigeons to send field reports back from the front [102]. The use of messenger pigeons would eventually expand to other domains (e.g., news, financiers, and stockbrokers) as it became advantageous to receive and transmit information faster than a competitor. Paul J. Reuters, who founded the eponymous news agency, used homing pigeons to carry news and stock quotes between London and Paris [170]. Perhaps it is not surprising that the Ancient Romans and Chinese were early adopters of these technologies, although they did not invent them. Both the Roman Empire and Imperial China encompassed vast swathes of territory. Being able to send messages quickly must have been especially useful concerning military operations where time is of the essence.

The 19th century witnessed the invention of the electric telegraph. The telegraph was the first device that used electricity to communicate at great distances. This device allowed messages to be transmitted almost instantly between two places. Standard time which is the synchronization of clocks within a region was adopted to schedule trains and steamships. Doing so was made possible by the telegraph. Railroads could now effectively coordinate the arrival and departure of trains. Newspapers could receive information from far away, and financial markets could centralize prices. The New York Stock Exchange became a national market, absorbing many regional exchanges [182]. Du Boff notes that many observers at the time predicted the

telegraph would have a decentralizing effect on the economy, while the opposite turned out to be the case [43]. The rise of digital media appears to be having the same effect on the news industry, with a decline in local and regional news but subscription surges for the largest American newspapers [17]. However, it has also had a powerful decentralizing effect by democratizing mass communication. These two diverging trends are interesting and worth considering. Here we jump directly to the internet and skip over some notable advances in communication technology (e.g., telephone, radio, and television).

The internet has revolutionized how we communicate. Social networking services, blogging, and digital publishing platforms have made it possible for ordinary people to share information with many individuals and followers. A local newspaper may have a few thousand subscribers; an influencer on social media can have millions of subscribers worldwide and transmit information to them almost instantly at no cost. This new paradigm has blurred the distinction between influencers and news outlets subject to editorial oversight. Before the internet, only news media (e.g., newspapers and broadcasting via radio and television) had this capacity. Overall, this has decentralized information sharing as everyone can have a blog or media channel. However, it appears to be having the opposite effect on the news industry. Let us consider how newspapers have traditionally operated to understand this.

4.1.1 News distribution

Newspapers are perishable products as the newsworthiness of a story naturally decays over time [99]. Yesterday's newspaper is less valuable than it was at the time of publication. As the saying goes, "Today's news is tomorrow's birdcage liner." Newer and more relevant stories necessarily replace older stories that we forget. Wu and Huberman studied the collective attention of a million users on many online news stories and found that novelty within groups decays with a stretched exponential law [181]. Thus an event occupies a transient state of newsworthiness before being forgotten or becoming history. The newspaper distribution problem has been treated in some publications [99, 125]. Distributing newspapers to people living further away becomes increasingly arduous due to the cost of transportation and the diminishing value of aging news. These two factors favor local newspapers by making it difficult for one newspaper to cover a large region. The likelihood of a news story becoming obsolete increases as the distribution network extends farther away. New technology has enabled a more centralized news industry. News broadcasting (e.g., radio and television) is not affected by this limitation. Until the 1990s, three commercial television networks (CBS, NBS, and ABC) dominated broadcast television in the United States, known collectively as the Big Three [91].

A paper from 2006 found that technological change had reduced the cost of distributing newspapers in local markets. Local newspaper circulation was lower in areas with high New York Times penetration, suggesting that advances in technology promote consolidation of the news industry. Hayes

et al. found that local news has declined somewhat over the recent years [87]. Overall, newspaper circulation has declined in the United States [17]. Meanwhile, the New York Times has added millions of digital subscribers, while the printed circulation was cut in half from 2005 to 2017 [17]. A digital subscriber can live anywhere in the world and read about stories immediately as they are published. Thus, the digital transformation has solved the distribution problem, which helps the largest newspapers expand into new markets.

4.1.2 News factors

What makes news news? There are many relevant factors other than being novel, although it is perhaps the defining property of news. For example, a local newspaper can cover stories that are relevant to its community. Many factors affect the newsworthiness of an event. Galtung and Ruge made the first attempt to classify these factors in their seminal paper [70]. Much work has gone into identifying all these news values. However, there is some disagreement about what constitutes a news value[18, 19, 25, 155]. It has to be said that news values are not a set of objective metrics for what deserves coverage but simply what is likely to be selected for coverage. Let us consider a few pertinent examples.

We have already encountered two values so far. Timeliness concerns news about current or ongoing events. This factor is arguably the principal news value — after all, there is no such thing as old news. Familiarity concerns events that are relatable to the audience. Here a local news outlet has an edge because it can tailor its stories to a specific audience. Conversely, this is more difficult for a prominent newspaper with a more heterogeneous group of subscribers. Frequency is a news value related to timeliness, asserting that sudden events are more likely to receive coverage than long-term trends or events that fit poorly into the schedule of the news organization. For example, a terrorist attack is more likely to receive coverage than a story about the gradual decline of poverty or violence. Bad news events also tend to receive more coverage than positive stories. However, it has been suggested that positivity is also a news value. A scientific breakthrough or a successful space mission will tend to receive some media coverage. There are other news values, but it is unnecessary to go through them, as we only draw upon timeliness and frequency in work ahead.

4.1.3 Modes of transmission

The internet allows everyone to become a news outlet. Becoming a news outlet (e.g., newspaper, radio, or television station) was capital intensive before the internet. Still, now everyone with a blog or a presence on a video-sharing platform is effectively a news outlet able to transfer information to everyone else on the network. Here we differentiate between two modes of communication. Mass communication is where a news outlet (e.g., an influencer, blogger, or a newspaper or news broadcast) imparts information to a large

population segment. This mode is directed, as there is no exchange taking place. The information flows from the news outlet to the receiver. In contrast, communication between two persons is undirected as information can flow in both directions. The following section introduces a model that combines many of the concepts we have discussed above. Here influencers battle for followers on a social network by spreading information. Individuals are more susceptible to new information. Recent news events are more contagious while information loses its infectious as it ages.

4.2 Modeling spread of news and rumors

Here we propose a model for the spread of news and rumors. This model concerns how information spreads and how news outlets or influencers compete for attention by spreading this information. To do so, we combine many concepts from the previous section. First, we consider a population of individuals represented by a collection of nodes. Each person can occupy one of two mutually exclusive states, follower or influencer. All nodes have a set of static undirected links independent of their state that represents person-to-person communication. The links are assumed to be fixed because an individual's social relationships are relatively stable. There is a multitude of ways to set up this reciprocal network. We start by using nearest neighbor interactions. Thus, a person is friends with his four nearest neighbors, subject to periodic boundary conditions. We will consider more realistic network topologies during the analysis. The effect of increasing the number of these links is also explored. Dunbar's seminal paper on neocortex and group size suggests that humans maintain around 150 stable relationships, so four is obviously in the lower end [45, 46, 143] Superimposed on this static network is a directed network of links between influencers and followers. These links are not fixed but can change over time. A follower can maintain only one directed connection to an influencer or news outlet, as attention is a finite resource. The influencers compete for attention by capturing followers from each other. This competition is driven by new information. In the previous section, we spend an entire paragraph arguing that novelty is a vital determinant of information spreading. Of course, one could include other parameters, but avoid this to keep the model as simple as possible. A person has a news value τ that measures its knowledge of current affairs. The network is updated stochastically in discrete steps. With each update, a node has a chance of discovering a news event, which has the following state-dependent effects. If a follower triggers a news event, it is promoted to an influencer and gains a news value equal to the current time step, i.e., $\tau = t$. An influencer also updates its followers' news value to t upon discovering a news event. With each step, a node also communicates with a random member of its reciprocal network. If the neighbor has a lower news value than its friend, it will shift its directed link to the friends' influencer while breaking the link to its previous information source. This mechanism allows influencers to capture followers by spreading new information. Meanwhile, influencers who fail to discover news will lose followers to those who do.

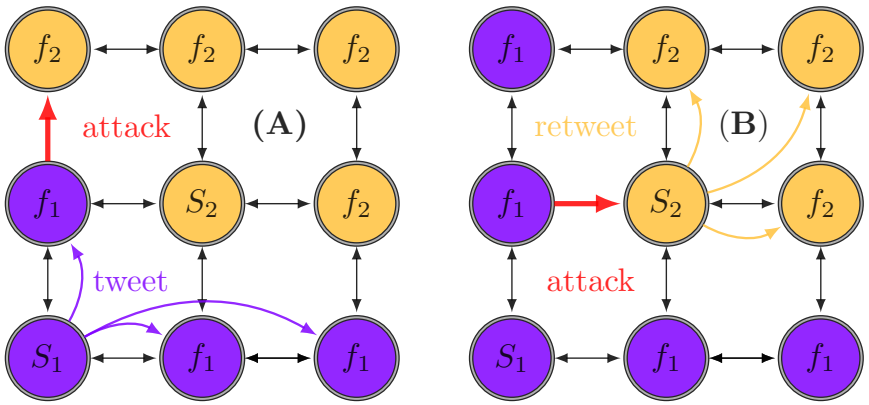

Figure 4.1: **Schematic diagram of the model**. Nodes represent users on an undirected social network. Color and subscript indicate followers' adherence to a news outlet. (a) shows the discovery of a news event, and the capture of a node. (b) shows how an influencer (S_2) can immunize its followers by appropriating the news event.

However, if a node attacks an influencer with a superior news value, it will appropriate the information and copy the news value onto itself and its followers. Thus, one can either discover news or copy it from others. The network will freeze up with influencers impervious to capture without occasionally demoting them to the follower state. To overcome this issue, we downgrade influencers who lose all subscribers to the follower state. Thus, an influencer must first lose all subscribers before becoming vulnerable to being absorbed by another subculture. To ensure the reproducibility of the model, we include a brief description of the computational algorithm.

4.2.1 Algorithm description

Define N nodes with a given undirected network topology (e.g., nearest-neighbor, Erdős–Rényi, small-world). Each node occupies either a follower state f or an influencer state S and has a current information state τ equal to the time of origin of the last news update it has received. Nodes are assigned an index $i, j, \ldots n$ designating the influencer it belongs to. That is to say that each subculture encompassing an influencer and all its subsequent followers inherits the same index. Time is increased by one increment for each N update. To perform an update, do the following.

Select a random node a. This node discovers a news event with probability p_0. If it is a follower node, it gains a news value $\tau = t$ and is promoted to an influencer, i.e., $a \in f \to S$. If an influencer discovers a news event, all nodes with that corresponding index gains news value $\tau = t$.

Select a random neighbour b to a. If $\tau(a) > \tau(b)$ then b abandons it influencers and establish a link to a's influencer. If $\tau(a) > \tau(b)$ and $b \in S$ then all nodes with b's index gains news value $\tau(a)$. For each sweep of N updates, influencers with no followers are demoted to followers. Although these demoted notes are not following anyone, they are no longer impervious to capture and can be absorbed by another subculture.

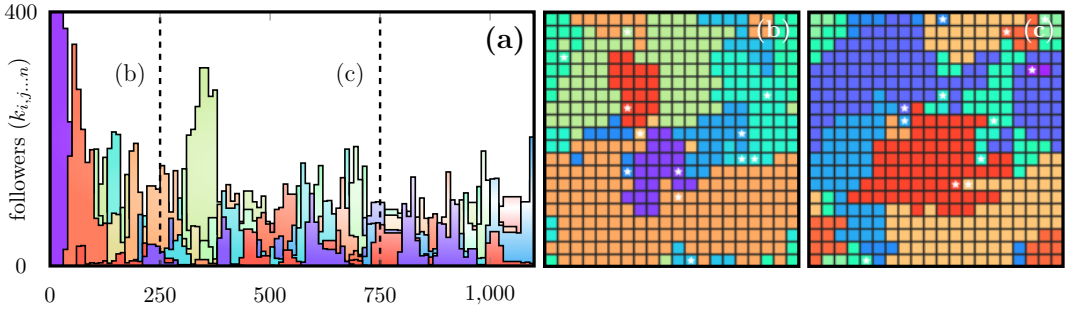

Figure 4.2: **Simulation on a small** 20×20 **lattice**. (a) shows the size of each subculture over 1.100 time steps. (b-c) show snapshots of the simulation at the vertical lines. Subcultures are assigned a unique color, and the white stars represent influencers. The system occupies a fragmented state where no subculture dominates for an extended period. The simulation was performed with $p_0 = 2.5 \times 10^{-4}$. The stars are only updated each time a full sweep of 400 updates has been performed.

4.3 Stochastic simulation of the model

Here we investigate the model under a wide range of conditions. Fig 4.2 shows a model simulation on a small system of 20×20 nodes with $p_0 = 2.5 \times 10^{-4}$ that is probability of discovering news. The p_0 parameter determines how difficult it is to become a news outlet, but it is also a measure of the overall occurrence of notable events that are discovered. We will expound on this in the discussion as this section is dedicated to analysis and simulation. Fig 4.2 shows that the network occupies a perpetually fragmented state without a dominating subculture. The number of influencers grows to some steady-state where the removal rate balances out the creation of new ones.

The p_0 parameter determines how difficult it is to become a news outlet. Careful inspection of Fig 4.2 shows that influencers represented by white stars tend to be located on the boundary between different subcultures. This pattern is not a coincidence; the system will self-organize into a state where influencers are situated on the border between subcultures for the following reason. Whenever a subculture encroaches on another with a lower news value, it will capture followers until it reaches the influencer. The influencer copies the news value of the attacker onto its followers, thereby immunizing from further capture. The influencer is left on a stable interface between the two subcultures, as these have the same news value. Self-organizing into this state dramatically increases the speed at which information can spread on the network. A news event can rarely trigger a cascade that travels through the system using the influencer networks, leaving the subcultures largely intact because the information imbalance is restored almost instantly. A non-uniform distribution of information drives the conflict between influencers. There is no competition or flow if all nodes have the same news value. In this sense, the system is never in equilibrium unless p_0 is small.

Fig 4.3 shows the news value of each site in a simulation on a 100×100 system. Here information spreads from person to person in the early stage of

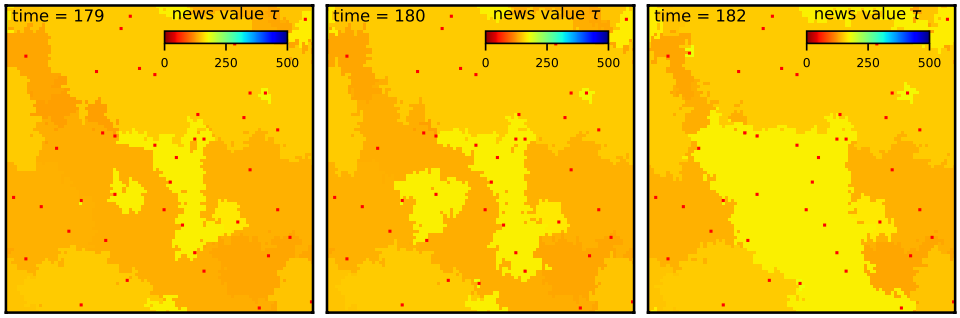

Figure 4.3: **News cascades on a large** 100×100 **lattice**. The color shows the news value of each node. Model parameter was $p_0 = 2.5 \times 10^{-5}$. Red squares represent influencers. A massive information cascade occurs between $t = 180$ and $t = 182$.

the simulation. Once a collection of subcultures has been established, news can spread faster using the directed influencer networks. The influencers act as hubs that instantly spread information to all their followers. Fig 4.3 shows how the influencer networks can trigger information cascades. Because influencers are likely to be located on the boundary between subcultures, this may trigger secondary or tertiary cascades.

4.3.1 Feedback-induced stability

Feedback is when the output of a system or process feeds back into the system as input. There are two forms of feedback. Positive feedback occurs when a perturbation is self-reinforcing. Conversely, negative feedback promotes stability by counteracting the disturbance. Feedback is pervasive in biological, economic, and climate systems [10, 21, 29]. Negative feedback occurs in many biological processes because of its stabilizing effect. Homeostasis is a process by which biological systems maintain stable internal conditions (e.g., body temperature, fluid balance, blood sugar level) while interacting with the external environment. Negative feedback mechanisms govern this process. The presence of multiple interacting feedback loops obscures climate modeling. Ice–albedo feedback is an example of positive feedback. Rising surface temperatures cause ice sheets to melt at the higher latitudes decreasing its albedo and increasing the proportion of sunlight absorbed by the surface. This mechanism then causes more ice to melt, and thus, we have a feedback circuit. Here we add a positive feedback loop between subscriber count and the news generation probability. An influencer with many subscribers should have a higher likelihood of producing or discovering news. For example, a newspaper with many subscribers can afford to hire more people, which allows it to find more news events. Aside from the monetary benefit, a journalist from a newspaper with many subscribers may receive more news tips. An influencer with index i now has probability

$$p_i = p_0(1 + \eta\kappa_i) \tag{4.1}$$

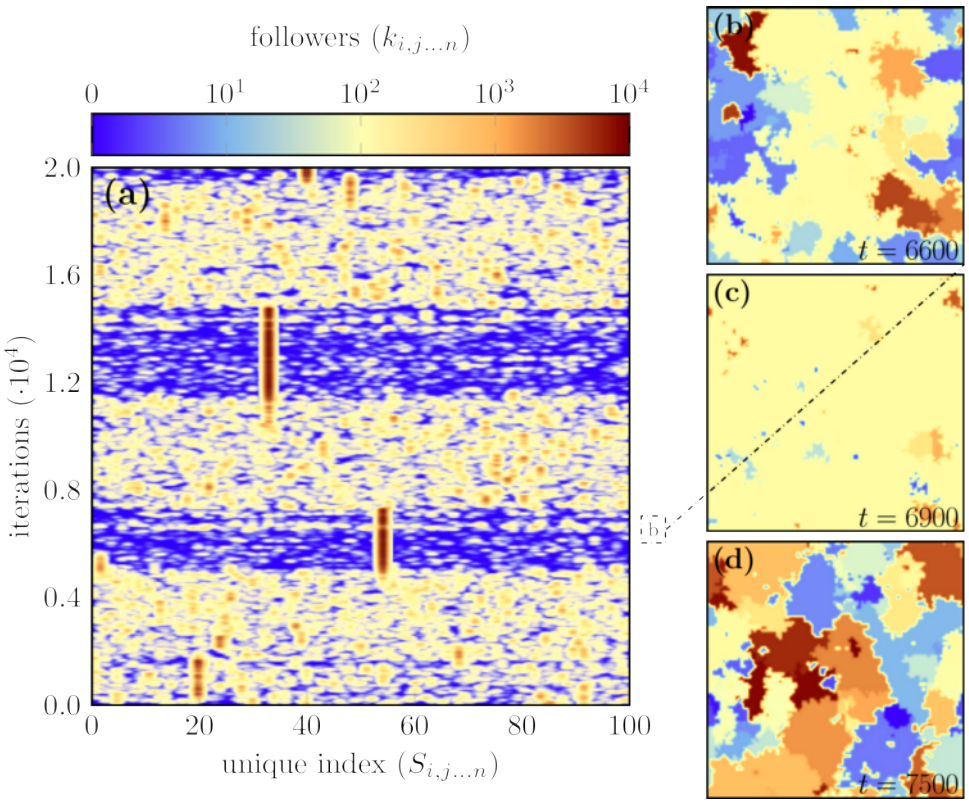

Figure 4.4: **Simulation with positive feedback on a** 100×100 **lattice**. (a) shows the size of each subculture. Vertical lines represent the time evolution of a subculture. The red lines are metastable states where the vast majority of followers belong to the same influencer. The bright blankets are fragmented states encompassing many subcultures of varying sizes. (a) shows the emergence of the first metastable state around $t = 5 \cdot 10^3$. (b-d) show snapshots of the simulation at different points in time. (b) shows the ordered domain on the verge of collapse as many emerging subcultures siphons followers from it. This subculture makes a swift recovery in (c) before collapsing in (d) into a fragmented state. Simulation was done with parameters $\eta = 0.30$, and $p_0 = 4.0 \cdot 10^{-5}$. The color in (a) displays a subculture's size. In (b-d) it displays affiliation with identical color nodes belonging to the same subculture.

to discover a news event. Here η is a feedback parameter and κ_i its number of followers. We define p_0 and η to be sufficiently small such that p_i never exceeds unity, i.e. $p_i = p_0(1 + \eta k_i) \leq 1$. An influencer is also a node and can therefore have no more than $N - 1$ followers. Therefore, if $p_0 = 1/N$ and $\eta = 1.0$ then $p_i = 1$. To avoid that p_i exceeds one we shall impose the following bounds $\eta \leq 1$ and $p_0 \leq \frac{1}{N}$ on the model's parameters.

4.3.2 Metastability and decay

Fig. 4.4 shows a simulation of a system with positive feedback. Model parameters are $p_0 = 4.0 \cdot 10^{-5}$, and $\eta = 0.30$. (a) shows the size of subcultures

over the simulation. Influencers can now increase p_i by capturing more followers. This positive feedback loop allows one influencer to maintain dominance for a sustained period. The probability of discovering a news event increases by ηp_0 for each subscriber. If p_0 is sufficiently high, there is a critical η where a subculture grows to encompass the entire system. The system can reside in an ordered metastable state, a fragmented configuration, or a completely disordered phase if p_0 is very large and η is negligible. It might seem paradoxical that p_0 is promoting stability through feedback and disorder by adding noise, but this is just a consequence of how we defined p_i. We return to this conundrum to further clarify it later on.

Metastability is commonly encountered in physics and chemistry. Consider, for example, a marble resting in a hole corresponding to a local minimum in the energy landscape or an atom in an excited state with a long lifetime. Dynamical systems with feedback, such as this one, can also exhibit stable and metastable states. Here the p_0 which adds noise to the system is somewhat analogous to a temperature which increases the probability of pushing the state out of a metastable configuration. The metastable phase is about to decay in (b) but bounces back in (c). This behavior is characteristic of systems with alternate stable states. Consider, for instance, the marble we alluded to above. Move it up the slope, and it simply rolls back down to its previous position. The decay of the metastable phase occurs between (c) and (d). This decay is a stochastic event facilitated by new subcultures that siphon followers from the dominating network, thereby lowering its p_i value. We use a random updating scheme where an arbitrary node is selected with each update. Hence there is no guarantee that the influencer of a large subculture is chosen during a sweep of N^2 updates. Of course, this influencer may also be selected multiple times during a sweep, but there is no benefit to this as they are assigned the same τ value. This asymmetry reduces the lifetimes of the metastable phase.

The model was also simulated on a one-dimensional ring. Here there was no transition to an ordered state, even for large values of η. Van Hoves' non-existence theorem prohibits phase transitions from occurring in one-dimensional systems with short-range interactions, but it only applies a certain class of systems [167]. Models with phase transitions in one dimension do exist [34]. Consider the following scenario to understand why this model does not have a phase transition in one dimension. An influencer S_1 on the ring lattice has amassed a large number of subscribers and reaches another influencer S_2 with few followers. S_2 will block any progress in this direction. To demote S_2 from the influencer state, it must lose all its followers. However, some of its followers are likely placed on the other side, so S_1 cannot capture them. Moreover, because S_2 borders the S_1 subculture, it can copy all of its news events and use this to capture followers on the other side. Thus, because of its juxtaposition to S_1, it is unlikely ever to be demoted. Subcultures on the ring lattice will tend to freeze up due to this, while the stasis is occasionally interrupted by the promotion of new influencers.

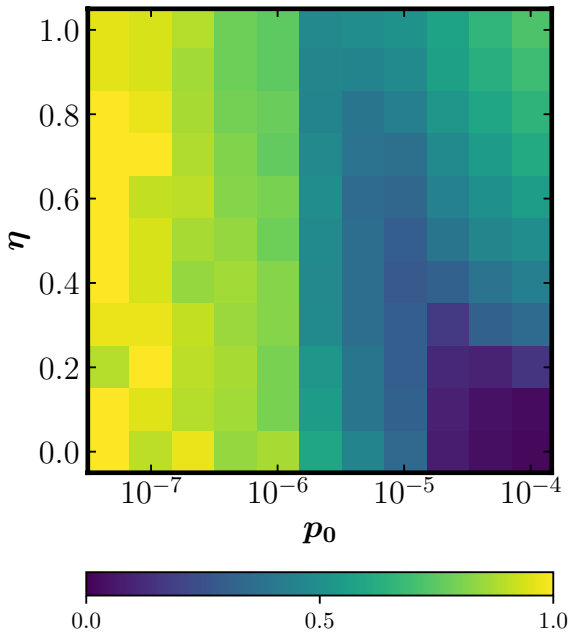

Figure 4.5: **Virality of information**. Here the color shows the fraction of viral news events that infect at least half of the network. Each point in the parameter space was averaged over 20.000 iterations on a 100×100 lattice

4.3.3 Viral information

Viral news events are events that spread quickly and widely on social media. It is possible to explore the viral properties of information in this model. Here we define *viral news events* as events that spread to half or more of the network. News events with the same τ are considered to be identical to avoid additional bookkeeping. Figure 4.5 shows the virality of information for a range of parameters [1]. Viral news events make up almost all of the news events for very low p_0 because an event has ample time to spread to a large part of the system before another replaces it. That is, in a world where noteworthy events seldom occur, the few noteworthy events that do occur are likely to attract attention. The competition between news events intensifies with p_0. Here it is difficult to capture the collective attention of the system because the network is inundated with news events. Viral news events are relatively common in the top right corner. Here most followers belong to the same influencer. This influencer has a high probability of generating news and can instantly pass on this information to its followers, and only this influencer can spread viral information.

[1] There are some minor discrepancies between Fig. 4.5 and the corresponding figure in the publication. Here the viral news events generated by influencers are not counted. This introduces an error along the vertical axis as the news events produced by influencers make up a significant fraction of all news events for large η, but changes nothing significant.

4.4 Complex network topologies

We have performed extensive simulations on a lattice model with many interesting qualities (e.g., boundary clustering, network cascades). Real social networks are characterized by variable degree distributions, nontrivial clustering, and assortative mixing [132]. The lattice has none of those properties except high clustering but with no cliques. Each node on the lattice has exactly four neighbors, so there is no variation in the number of edges assigned to them. Here the words *node* and *vertex* together with *link* and *edge* are used interchangeably. Clustering is a propensity for nodes with a mutual neighbor to be connected. The local clustering coefficient of a node introduced by Watts and Strogatz quantifies how close it is to a clique [173]. Here a clique or a complete subgraph is a subset of mutually adjacent vertices. Nontrivial clustering is related to homophily or assortative mixing. Assortative mixing is a tendency to form connections between nodes with similar characteristics. This tendency likely exacerbates fake news and polarization by creating echo chambers. However, since we do not assign specific characteristics to individual nodes (e.g., beliefs and preferences), exploring homophily with this model is not meaningful. We now proceed to simulate the model on more complex networks substrates. First, however, it is helpful to introduce them properly to clarify how they differ from the simple lattice.

4.4.1 Erdős–Rényi networks

The Erdős–Rényi model is one of two related algorithms for generating random graphs. The one introduced by Paul Erdős and Alfred Rényi generates a random network $G(N, k)$ from a predefined number of vertices N and edges

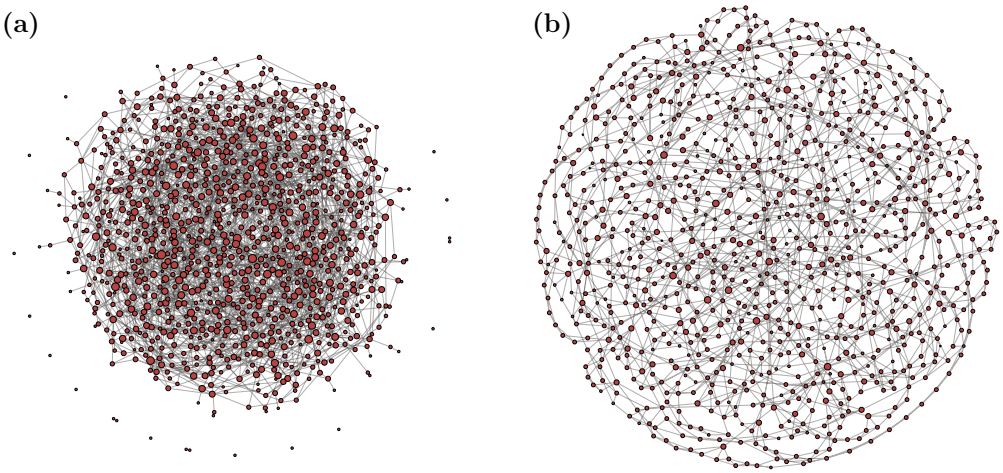

Figure 4.6: (a) random graph $G(N, p)$ with $N = 10^3$ and probability $p = 0.004$ of edge creation between vertice pairs. The expected number of links for this graph is 1998. (b) small-world graph with $N = 10^3$ and a $\beta = 0.1$ rewiring probability. Each node was assigned $k = 4$ neighbours.

k [49]. The other model introduced contemporaneously by Edgar Gilbert assigns a probability p to an edge being formed independently of other edges [72]. These random networks $G(N, p)$ are sometimes called random binomial graphs because the degree distribution of any particular vertex follows a binomial distribution. The probability that a node is given k links is

$$P(k) = \binom{N-1}{k} p^k (1-p)^{n-1-k}, \tag{4.2}$$

and the graph has an expected sum of $p\binom{N}{2}$ edges. Overall, random graphs have somewhat variable degree distributions (some vertices have many edges and some have few or no edges), but low clustering coefficients [173].

4.4.2 Small-world networks

Small-world networks are similar to lattices in that most nodes are not connected. They differ from lattices by having a low path length L. More precisely, the average distance L between two random vertices grows logarithmically with the size of the network N. The basic idea is that a few well-connected nodes dramatically reduces the distance between nodes by acting as transportation hubs. Thus, a node can use the links of its neighbors and so forth. Watts and Strogatz proposed a method for generating small-world networks. Starting from a regular lattice, we randomly rewire each link with probability β. We have a regular lattice at $\beta = 0$, a random network at $\beta = 1$, and small-world networks somewhere between those extremes. Watts and Strogatz showed that we obtain networks with low path length and high clustering for low β [173].

4.4.3 Model's parameter space

Figure 4.7 shows the average size of the largest subculture for a range of parameters on different networks. (a) shows the familiar lattice as a reference point. (b) show random-neighbor interactions. That is a complete network. (c) show simulations on random graphs generated by the Erdős–Rényi model with $p = 0.0004$. (d) show simulations on small-world networks generated by the Watts–Strogatz model with $\beta = 0.1$. Dark fields are ordered domains with a dominating subculture, and disorder increases with brightness. The information generation probability p_i increases by ηp_0 for each captured follower. The effect of feedback is proportional to p_0, which is why there is no ordered domain for low p_0. Alternatively, we could increase p_i by a fixed amount for each subscriber independent of p_0.

The time-averaged size of the largest subculture begins to increase for low p_0 because an influencer with new news has more time to capture followers before the information is made obsolete. This effect is more pronounced on the regular lattice with a high average path length than the other networks.

The highly clustered lattice and the small-world network have a solid boundary to the ordered domain. Conversely, the Erdős–Rényi random graphs

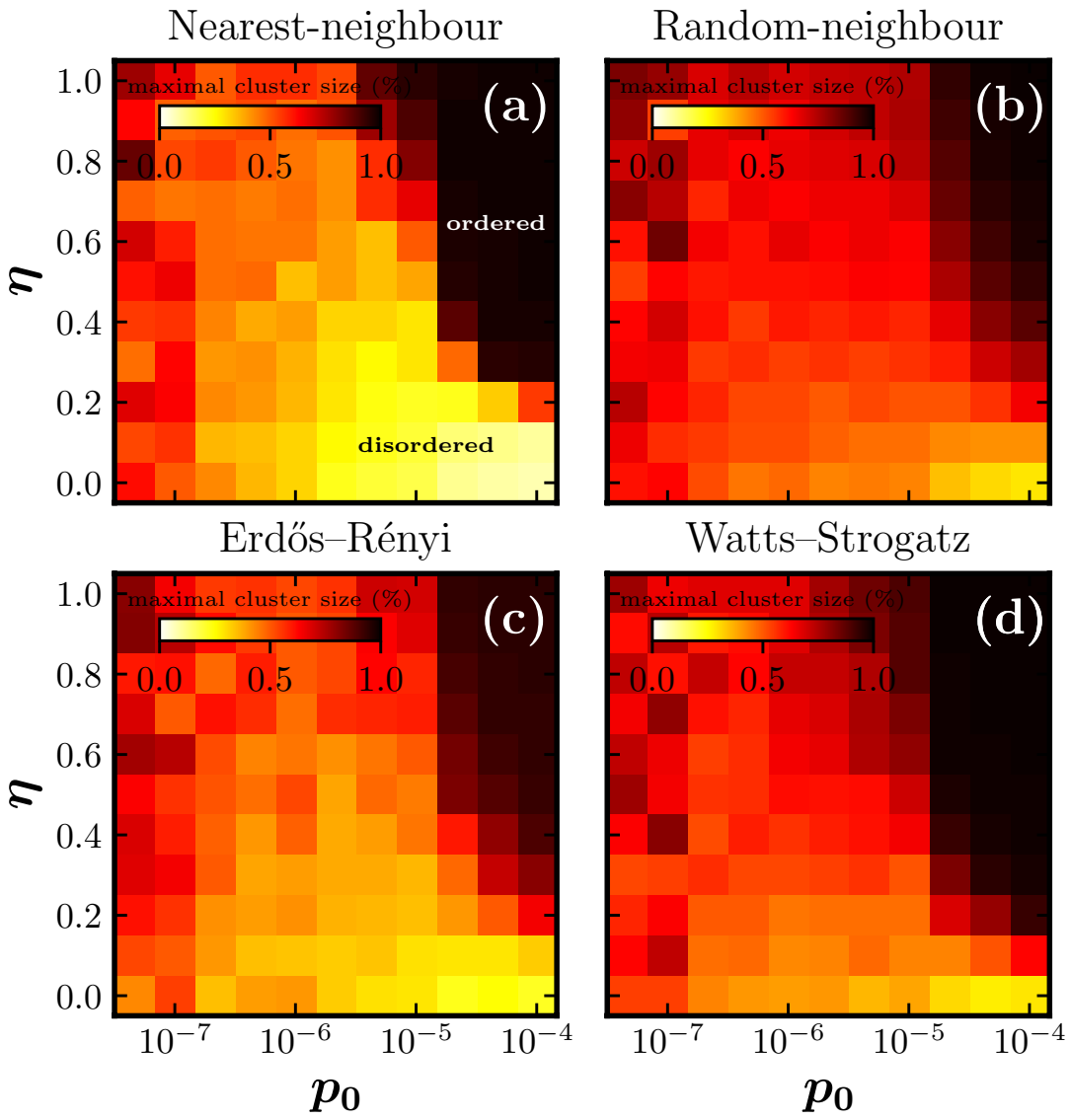

Figure 4.7: **Phase diagrams showing the average size of the largest subculture**. (a) regular lattice. (b) each node interacts with a random node. (c) Erdős–Rényi random graph with $p = 0.0004$. (d) Watts-Strogatz generated small-world network with $\beta = 0.1$. Dark regions mark the ordered domain. Disorder increases with brightness. Each point in the parameter space was averaged over 20.000 iterations on a network with 10^4 nodes.

and the complete networks have a fuzzy boundary. Subcultures grow exponentially on the "mean-field" networks. Thus, emerging influencers can siphon followers from the dominating subculture much faster compared to the regular lattice. We already mentioned how the stochastic updating scheme asymmetrically favors the emerging subcultures, now compounded by exponential growth. Concerning the Erdős–Rényi random graphs, the ordered domain is slightly brighter than the other diagrams. The largest component in the Erdős–Rényi random graphs never controls the entire network. Inspection of Fig. 4.6 reveals poorly connected nodes at the network's periphery, with some nodes being completely disjointed. Thus it is difficult for the

dominating subculture to absorb these low degree nodes. Remember that the network in Fig. 4.6 is an order of magnitude smaller than in Fig. 4.7.

4.4.4 Mutual co-existence in scale-free networks

Scale-free networks denote a class of networks whose degree distribution follows a power law. Thus, most nodes have a few links, while a few nodes have disproportionately many links. The Barabási–Albert model grows a scale-free network by preferentially attaching nodes with m to pre-existing nodes [16]. The probability of connecting a new node to a is

$$p_a = \frac{k_a}{\sum_b k_b}, \tag{4.3}$$

here k_a is the degree of a, and the sums run over the existing nodes b [4]. Hence nodes of a high degree accumulate links faster.

Figure 4.9 show a simulation of the model on a scale-free network. Here the nodes with disproportionately many neighbors are like massive news networks whose links reach every corner of the network. These links allow them to pick up news events around the network. This capability to quickly copy information allows them to immunize their followers while attacking

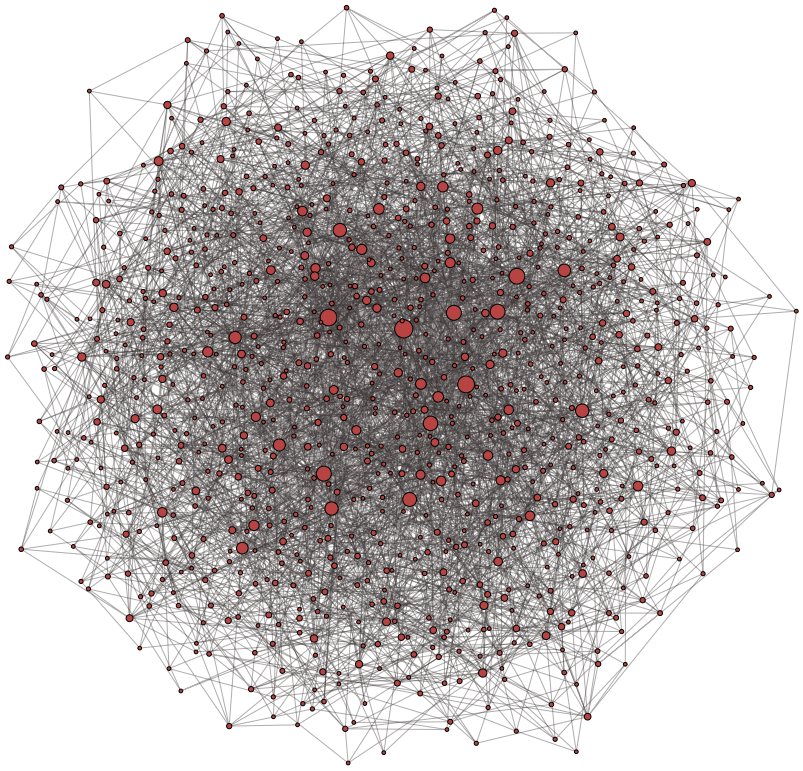

Figure 4.8: Scale-free network of $N = 10^3$ nodes with $m = 4$.

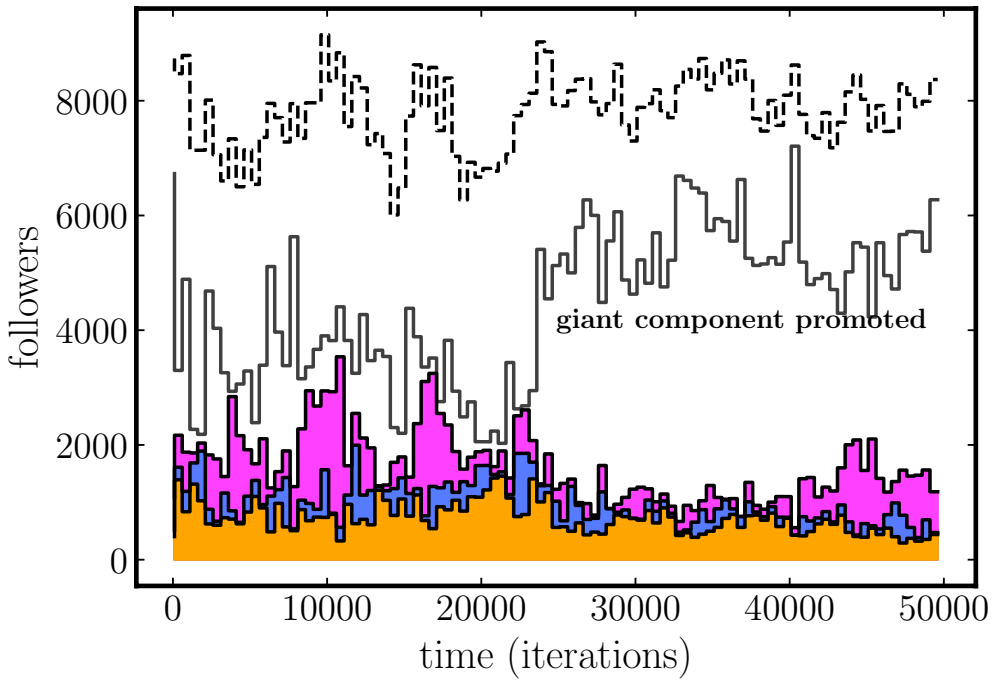

Figure 4.9: Simulation of the model on a scale-free network showing the four largest subcultures. The dashed line on top shows the sum of these four subcultures. Model parameters are $p_0 = 0.05$, and $\eta = 0$. The Barabási–Albert model was used to generate a scale-free network with $N = 10^4$ nodes with $m = 4$.

other less connected nodes. Mutual co-existence between highly connected influencers occurs in simulation. Here the node with the most links is promoted about halfway through the simulation. This highly connected node dominates about half of the network for a sustained period. Despite this abrupt shift, the number of subscribers belonging to the four largest subcultures fluctuates around a steady state. We conjecture that the network will converge to a stable state of mutual co-existence when all the high-degree nodes have been promoted, which appears to have occurred in the last half of the simulation. It is, therefore, necessary to simulate for a very long time if p_0 is low to ensure the promotion of high-degree nodes. The phase diagram of the scale-free network was deemed prohibitively time-consuming to make, although it is not impossible.

4.4.5 Summary and concluding remarks

To summarize, we modeled a social network that exhibits transitions between a dominating monoculture and a disaggregated collection of subcultures. It is posited that online social networks have brought about a similar transition by allowing everyone to be a news outlet. The effect of feedback was more pronounced than network topology, except on the scale-free network that exhibits some stability without feedback. However, the scale-free

network is not a realistic model of social networks because the high-degree nodes have connections that exceed Dunbar's number. It can, however, be interpreted as a model of competing news networks. The big three news networks used to dominate mass media in the United States, as previously stated [91].

There is growing concern that the internet has brought about an epidemic of fake news by lowering the cost of entry to new competitors, many of whom reject journalistic norms [113]. Vosoughi et al. showed that fake news stories spread more than the truth [169]. Fake news outlets can fabricate stories of greater newsworthiness, so it should not be surprising that false news spreads more than the truth. However, some studies dispute the prevalence of fake news. Findings by Allen et al. [5] suggest that fake news only makes up a small percentage of Americans' daily media diets. Whether true or false, there is a perception of fake news as a widespread problem. Individuals in a fragmented information ecosystem are exposed to information from many different sources. Exposure to conflicting narratives could exacerbate the perception of fake news. Conversely, individuals in a monoculture are exposed only to the information passed on to them from the dominating news outlet. These individuals could be exposed to much more fake news because a single news outlet generally controls the flow of information in autocratic societies.

The content of news events was not explicitly modeled, nor was there any differentiation between real and fake news outlets. An extension of the model could give fake news outlets a high news generation probability. Here it would be necessary to introduce a measure of credibility to penalize outlets that disseminate fake news. Respectable news outlets would then find themselves in a delicate situation when deciding whether or not to pass on information from another source. The risk of passing on false information entails a loss of reputation. However, journalists often face this dilemma because the race to report on a breaking news event first can drive even respectable news outlets to publish information before adequately vetting it.

Our findings suggest that either fake news or the perception of fake news as being ubiquitous is endemic to our society because everyone can become a news outlet (e.g., influencer).

Bibliography

[1] David Adam. "Special report: The simulations driving the world's response to COVID-19." In: *Nature* 580.7802 (2020), pp. 316–319.

[2] Avner Ahituv, V Joseph Hotz, and Tomas Philipson. "The responsiveness of the demand for condoms to the local prevalence of AIDS". In: *Journal of Human Resources* (1996), pp. 869–897.

[3] Marco Ajelli et al. "Spatiotemporal dynamics of the Ebola epidemic in Guinea and implications for vaccination and disease elimination: a computational modeling analysis". In: *BMC medicine* 14.1 (2016), pp. 1–10.

[4] Réka Albert and Albert-László Barabási. "Statistical mechanics of complex networks". In: *Reviews of modern physics* 74.1 (2002), p. 47.

[5] Jennifer Allen et al. "Evaluating the fake news problem at the scale of the information ecosystem". In: *Science Advances* 6.14 (2020), eaay3539.

[6] Christian L Althaus. "Estimating the reproduction number of Ebola virus (EBOV) during the 2014 outbreak in West Africa". In: *PLoS currents* 6 (2014).

[7] Roy M Anderson and Robert M May. *Infectious diseases of humans: dynamics and control*. Oxford university press, 1992.

[8] Sigrún Andradóttir et al. "Simulation of strategies for containing pandemic influenza". In: *Proceedings of the 2010 Winter Simulation Conference*. IEEE. 2010, pp. 2221–2229.

[9] Melissa M Arons et al. "Presymptomatic SARS-CoV-2 infections and transmission in a skilled nursing facility". In: *New England journal of medicine* 382.22 (2020), pp. 2081–2090.

[10] W Brian Arthur. "Positive feedbacks in the economy". In: *Scientific american* 262.2 (1990), pp. 92–99.

[11] Christie Aschwanden. *How COVID is changing the study of human behaviour*. 2021.

[12] Rapid Risk Assessment. "Detection of new SARS-CoV-2 variants related to mink". In: *Eur. Cent. Dis. Prev. Control* (2020).

[13] Robert Axelrod. "The dissemination of culture: A model with local convergence and global polarization". In: *Journal of conflict resolution* 41.2 (1997), pp. 203–226.

[14] Sylvain Baize et al. "Emergence of Zaire Ebola virus disease in Guinea". In: *New England Journal of Medicine* 371.15 (2014), pp. 1418–1425.

[15] Shweta Bansal, Bryan T Grenfell, and Lauren Ancel Meyers. "When individual behaviour matters: homogeneous and network models in epidemiology". In: *Journal of the Royal Society Interface* 4.16 (2007), pp. 879–891.

[16] Albert-László Barabási and Réka Albert. "Emergence of scaling in random networks". In: *science* 286.5439 (1999), pp. 509–512.

[17] Michael Barthel. "Despite subscription surges for largest US newspapers, circulation and revenue fall for industry overall". In: *Pew Research Center* 1 (2017).

[18] Monika Bednarek and Helen Caple. *The discourse of news values: How news organizations create newsworthiness*. Oxford University Press, 2017.

[19] Allan Bell. *The language of news media*. Blackwell Oxford, 1991.

[20] Sally Blower and Daniel Bernoulli. "An attempt at a new analysis of the mortality caused by smallpox and of the advantages of inoculation to prevent it. 1766." In: *Reviews in medical virology* 14 (Sept. 2004), pp. 275–88. DOI: 10.1002/rmv.443.

[21] Sandrine Bony et al. "How well do we understand and evaluate climate change feedback processes?" In: *Journal of Climate* 19.15 (2006), pp. 3445–3482.

[22] Benny Borremans et al. "The shape of the contact–density function matters when modelling parasite transmission in fluctuating populations". In: *Royal Society open science* 4.11 (2017), p. 171308.

[23] Declan Butler. "Models overestimate Ebola cases". In: *Nature News* 515.7525 (2014), p. 18.

[24] Edward W Campion et al. "Ebola and quarantine". In: *N Engl J Med* 371 (2014), pp. 2029–30.

[25] Helen Caple and Monika Bednarek. "Delving into the discourse: Approaches to news values in journalism studies and beyond". In: (2013).

[26] Damon Centola and Michael Macy. "Complex contagions and the weakness of long ties". In: *American journal of Sociology* 113.3 (2007), pp. 702–734.

[27] Matteo Chinazzi et al. "The effect of travel restrictions on the spread of the 2019 novel coronavirus (COVID-19) outbreak". In: *Science* 368.6489 (2020), pp. 395–400.

[28] Jean-Paul Chretien, Steven Riley, and Dylan B George. "Mathematical modeling of the West Africa Ebola epidemic". In: *Elife* 4 (2015), e09186.

[29] Olivier Cinquin and Jacques Demongeot. "Roles of positive and negative feedback in biological systems". In: *Comptes rendus biologies* 325.11 (2002), pp. 1085–1095.

[30] Vittoria Colizza et al. "Modeling the worldwide spread of pandemic influenza: baseline case and containment interventions". In: *PLoS medicine* 4.1 (2007), e13.

[31] Vittoria Colizza et al. “The role of the airline transportation network in the prediction and predictability of global epidemics”. In: *Proceedings of the National Academy of Sciences* 103.7 (2006), pp. 2015–2020.

[32] Ben S Cooper et al. “Delaying the international spread of pandemic influenza”. In: *PLoS medicine* 3.6 (2006), e212.

[33] Gabriel Crossley. “Wuhan lockdown unprecedented, shows commitment to contain virus: WHO representative in China”. In: *Thomson Reuters* (2020).

[34] José A Cuesta and Angel Sánchez. “General non-existence theorem for phase transitions in one-dimensional systems with short range interactions, and physical examples of such transitions”. In: *Journal of statistical physics* 115.3 (2004), pp. 869–893.

[35] Daryl J Daley and David G Kendall. “Epidemics and rumours”. In: *Nature* 204.4963 (1964), pp. 1118–1118.

[36] Nicholas G Davies et al. “Association of tiered restrictions and a second lockdown with COVID-19 deaths and hospital admissions in England: a modelling study”. In: *The Lancet Infectious Diseases* 21.4 (2021), pp. 482–492.

[37] Erik Dietzel et al. “Functional characterization of adaptive mutations during the West African Ebola virus outbreak”. In: *Journal of virology* 91.2 (2017), e01913–16.

[38] Ivan Djordjevic, William Ryan, and Bane Vasic. *Coding for optical channels*. Springer Science & Business Media, 2010.

[39] Scott F Dowell et al. “Transmission of Ebola hemorrhagic fever: a study of risk factors in family members, Kikwit, Democratic Republic of the Congo, 1995”. In: *The Journal of infectious diseases* 179.Supplement_1 (1999), S87–S91.

[40] John M Drake et al. “Ebola cases and health system demand in Liberia”. In: *PLoS biology* 13.1 (2015), e1002056.

[41] P Van den Driessche. “Spatial structure: Patch models”. In: *Mathematical epidemiology*. Springer, 2008, pp. 179–189.

[42] Jeremy P D’Silva and Marisa C Eisenberg. “Modeling spatial invasion of Ebola in West Africa”. In: *Journal of theoretical biology* 428 (2017), pp. 65–75.

[43] Richard B Du Boff. “The telegraph in nineteenth-century America: Technology and monopoly”. In: *Comparative Studies in Society and History* 26.4 (1984), pp. 571–586.

[44] Gytis Dudas et al. “Virus genomes reveal factors that spread and sustained the Ebola epidemic”. In: *Nature* 544.7650 (2017), pp. 309–315.

[45] Robin IM Dunbar. “Coevolution of neocortical size, group size and language in humans”. In: *Behavioral and brain sciences* 16.4 (1993), pp. 681–694.

[46] Robin IM Dunbar. "Neocortex size as a constraint on group size in primates". In: *Journal of human evolution* 22.6 (1992), pp. 469–493.

[47] Murray Eden et al. "A two-dimensional growth process". In: *Proceedings of the fourth Berkeley symposium on mathematical statistics and probability*. Vol. 4. University of California Press Berkeley. 1961, pp. 223–239.

[48] Joshua M Epstein et al. "Controlling pandemic flu: the value of international air travel restrictions". In: *PloS one* 2.5 (2007), e401.

[49] Paul Erdös and Alfréd Rényi. "On the evolution of random graphs". In: *The structure and dynamics of networks*. Princeton University Press, 2011, pp. 38–82.

[50] Shannon M Fast et al. "The role of social mobilization in controlling Ebola virus in Lofa County, Liberia". In: *PLoS currents* 7 (2015).

[51] Huang Fei et al. "The impact of the COVID-19 epidemic on tuberculosis control in China". In: *The Lancet Regional Health-Western Pacific* 3 (2020), p. 100032.

[52] Heinz Feldmann, Armand Sprecher, and Thomas W Geisbert. "Ebola". In: *New England Journal of Medicine* 382.19 (2020), pp. 1832–1842.

[53] Heinz Feldmann et al. "Ebola virus: from discovery to vaccine". In: *Nature Reviews Immunology* 3.8 (2003), pp. 677–685.

[54] Neil Ferguson. "Capturing human behaviour". In: *Nature* 446.7137 (2007), pp. 733–733.

[55] Neil M Ferguson et al. "Planning for smallpox outbreaks". In: *Nature* 425.6959 (2003), pp. 681–685.

[56] Neil M Ferguson et al. "Strategies for containing an emerging influenza pandemic in Southeast Asia". In: *Nature* 437.7056 (2005), pp. 209–214.

[57] Neil M Ferguson et al. "Strategies for mitigating an influenza pandemic". In: *Nature* 442.7101 (2006), pp. 448–452.

[58] Harold Henry Fisher et al. "famine in Soviet Russia, 1919-1923". In: (1927).

[59] David Fisman, Edwin Khoo, and Ashleigh Tuite. "Early epidemic dynamics of the West African 2014 Ebola outbreak: estimates derived with a simple two-parameter model". In: *PLoS currents* 6 (2014).

[60] Antoine Flahault et al. "Strategies for containing a global influenza pandemic". In: *Vaccine* 24.44-46 (2006), pp. 6751–6755.

[61] Seth Flaxman et al. "Estimating the effects of non-pharmaceutical interventions on COVID-19 in Europe". In: *Nature* 584.7820 (2020), pp. 257–261.

[62] Fiona Fleck. "How SARS changed the world in less than six months". In: *Bulletin of the World Health Organization* 81 (2003), pp. 625–626.

[63] Pierre Formenty et al. “Human infection due to Ebola virus, subtype Cote d’Ivoire: clinical and biologic presentation”. In: *The Journal of infectious diseases* 179.Supplement_1 (1999), S48–S53.

[64] Paolo Francesconi et al. “Ebola hemorrhagic fever transmission and risk factors of contacts, Uganda”. In: *Emerging infectious diseases* 9.11 (2003), p. 1430.

[65] HL Frisch and JM Hammersley. “Percolation processes and related topics”. In: *Journal of the society for industrial and applied mathematics* 11.4 (1963), pp. 894–918.

[66] Sebastian Funk, Gwenan M Knight, and Vincent AA Jansen. “Ebola: the power of behaviour change”. In: *Nature* 515.7528 (2014), pp. 492–492.

[67] Sebastian Funk et al. “The impact of control strategies and behavioural changes on the elimination of Ebola from Lofa County, Liberia”. In: *Philosophical Transactions of the Royal Society B: Biological Sciences* 372.1721 (2017), p. 20160302.

[68] Sebastian Funk et al. “The spread of awareness and its impact on epidemic outbreaks”. In: *Proceedings of the National Academy of Sciences* 106.16 (2009), pp. 6872–6877.

[69] Nathan W Furukawa, John T Brooks, and Jeremy Sobel. “Evidence supporting transmission of severe acute respiratory syndrome coronavirus 2 while presymptomatic or asymptomatic”. In: *Emerging infectious diseases* 26.7 (2020).

[70] Johan Galtung and Mari Holmboe Ruge. “The structure of foreign news: The presentation of the Congo, Cuba and Cyprus crises in four Norwegian newspapers”. In: *Journal of peace research* 2.1 (1965), pp. 64–90.

[71] Zhiru Gao et al. “A systematic review of asymptomatic infections with COVID-19”. In: *Journal of Microbiology, Immunology and Infection* 54.1 (2021), pp. 12–16.

[72] Edgar N Gilbert. “Random graphs”. In: *The Annals of Mathematical Statistics* 30.4 (1959), pp. 1141–1144.

[73] Amaya M Gillespie et al. “Social mobilization and community engagement central to the Ebola response in West Africa: lessons for future public health emergencies”. In: *Global Health: Science and Practice* 4.4 (2016), pp. 626–646.

[74] Daniel T Gillespie. “A general method for numerically simulating the stochastic time evolution of coupled chemical reactions”. In: *Journal of computational physics* 22.4 (1976), pp. 403–434.

[75] Daniel T Gillespie. “Exact stochastic simulation of coupled chemical reactions”. In: *The journal of physical chemistry* 81.25 (1977), pp. 2340–2361.

[76] Daniel T Gillespie. "Stochastic simulation of chemical kinetics". In: *Annu. Rev. Phys. Chem.* 58 (2007), pp. 35–55.

[77] Alina Glaubitz and Feng Fu. "Oscillatory dynamics in the dilemma of social distancing". In: *Proceedings of the Royal Society A* 476.2243 (2020), p. 20200686.

[78] Judith R Glynn et al. "Asymptomatic infection and unrecognised Ebola virus disease in Ebola-affected households in Sierra Leone: a cross-sectional study using a new non-invasive assay for antibodies to Ebola virus". In: *The Lancet infectious diseases* 17.6 (2017), pp. 645–653.

[79] William Goffman. "An epidemic process in an open population". In: *Nature* 205.4973 (1965), pp. 831–832.

[80] William Goffman and V Newill. "Generalization of epidemic theory". In: *Nature* 204.4955 (1964), pp. 225–228.

[81] William Goffman and Vaun A Newill. "Communication and epidemic processes". In: *Proceedings of the Royal Society of London. Series A. Mathematical and Physical Sciences* 298.1454 (1967), pp. 316–334.

[82] Patricio Goldstein, Eduardo Levy Yeyati, and Luca Sartorio. "Lockdown fatigue: The diminishing effects of quarantines on the spread of COVID-19". In: (2021).

[83] Tracey Goldstein et al. "The discovery of Bombali virus adds further support for bats as hosts of ebolaviruses". In: *Nature microbiology* 3.10 (2018), pp. 1084–1089.

[84] Peter Grassberger. "On the critical behavior of the general epidemic process and dynamical percolation". In: *Mathematical Biosciences* 63.2 (1983), pp. 157–172.

[85] Trisha Greenhalgh et al. "Ten scientific reasons in support of airborne transmission of SARS-CoV-2". In: *The lancet* 397.10285 (2021), pp. 1603–1605.

[86] Sumedha Gupta et al. *Tracking public and private responses to the COVID-19 epidemic: evidence from state and local government actions*. Tech. rep. National Bureau of Economic Research, 2020.

[87] Danny Hayes and Jennifer L Lawless. "The decline of local news and its effects: New evidence from longitudinal data". In: *The Journal of Politics* 80.1 (2018), pp. 332–336.

[88] Daihai He et al. "The relative transmissibility of asymptomatic COVID-19 infections among close contacts". In: *International Journal of Infectious Diseases* 94 (2020), pp. 145–147.

[89] Stephane Helleringer and Andrew Noymer. "Magnitude of Ebola relative to other causes of death in Liberia, Sierra Leone, and Guinea". In: *The Lancet Global Health* 3.5 (2015), e255–e256.

[90] Barry S Hewlett and Bonnie L Hewlett. *Ebola, culture and politics: the anthropology of an emerging disease*. Cengage Learning, 2007.

[91] Douglas Blanks Hindman and Kenneth Wiegand. "The big three's prime-time decline: a technological and social context". In: *Journal of Broadcasting & Electronic Media* 52.1 (2008), pp. 119–135.

[92] T Déirdre Hollingsworth, Neil M Ferguson, and Roy M Anderson. "Will travel restrictions control the international spread of pandemic influenza?" In: *Nature medicine* 12.5 (2006), pp. 497–499.

[93] Michelle L Holshue et al. "First case of 2019 novel coronavirus in the United States". In: *New England Journal of Medicine* (2020).

[94] David Holtz et al. "Interdependence and the cost of uncoordinated responses to COVID-19". In: *Proceedings of the National Academy of Sciences* 117.33 (2020), pp. 19837–19843.

[95] U.S Department of Homeland Security. *DHS Issues Supplemental Instructions for Inbound Flights with Individuals Who Have Been In China*. URL: https://www.dhs.gov/news/2020/02/02/dhs-issues-supplemental-instructions-inbound-flights-individuals-who-have-been-china.

[96] Hao Hu, Karima Nigmatulina, and Philip Eckhoff. "The scaling of contact rates with population density for the infectious disease models". In: *Mathematical biosciences* 244.2 (2013), pp. 125–134.

[97] Lars Hufnagel, Dirk Brockmann, and Theo Geisel. "Forecast and control of epidemics in a globalized world". In: *Proceedings of the National Academy of Sciences* 101.42 (2004), pp. 15124–15129.

[98] Christine E Hulseberg et al. "Molecular analysis of the 2012 Bundibugyo virus disease outbreak". In: *Cell Reports Medicine* 2.8 (2021), p. 100351.

[99] Arthur P Hurter and Michael G Van Buer. "The newspaper production/distribution problem". In: *Journal of Business Logistics* 17.1 (1996), p. 85.

[100] Oly Ilunga Kalenga et al. "The ongoing Ebola epidemic in the Democratic Republic of Congo, 2018–2019". In: *New England Journal of Medicine* 381.4 (2019), pp. 373–383.

[101] Center for International Earth Science Information Network CIESIN Columbia University. *Gridded Population of the World, Version 4 (GPWv4): Population Density, Revision 11. Palisades, NY: NASA Socioeconomic Data and Applications Center (SEDAC)*. https://doi.org/10.7927/H49C6VHW. 2018.

[102] Colin Jerolmack. "Animal archeology: domestic pigeons and the nature-culture dialectic". In: *Qualitative Sociology Review* 3.1 (2007).

[103] Christel Kamp, Mathieu Moslonka-Lefebvre, and Samuel Alizon. "Epidemic spread on weighted networks". In: *PLoS computational biology* 9.12 (2013), e1003352.

[104] Matthew J Keeling et al. "The effects of local spatial structure on epidemiological invasions". In: *The Structure and Dynamics of Networks*. Princeton University Press, 2011, pp. 480–488.

[105] William Ogilvy Kermack and Anderson G McKendrick. "A contribution to the mathematical theory of epidemics". In: *Proceedings of the royal society of london. Series A, Containing papers of a mathematical and physical character* 115.772 (1927), pp. 700–721.

[106] Maria Kiskowski and Gerardo Chowell. "Modeling household and community transmission of Ebola virus disease: epidemic growth, spatial dynamics and insights for epidemic control". In: *Virulence* 7.2 (2016), pp. 163–173.

[107] Stephen M Kissler et al. "Projecting the transmission dynamics of SARS-CoV-2 through the postpandemic period". In: *Science* 368.6493 (2020), pp. 860–868.

[108] Alden S Klovdahl. "Social networks and the spread of infectious diseases: the AIDS example". In: *Social science & medicine* 21.11 (1985), pp. 1203–1216.

[109] Andrew M Kramer et al. "Spatial spread of the West Africa Ebola epidemic". In: *Royal Society open science* 3.8 (2016), p. 160294.

[110] Jens H Kuhn et al. "Proposal for a revised taxonomy of the family Filoviridae: classification, names of taxa and viruses, and virus abbreviations". In: *Archives of virology* 155.12 (2010), pp. 2083–2103.

[111] Max SY Lau et al. "Spatial and temporal dynamics of superspreading events in the 2014–2015 West Africa Ebola epidemic". In: *Proceedings of the National Academy of Sciences* 114.9 (2017), pp. 2337–2342.

[112] Glenn Laverack and Erma Manoncourt. "Key experiences of community engagement and social mobilization in the Ebola response". In: *Global health promotion* 23.1 (2016), pp. 79–82.

[113] David MJ Lazer et al. "The science of fake news". In: *Science* 359.6380 (2018), pp. 1094–1096.

[114] Vernon J Lee, David C Lye, and Annelies Wilder-Smith. "Combination strategies for pandemic influenza response-a systematic review of mathematical modeling studies". In: *BMC medicine* 7.1 (2009), pp. 1–8.

[115] Dyani Lewis. "COVID-19 rarely spreads through surfaces. So why are we still deep cleaning". In: *Nature* 590.7844 (2021), pp. 26–28.

[116] Joseph A Lewnard et al. "Dynamics and control of Ebola virus transmission in Montserrado, Liberia: a mathematical modelling analysis". In: *The Lancet Infectious Diseases* 14.12 (2014), pp. 1189–1195.

[117] Qun Li et al. "Early transmission dynamics in Wuhan, China, of novel coronavirus–infected pneumonia". In: *New England journal of medicine* (2020).

[118] Ruiyun Li et al. "Substantial undocumented infection facilitates the rapid dissemination of novel coronavirus (SARS-CoV-2)". In: *Science* 368.6490 (2020), pp. 489–493.

[119] Yuan Liu et al. "Aerodynamic analysis of SARS-CoV-2 in two Wuhan hospitals". In: *Nature* 582.7813 (2020), pp. 557–560.

[120] Alun L Lloyd and Robert M May. "Spatial heterogeneity in epidemic models". In: *Journal of theoretical biology* 179.1 (1996), pp. 1–11.

[121] James O Lloyd-Smith et al. "Superspreading and the effect of individual variation on disease emergence". In: *Nature* 438.7066 (2005), pp. 355–359.

[122] Ira M Longini et al. "Containing pandemic influenza at the source". In: *Science* 309.5737 (2005), pp. 1083–1087.

[123] Philip A Mackowiak and Paul S Sehdev. "The origin of quarantine". In: *Clinical Infectious Diseases* 35.9 (2002), pp. 1071–1072.

[124] Angellar Manguvo and Benford Mafuvadze. "The impact of traditional and religious practices on the spread of Ebola in West Africa: time for a strategic shift". In: *The Pan African Medical Journal* 22.Suppl 1 (2015).

[125] RJ Mantel and M Fontein. "A practical solution to a newspaper distribution problem". In: *International Journal of Production Economics* 30 (1993), pp. 591–599.

[126] Martin I Meltzer et al. "Estimating the future number of cases in the Ebola epidemic–Liberia and Sierra Leone, 2014–2015". In: (2014).

[127] Stefano Merler et al. "Spatiotemporal spread of the 2014 outbreak of Ebola virus disease in Liberia and the effectiveness of non-pharmaceutical interventions: a computational modelling analysis". In: *The Lancet Infectious Diseases* 15.2 (2015), pp. 204–211.

[128] Stefano Merler et al. "Strategies for containing an influenza pandemic: the case of Italy". In: *Proceedings of the 1st international conference on Bio inspired models of network, information and computing systems*. 2006, 11–es.

[129] Lauren Ancel Meyers, MEJ Newman, and Babak Pourbohloul. "Predicting epidemics on directed contact networks". In: *Journal of theoretical biology* 240.3 (2006), pp. 400–418.

[130] Joël Mossong et al. "Social contacts and mixing patterns relevant to the spread of infectious diseases". In: *PLoS medicine* 5.3 (2008), e74.

[131] János Neumann, Arthur W Burks, et al. *Theory of self-reproducing automata*. Vol. 1102024. University of Illinois press Urbana, 1966.

[132] Mark EJ Newman and Juyong Park. "Why social networks are different from other types of networks". In: *Physical review E* 68.3 (2003), p. 036122.

[133] Julia V Noble. "Geographic and temporal development of plagues". In: *Nature* 250.5469 (1974), pp. 726–729.

[134] Bianca Nogrady. "What the data say about asymptomatic COVID infections". In: *Nature* 587.7835 (2020), pp. 534–535.

[135] Johnson OE and AE Ijezie. "Control of Ebola virus disease (EVD): An entry point for personal and environmental hygiene in the West African sub-region". In: *Journal of Medicine and Medical Sciences* 6.3 (2015), pp. 53–57.

[136] Yoshiyuki Okada et al. "SIR-extended information diffusion model of false rumor and its prevention strategy for twitter". In: *Journal of Advanced Computational Intelligence and Intelligent Informatics* 18.4 (2014), pp. 598–607.

[137] Comfort K Panda. "Kono Members' Perceptions of Burial Practices and the Spread of Ebola Virus Disease". PhD thesis. Walden University, 2018.

[138] Abhishek Pandey et al. "Strategies for containing Ebola in west Africa". In: *Science* 346.6212 (2014), pp. 991–995.

[139] Romualdo Pastor-Satorras and Alessandro Vespignani. "Epidemic spreading in scale-free networks". In: *Physical review letters* 86.14 (2001), p. 3200.

[140] John Perry and T Debey Sayndee. *Social mobilization and the Ebola virus disease in Liberia*. Rowman & Littlefield, 2016.

[141] Peter Piot. *Ebola's perfect storm*. 2014.

[142] Peter Piot. *No time to lose: a life in pursuit of deadly viruses*. WW Norton & Company, 2012.

[143] Dale Purves et al. *Cognitive neuroscience*. Sunderland: Sinauer Associates, Inc, 2008.

[144] Amira Rachah and Delfim FM Torres. "Mathematical modelling, simulation, and optimal control of the 2014 Ebola outbreak in West Africa". In: *Discrete dynamics in nature and society* 2015 (2015).

[145] Andrew Rhodes et al. "The variability of critical care bed numbers in Europe". In: *Intensive care medicine* 38.10 (2012), pp. 1647–1653.

[146] Steven Riley. "Large-scale spatial-transmission models of infectious disease". In: *Science* 316.5829 (2007), pp. 1298–1301.

[147] Steven Riley and Neil M Ferguson. "Smallpox transmission and control: spatial dynamics in Great Britain". In: *Proceedings of the National Academy of Sciences* 103.33 (2006), pp. 12637–12642.

[148] Caitlin M Rivers et al. "Modeling the impact of interventions on an epidemic of Ebola in Sierra Leone and Liberia". In: *PLoS currents* 6 (2014).

[149] Ronald Ross. "An application of the theory of probabilities to the study of a priori pathometry.—Part I". In: *Proceedings of the Royal Society of London. Series A, Containing papers of a mathematical and physical character* 92.638 (1916), pp. 204–230.

[150] Ronald Ross and Hilda P Hudson. "An application of the theory of probabilities to the study of a priori pathometry.—Part II". In: *Proceedings of the Royal Society of London. Series A, Containing papers of a mathematical and physical character* 93.650 (1917), pp. 212–225.

[151] Ronald Ross and Hilda P Hudson. "An application of the theory of probabilities to the study of a priori pathometry.—Part III". In: *Proceedings of the Royal Society of London. Series A, Containing papers of a mathematical and physical character* 89.621 (1917), pp. 215–240.

[152] Leonid A Rvachev and Ira M Longini Jr. "A mathematical model for the global spread of influenza". In: *Mathematical biosciences* 75.1 (1985), pp. 3–22.

[153] Thomas C Schelling. "Dynamic models of segregation". In: *Journal of mathematical sociology* 1.2 (1971), pp. 143–186.

[154] Arthur Schlesinger. "Origins of the Cold War". In: *Foreign Affairs* 46.1 (1967), pp. 22–52.

[155] Philip Schlesinger. *Putting'reality'together: BBC news*. Constable, 1978.

[156] Anne Schuchat, CDC Covid, and Response Team. "Public health response to the initiation and spread of pandemic COVID-19 in the United States, February 24–April 21, 2020". In: *Morbidity and mortality weekly Report* 69.18 (2020), p. 551.

[157] Phillip Schumm et al. "Epidemic spreading on weighted contact networks". In: *2007 2nd Bio-Inspired Models of Network, Information and Computing Systems*. IEEE. 2007, pp. 201–208.

[158] MW Shaw. "Simulation of population expansion and spatial pattern when individual dispersal distributions do not decline exponentially with distance". In: *Proceedings of the Royal Society of London. Series B: Biological Sciences* 259.1356 (1995), pp. 243–248.

[159] Trevor Shoemaker et al. "Reemerging Sudan ebola virus disease in Uganda, 2011". In: *Emerging infectious diseases* 18.9 (2012), p. 1480.

[160] James M Shultz, Florence Baingana, and Yuval Neria. "The 2014 Ebola outbreak and mental health: current status and recommended response". In: *Jama* 313.6 (2015), pp. 567–568.

[161] Juen Kiem Tan et al. "The prevalence and clinical significance of Presymptomatic COVID-19 patients: how we can be one step ahead in mitigating a deadly pandemic". In: *BMC infectious diseases* 21.1 (2021), pp. 1–10.

[162] AE Tchahou Tchendjeu et al. "Dynamics of the competition between two languages". In: *SeMA Journal* 77 (2020), pp. 351–373.

[163] International Ebola Response Team et al. "Exposure patterns driving Ebola transmission in West Africa: a retrospective observational study". In: *PLoS medicine* 13.11 (2016), e1002170.

[164] WHO Ebola Response Team. "Ebola virus disease in West Africa—the first 9 months of the epidemic and forward projections". In: *New England Journal of Medicine* 371.16 (2014), pp. 1481–1495.

[165] Jonathan S Towner et al. "Newly discovered ebola virus associated with hemorrhagic fever outbreak in Uganda". In: *PLoS pathogens* 4.11 (2008), e1000212.

[166] Neeltje Van Doremalen et al. "Aerosol and surface stability of SARS-CoV-2 as compared with SARS-CoV-1". In: *New England journal of medicine* 382.16 (2020), pp. 1564–1567.

[167] Léon Van Hove. "Sur l'intégrale de configuration pour les systèmes de particules à une dimension". In: *Physica* 16.2 (1950), pp. 137–143.

[168] Cécile Viboud et al. "The RAPIDD ebola forecasting challenge: Synthesis and lessons learnt". In: *Epidemics* 22 (2018), pp. 13–21.

[169] Soroush Vosoughi, Deb Roy, and Sinan Aral. "The spread of true and false news online". In: *Science* 359.6380 (2018), pp. 1146–1151.

[170] Steven Waldman. *Information needs of communities: The changing media landscape in a broadband age*. Diane Publishing, 2011.

[171] Joseph F Wamala et al. "Ebola hemorrhagic fever associated with novel virus strain, Uganda, 2007–2008". In: *Emerging infectious diseases* 16.7 (2010), p. 1087.

[172] Chia C Wang et al. "Airborne transmission of respiratory viruses". In: *Science* 373.6558 (2021), eabd9149.

[173] Duncan J Watts and Steven H Strogatz. "Collective dynamics of 'small-world'networks". In: *nature* 393.6684 (1998), pp. 440–442.

[174] Christopher JM Whitty et al. "Infectious disease: tough choices to reduce Ebola transmission". In: *Nature News* 515.7526 (2014), p. 192.

[175] World Health Organization (WHO). *Coronavirus disease (COVID-19)*. URL: https://www.who.int/emergencies/diseases/novel-coronavirus-2019/question-and-answers-hub/q-a-detail/coronavirus-disease-covid-19. (accessed: 03/10/2021).

[176] World Health Organization (WHO). *Ebola virus disease*. URL: https://www.who.int/news-room/fact-sheets/detail/ebola-virus-disease. (accessed: 19/09/2021).

[177] Report of a WHO/International Study Team et al. "Ebola haemorrhagic fever in Sudan, 1976". In: *Bulletin of the World Health Organization* 56.2 (1978), p. 247.

[178] Edwin B Wilson and Jane Worcester. "The law of mass action in epidemiology". In: *Proceedings of the National Academy of Sciences of the United States of America* 31.1 (1945), p. 24.

[179] Luzie U Wingen, James KM Brown, and Michael W Shaw. "The population genetic structure of clonal organisms generated by exponentially bounded and fat-tailed dispersal". In: *Genetics* 177.1 (2007), pp. 435–448.

[180] ZSY Wong et al. "A systematic review of early modelling studies of Ebola virus disease in West Africa". In: *Epidemiology & Infection* 145.6 (2017), pp. 1069–1094.

[181] Fang Wu and Bernardo A Huberman. "Novelty and collective attention". In: *Proceedings of the National Academy of Sciences* 104.45 (2007), pp. 17599–17601.

[182] JoAnne Yates. “The telegraph’s effect on nineteenth century markets and firms”. In: *Business and economic history* (1986), pp. 149–163.

[183] Na Zhu et al. “A novel coronavirus from patients with pneumonia in China, 2019”. In: *New England journal of medicine* (2020).

Estimating the effect of coordinating lockdowns betweeen recurring SARS CoV-2 outbreaks

Gustav S. Halvorsen[1,*]

[1]Copenhagen University, Niels Bohr Institute, Blegdamsvej 17, 2100 Copenhagen, Denmark

ABSTRACT

The ongoing SARS-CoV-2 pandemic has prompted governments around the world to lockdown society. Suppression and mitigation strategies have nonetheless varied considerably within and among countries. This work estimates the effects of synchronizing lockdowns between jurisdictions hit by recurring infectious disease outbreaks. It is shown that a coordinated strategy is likely better at postponing susceptible depletion using the same amount of disposable resources.

1 Introduction: SARS-CoV-2 pandemic

The SARS-CoV-2 pandemic has upended life worldwide and prompted governments to enact stay-at-home orders, closing schools, non-essential shops, and public places. Strategies to control an infectious disease outbreak have been studied extensively. Ferguson et al. showed how a nascent influenza pandemic could be contained using a combination of pharmaceutical interventions and social distancing measures[1].

Lockdowns were put in place to slow the spread of disease and prevent intensive care units from overflowing with patients as neither vaccines nor antiviral drugs were available at the outset of the pandemic.[2–5]. Handel et al. proposed an optimal control strategy for multiple infectious disease outbreaks that minimize overshooting[6]. However, the current pandemic affects many different jurisdictions that do not necessarily follow the same containment policy. The response to SARS-CoV-2 in the United States was characterized by significant variation across state lines. England enforced localized, tiered restrictions in an attempt to control a second wave, which was found to be less effective than a national lockdown[7]. Denmark restricted the movement of citizens in 7 municipalities between November 5-19, 2020, to thwart a novel spike mutation (cluster 5 variant)[8]. Findings by Ruktanonchai et al. suggest that coordinating lockdowns increased the likelihood of eliminating community transmission in Europe and that fewer lockdown periods would be necessary to end continent-wide community transmission[9].

Here a simple epidemic model is used to explore the effects of coordinating intermittent lockdowns between jurisdictions that experience multiple unsynchronized epidemic waves. The idea is to simulate the model with unsynchronized lockdown (**UL**) and synchronized lockdown (**SL**) for a range of parameters to compare outcomes.

2 Model

Two related suppression strategies shall be considered.

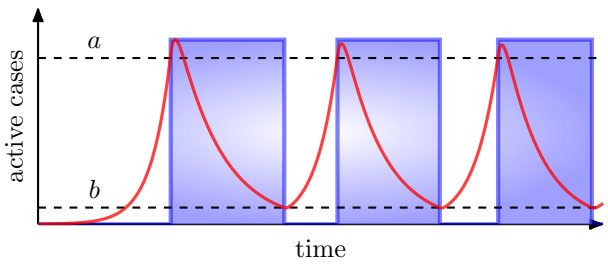

Figure 1. Sketch of the lockdown mechanism. **UL** activates a lockdown when cases surpass a. The contact rate β is reduced by a factor of $(1-s)$ while lockdown is activated. The lockdown is annulled when cases drop below b. **SL** activates lockdown if just one jurisdiction surpasses a and undo the policy only when all jurisdictions have below b cases. The latent period causes the epidemic waves to peak above a.

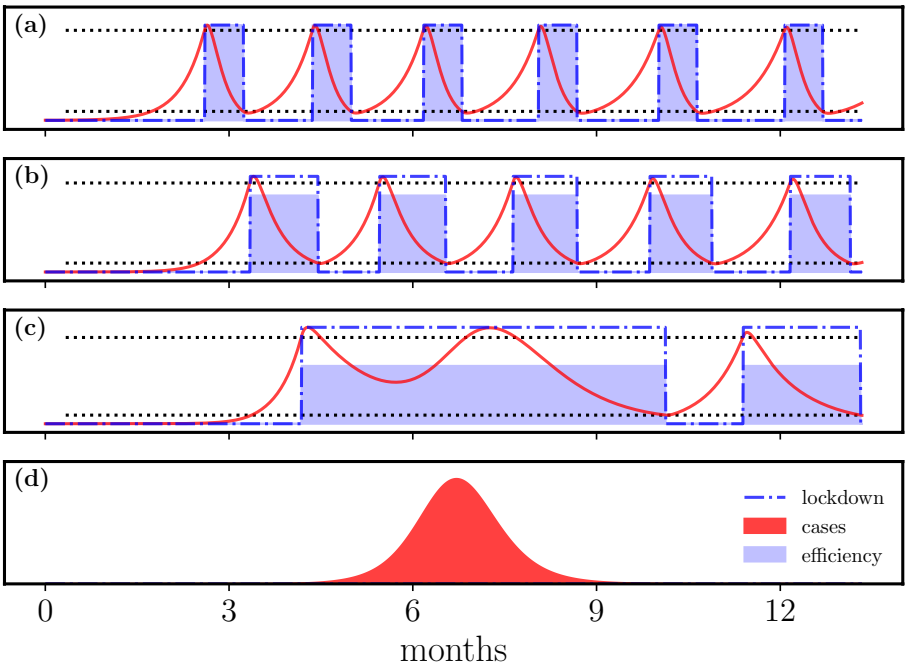

Figure 2. Disease transmission between 4 jurisdictions. Each jurisdiction is executing its own suppression policy with decreasing commitment from top to bottom. The top panel (a) does a draconian lockdown that nullifies transmission. (b) is using a hard lockdown with 80% efficiency. (c) is using a soft lockdown with a 60% efficiency. The bottom panel (d) is not doing lockdown. Cross-transmission from (d) is causing a surge of cases in (c) despite being in lockdown. Initial conditions are $I_a(t_0) = 1$ and the remaining population is susceptible at $t = t_0$. Each jurisdiction contains $N = 100.000$ persons. Model parameters: $R_0 = 2.0, \sigma = 1/5$, $\gamma = 1/4$, $g_{ab} = g_{bc} = g_{cd} = 0.01$ and $g_{dc} = 0.05$. Lockdown parameters: $a = 500$, and $b = 50$.

Unsynchronized lockdown **(UL)** is activated in i when cases in $I_i(t)$ exceed a and anulled when cases drop below b. Mathematically, we can write this as a sequence of dynamic boundary conditions. If lockdown is not active then $\beta_i = \beta$ while $a \geq I_i(t)$ until $a < I_i(t)$ at which instant lockdown becomes active and $\beta_i = \beta(1 - s_i)$. Then $\beta_i = \beta(1 - s_i)$ while $I_i(t) \geq b$ until $I_i(t) < b$ at which point lockdown is no longer active and $\beta_i = \beta$.

Synchronized lockdown **(SL)** follow the same rule but is activated in **all** jurisdictions if cases in just one of them exceed a and undone only when cases in **all** them drops below b.

Closing and re-opening parameters could vary between jurisdictions using **UL**. The risk of depleting critical care capacity has been widely used to support lockdown. Substantial variability exists in the number of intensive care beds even among wealthy nations[10]. The effect of lockdowns s_i also varies depending on compliance and rigor. A soft lockdown may entail closing schools, public places, and limits on gatherings, while a hard lockdown breaks down contact between people by forcing them to shelter in place. Estimates suggest a reduction in transmission by around 60-80 % can be expected[3,11].

2.1 coupled susceptible-exposed-infected model

Let us consider transmission inside and between n jurisdictions, each according to a susceptible-exposed-infected model with a small amount of cross-transmission between them.

$$\frac{dS_i}{dt} = -(1 - \sum_j g_{i,j})\beta_i I_i S_i - \sum_i g_{i,j}\beta_i S_i I_j, \tag{1}$$

$$\frac{dE_i}{dt} = (1 - \sum_j g_{i,j})\beta_i I_i S_i + \sum_i g_{i,j}\beta_i S_i I_j - \sigma E_i, \tag{2}$$

$$\frac{dI_i}{dt} = \sigma E_i - \gamma I_i. \tag{3}$$

Here the sum is over n jurisdictions interacting through a coupling matrix $g_{i,j}$. The coupling matrix $g_{i,j}$ gives the cross-transmission from one jurisdiction to another. The first term in the system above gives the transmission within i. The second term gives the transmission from other jurisdictions to i. The sum $\sum_j g_{i,j}$ gives the net contact rate out of i to other jurisdictions.

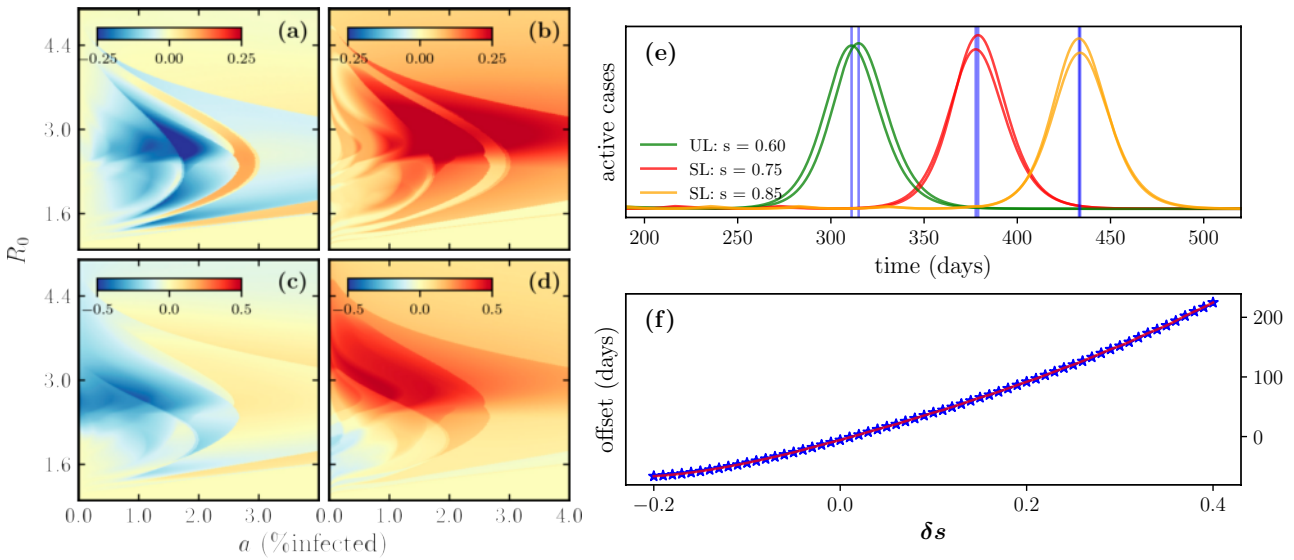

Figure 3. Disparities between the two strategies. Here **SL** performs better in blue and worse in red. (a) show the difference in attack rate between the two strategies after one year of transmission. (b) shows the difference in lockdown time measured as a fraction of one year. Each jurisdiction contains $N = 100.000$ persons. Model parameters: $\sigma = 1/3.69$, $\gamma = 1/3.48$, and $g_{1,2} = g_{2,1} = 0.01$. Lockdown parameters: $b = 0.1 \cdot a$, and $s = 0.6$. Bottom panel (c) and (d) shows the simulations with reduced effectiveness for **UL** decreased to $s = 0.5$. (e) show 3 simulations with a limit on lockdown time equal to 160 days. (f) shows the effect of varying s for **SL** on peak seperation. Effectiveness of **UL** is kept constant at $s = 0.6$. Model parameters for (e) and (f) are $R_0 = 2.0$, $a = 100$, $b = 10$, and otherwise equal to those above.

This value is subtracted from the transmission rate within i. Each jurisdiction contains the same number of persons N. The disease cannot go extinct owing to the continuous nature of the model. Onward transmission persists until susceptible depletion.

3 Model analysis and results

The ordinary differential equations (ODE's) are solved numerically with the suppression strategies as dynamic boundary conditions. Figure 2 shows transmission between $n = 4$ jurisdictions using **UL**. The effectiveness of lockdown varies, as shown by the blue filling. The jurisdiction in (d) has decided not to enact a lockdown but maintains a strong coupling to (c), which further drives transmission since lockdown here otherwise barely keeps R_0 below the epidemic threshold. Re-directing this coupling to (a) has no effect, and the effect on (b) is negligible. This finding would suggest that border closings are less pertinent if a hard lockdown is in effect. However, if only a soft lockdown is in effect, one should be more cautious about links to a large transmission cluster.

3.1 model's parameter space

The model is simulated on various parameters to measure performance on attack rate and time spend in lockdown. This analysis seeks to find variations in outcomes between the two suppression strategies. Here we consider transmission between two jurisdictions connected by a reciprocal coupling $g_{ij} = g_{ji} = 0.01$ to keep things as simple as possible. The latency σ^{-1} and infectious periods γ^{-1} are set to 3.69 and 3.48 days, respectively[12]. The transmission rate β and the lockdown trigger a, and b are free parameters. Lockdown is set to reduce transmission β by 60%. Figure 3 shows the output of simulations after one year of transmission. Here the horizontal axis shows the activation threshold a; b is set to 10% of this value, so cases must drop one order of magnitude below a to de-activate the lockdown. The vertical axis shows R_0 which reduces to $\frac{\beta}{\gamma}$ without vital dynamics. Fig. 3 (a) shows the difference in attack rate between the two strategies after one year. **SL** performs better in the blue and worse in the red. Fig. 3 (b) shows the difference in lockdown time measured as a fraction of the one-year simulation time.

UL generally gives a lower attack rate in exchange for a longer lockdown. It is not surprising that longer lockdowns tend to yield fewer cases, but there are some exceptions to this rule that we will return to. In practice, however, it may be more difficult to implement **UL** at a local level. It also opens up the possibility that persons from municipalities under lockdown carry on social activities in other places. Davies et al. found regional lockdowns to be less effective than a national lockdown in England[7]. While **UL** has increased flexibility over **SL**, it is likely not as effective at reducing the contact rate. The bottom

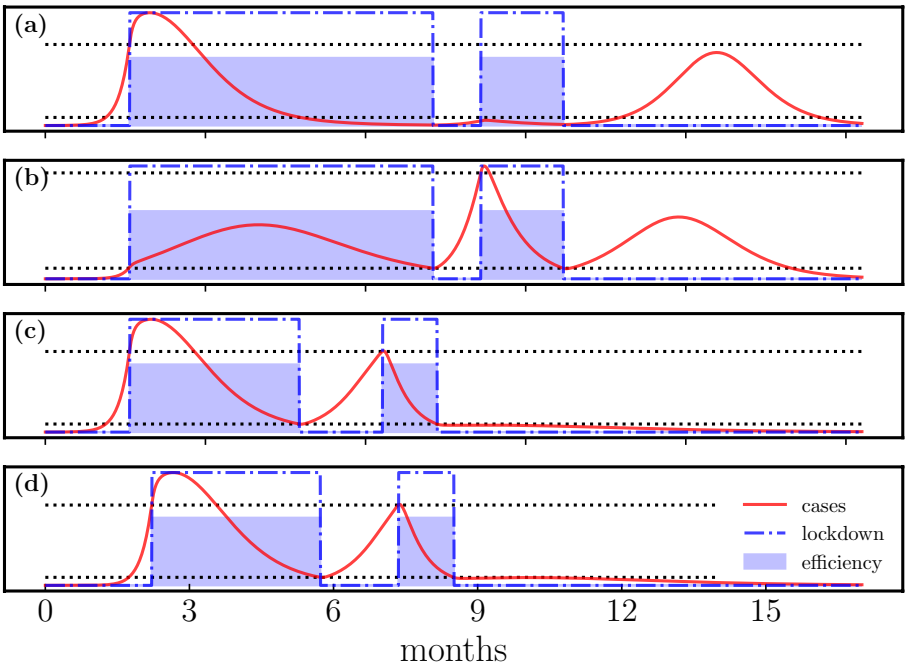

Figure 4. Top panels (a-b) show a simulation with **SL**. Overshooting is not minimized on the last wave as infection peaks just below a. Bottom panels (c-d) show the simulation with **UL**. Each jurisdiction contains $N = 100.000$ persons. Model parameters are $R_0 = 3.0$, $\gamma = 1/4$, $\sigma = 1/5$, and $g_{12} = g_{21} = 0.01$. Lockdown parameters: $a = 2100$, $b = 210$, and $s = 0.4$. Failure to minimize overshoot can also occur for **UL** depending on the input parameters.

panel (c) and (d) shows the simulations repeated but with effectiveness for **UL** decreased to $s = 0.5$. Here **SL** performs better and can repress transmission with greater R_0. Lockdown time is even higher now compared to **UL** for large R_0 because **UL** is unable to stop transmission. Susceptible depletion takes place early, resulting in less lockdown time at the cost of more cases. Unfortunately, the problem of weighing lockdown duration against attack rate persists. It is possible to overcome this problem by giving each municipality a maximum of 160 lockdown days and measure how long the two strategies can delay susceptible depletion. Lockdown is immediately de-activated when the 160 days have been spent. Fig. 3 (e) shows this for 3 simulations. Here **UL** is used as a reference with $s = 0.6$ and the effectiveness of **SL** is varied. Fig. 3 (f) shows the average peak separation as a function of δs. **UL** is slightly better at parity $\delta s = 0$. However, if $\delta s = 0.2$, then **SL** delays susceptible depletion for about 100 days more using the same amount of lockdown time. The effect of varying a and b on peak separation was small compared to s.

3.2 catastrophic overshooting

Figure 3 show that longer lockdown does not necessarily correlate with a lower attack rate—the red trajectory in (a-b) has a moderately higher attack rate despite a longer lockdown period. This effect is a result of the strategy failing to minimize overshoot. Overshooting is the excess infections that occur leading up to herd immunity. The effective reproduction number R_{eff} drops as the susceptible population is depleted. The infectious curve peaks when R_{eff} is one; from this point onward, the expected number of cases generated by each infection is equal to or less than one. The number of infected is maximum, so cases continue to pile up absent any effort to control the pandemic. These excess infections can be prevented with interventions to curb transmission temporarily. We arrive at herd immunity in both scenarios, but the latter's final attack rate is minimized. Recurring outbreaks are not possible if lasting immunity is gained from infection. This assumption is especially problematic concerning SARS-CoV-2 as the mutation of new variants is driven by a vast global reservoir.

SL and **UL** can fail to minimize overshooting because of the intransigent lockdown condition. Fig. 4 shows an example of this error. The top panels (a-b) show transmission between two jurisdictions using **SL**. The last waves are just below the threshold for lockdown activation, so the overshoot is not minimized on the final waves. The bottom panels (c-d) show the simulation repeated with **UL**. Here the epidemic is much faster but overshooting is minimized over the entire epidemic. **SL** performs worse on cases and significantly worse on lockdown time. Nonetheless, **SL** is generally better at delaying susceptible depletion given the same amount of lockdown time, assuming it is slightly more effective.

4 Discussion and summary

Outbreaks of novel infectious diseases pose a threat to global public health. Control strategies can blunt the impact. These efforts to control transmission are only temporary. Delaying transmission of SARS-CoV-2 by lockdown or contact tracing does not prevent outbreaks from erupting once infection controls are lifted. While, in theory, it is possible to eradicate SARS-CoV-2 with lockdown, these would need to be synchronized worldwide and maintained for very long, which is not realistic. In practice, some form of herd immunity through vaccination or infected persons recovering with immunity is the only way to prevent recurring outbreaks of an infectious disease that has escaped early containment.

This work suggests that **SL** is likely better at postponing susceptible depletion, while **UL** is better at minimizing overshooting using minimal lockdown time. **SL** is, therefore, promising if the goal is to postpone susceptible depletion until a vaccine becomes available. **UL** may be better if, for whatever reason, a vaccine is not possible to make in the foreseeable future, and the aim is to minimize overshooting with the fewest possible resources. The effort to quickly discover and distribute a COVID-19 vaccine has been an unprecedented success. It is, however, not clear from the onset of a novel infectious disease outbreak how long it takes to find a vaccine or whether it is possible to do so. Nor is not known how long intermittent lockdowns can be sustained before civil disobedience ensues. Maintaining social distancing for many years would likely not have been feasible if initial efforts fail to produce a safe and effective vaccine. Minimizing overshoot and expanding intensive care capacity to prevent overflow of critical cases may be better if it is impossible to delay transmission until a vaccine becomes available. However, allowing a significant fraction of a population to be infected entails more deaths and unknown risks. Some recovering COVID-19 patients show signs of chronic illness and cognitive impairment, a condition known as Long COVID. It is unknown if this condition is permanent, but it will be very costly if so.

It should be stressed that lockdown, coordinated or not, is an emergency brake to be used only when other options are unavailable. Being better prepared for future pandemics is better than having to close down society.

4.1 Acknowledgements

Thanks to Kim Sneppen for comments and feedback. This project has received funding from the European Research Council (ERC) under the European Union's Horizon 2020 research and innovation program under grant agreement No [740704].

Additional information

The author declare no competing interests.

References

1. Ferguson, N. M. *et al.* Strategies for containing an emerging influenza pandemic in southeast asia. *Nature* **437**, 209–214 (2005).
2. Ferguson, N. M. *et al.* Impact of non-pharmaceutical interventions (npis) to reduce covid-19 mortality and healthcare demand. 2020. *DOI* **10**, 77482 (2020).
3. Flaxman, S. *et al.* Estimating the effects of non-pharmaceutical interventions on covid-19 in europe. *Nature* **584**, 257–261 (2020).
4. Brauner, J. M. *et al.* Inferring the effectiveness of government interventions against covid-19. *Science* **371** (2021).
5. Hsiang, S. *et al.* The effect of large-scale anti-contagion policies on the covid-19 pandemic. *Nature* **584**, 262–267 (2020).
6. Handel, A., Longini Jr, I. M. & Antia, R. What is the best control strategy for multiple infectious disease outbreaks? *Proc. Royal Soc. B: Biol. Sci.* **274**, 833–837 (2007).
7. Davies, N. G. *et al.* Association of tiered restrictions and a second lockdown with covid-19 deaths and hospital admissions in england: a modelling study. *The Lancet Infect. Dis.* **21**, 482–492 (2021).
8. Assessment, R. R. Detection of new sars-cov-2 variants related to mink. *Eur. Cent. Dis. Prev. Control.* (2020).
9. Ruktanonchai, N. W. *et al.* Assessing the impact of coordinated covid-19 exit strategies across europe. *Science* **369**, 1465–1470 (2020).
10. Rhodes, A. *et al.* The variability of critical care bed numbers in europe. *Intensive care medicine* **38**, 1647–1653 (2012).
11. Kissler, S. M., Tedijanto, C., Goldstein, E., Grad, Y. H. & Lipsitch, M. Projecting the transmission dynamics of sars-cov-2 through the postpandemic period. *Science* **368**, 860–868 (2020).
12. Li, R. *et al.* Substantial undocumented infection facilitates the rapid dissemination of novel coronavirus (sars-cov-2). *Science* **368**, 489–493 (2020).

Spatial model of Ebola outbreaks contained by behavior change

G. S. Halvorsen [1], L. Simonsen [2], K. Sneppen [1],

1 Niels Bohr Institute, Blegdamsvej 17, 2100 Copenhagen, Denmark
2 Department of Science and Environment, Roskilde University, Roskilde, Denmark

* sneppen@nbi.ku.dk

Abstract

The West African Ebola (2014-2016) epidemic caused an estimated 11.310 deaths and massive social and economic disruption. The epidemic was comprised of many local outbreaks of varying sizes. However, often local outbreaks recede before the arrival of international aid or susceptible depletion. We modeled Ebola virus transmission under the effect of behavior changes acting as a local inhibitor. A spatial metapopulation model is used to simulate Ebola epidemics. Our findings suggest that behavior changes can explain why local Ebola outbreaks recede before substantial international aid was mobilized during the 2014-2016 epidemic.

1 Introduction

The West African Ebola epidemic was the deadliest outbreak of Ebola virus disease reported to this date. On March 23, 2014, local authorities notified the World Health Organization of an Ebola virus outbreak in southern Guinea. The virus quickly spread to neighboring countries, Liberia and Sierra Leone, causing a net count of 28.616 infections and 11.310 fatalities before ending in June 2016 [1]. The unprecedented scale of the epidemic resulted from dysfunctional healthcare systems, low trust in government following years of armed conflict, and a slow response to the crisis [2]. Risky cultural practices also compounded the severity of the outbreak, particularly burial rites that involve close contact with deceased Ebola patients.

Fig. 1 shows the cumulative number of confirmed or probable cases at the district level in Guinea. The time-series begin on January 5, 2014, ends on May 8, 2016, and advances in weekly increments. The outbreak originated in Guinea, in the Guéckédou prefecture, and quickly spread to Liberia and Sierra Leone. On August 8, 2014, several months after its beginning, the World Health Organization declared the outbreak in West Africa a Public Health Emergency of International Concern. On September 18, 2014, the United Nations established The United Nations Mission for Ebola Emergency Response (UNMEER). The West African Ebola epidemic was declared over by the World Health Organization on June 9, 2016.

The local outbreaks in Fig. 1 terminate at different times and the whole epidemic ends long before susceptible depletion. Before the United Nations convened to form UNMEER, many local outbreaks, including the outbreak in the Guéckédou prefecture where the epidemic originated, had already ceased. Naive epidemic theory predicts that onward transmission continues in the absence of interventions (e.g., contact tracing, isolation, or immunization) until herd immunity is reached. It is unclear if interventions

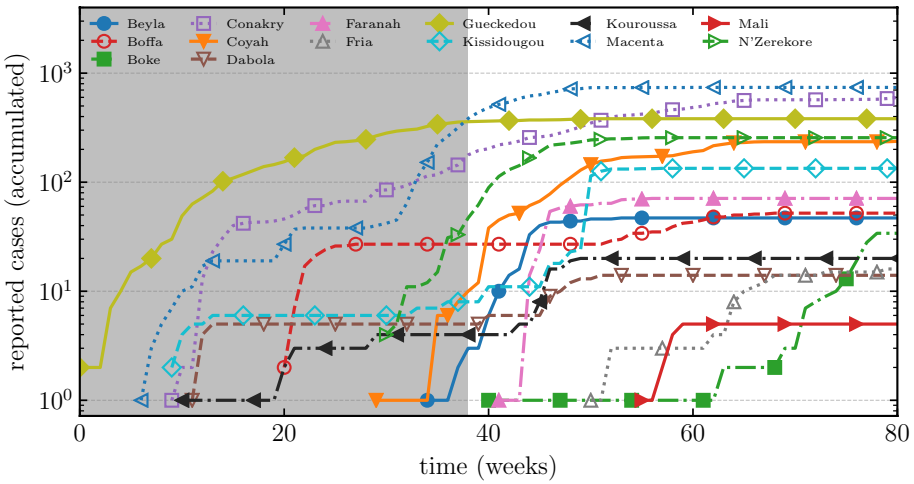

Fig 1. Ebola virus epidemic in Guinea. Shows the cumulative number of confirmed or probable cases at the district level. The time series begins on January 5, 2014, ends on May 8, 2016, and advances weekly increments. On August 8, 2014, several months after its beginning, the World Health Organization declared the outbreak in West Africa a Public Health Emergency of International Concern. On September 18, 2014, the United Nations established The United Nations Mission for Ebola Emergency Response (UNMEER). The grey shaded regions show the time before the creation of UNMEEER. Guinea was declared free of Ebola by the World Health Organization on June 1. We also show epidemic curves for 14 of 33 Guinean prefectures. The outbreak originated in the Guéckédou prefecture and quickly spread to Conakry, the capital city. Data from the World Health Organization.

or susceptible depletion can explain the abrupt termination of local outbreaks. Despite the large size of the outbreak compared to previous sporadic outbreaks of Ebola virus disease (EVD) in Sub-Saharan Africa, the total number of cases was also small compared to model projections [3]. Merler et al. modeled the spatial spread of Ebola virus disease in Liberia (2014) and concluded that Ebola treatment units (ETUs), safe burial procedures, and household protection kits explain the decrease in incidence [4,5]. Here we explore an alternate hypothesis; that behavior changes explain the surprisingly small number of cases.

1.1 Human behavior and the 2014 West Africa Ebola Outbreak

Ebola virus disease is transmitted by direct physical contact with infected bodily fluids [6]. According to the World Health Organization, avoiding direct contact with people who show Ebola symptoms reduces transmission. Asymptomatic infections are rare [7], suggesting that social distancing and isolation are effective in reducing the risk of human-to-human transmission. Burial rites are also a strong driver of Ebola transmission. Previous outbreaks in the Democratic Republic of Congo (DRC) and Uganda have shown that unsafe burial practices linger unless infection-control measures are adapted to local traditions [8]. Nonetheless, the 2014-2016 Ebola epidemic was massive compared to previously known outbreaks. An observational study found that of the cases exposed during funerals, 65% of those giving a response reported having touched the corpse. This proportion declined significantly after October 2014, suggesting that behavior changes had taken place [9]. Estimates of R_0 during the 2014-2016 Ebola

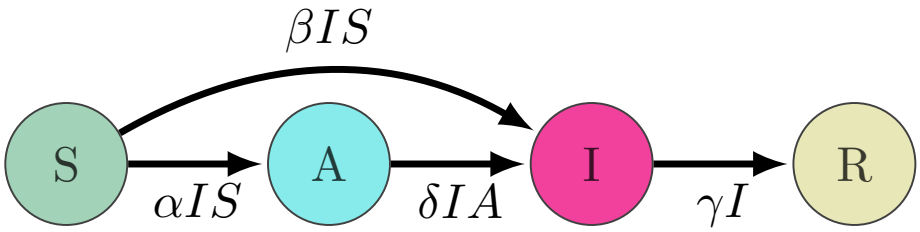

Fig 2. Diagram of the compartmental model. β is the contact rate, and γ is the rate of recovery. α is the rate of behavior change, and δ is the contact rate in the aware population.

epidemic in West Africa are low, ranging between 1.2 and 2.2 [10]. Hence, a moderate reduction in transmissibility is sufficient to push R_0 below the epidemic threshold [11].

It should be emphasized that the behavior changes mentioned above (i.e., avoiding direct contact with people who show Ebola symptoms, self-isolating, and not touching the corpse during a funeral or attending the ceremony) can occur autonomously. Findings by Drake et al. suggest behavior changes decreased the effective reproductive number in Liberia to almost one and that interventions further brought it down below the epidemic threshold [12]. Another study by Funk et al. found that healthcare-seeking behavior doubled throughout the outbreak in Lofa county, Liberia, but this was also linked to increased transmission inside treatment facilities [13]. The RAPID Ebola forecasting challenge compared the performance of eight independent modeling approaches on synthetic data and found that the top-performing models for short-term weekly incidence used reactive behavior changes [14].

2 Model

Consider the following system of ordinary differential equations (ODE's). Each equation represents a compartment of susceptible, aware, infectious, or removed agents [15].

$$\frac{dS}{dt} = -\beta IS - \alpha IS \tag{1}$$

$$\frac{dA}{dt} = \alpha IS - \delta AI, \tag{2}$$

$$\frac{dI}{dt} = \beta IS + \delta AI - \gamma I, \tag{3}$$

where β is the contact rate, and γ is the rate of removal. α is the rate of behavior change, and δ is the contact rate for aware individuals. A is assumed to grow by a rate that is proportional to I, meaning that only symptomatic carriers can spread awareness.

Spatial heterogeneity was a distinguishing feature of the 2014-16 Ebola epidemic. However, the mean-field model above assumes homogeneous mixing. The West African Ebola epidemic has been the subject of many spatial modeling studies [4, 16–20]. Funk et al. showed that the impact of behavior change is more pronounced in the presence of spatial structure [21]. The tendency of local Ebola outbreaks to flare up and subside quickly suggests the epidemic could be locally self-organized. To explore this possibility, we will consider a spatial version of the mean-field model.

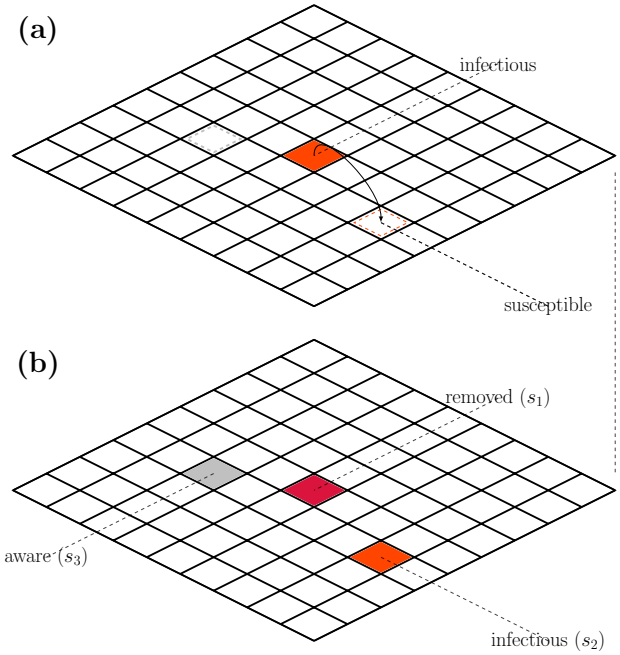

Fig 3. Diagram of the spatial model. Each site on the grid contains just one person. A small grid is with one infectious person in the center. (a) the infected person spreads disease and awareness to nearby squares. The transitions occur with probability β and α, respectively. The infected cell is removed with probability γ. (b) shows the updated state-space on the grid.

2.1 Stochastic lattice model

The spatial model is defined on a $L \times L$ lattice where one person occupies each site. A grid cell is either susceptible S, infectious I, aware A or removed R. Grid cells on the lattice are initialized in the susceptible state with a small number of infected sites to start the epidemic. Simulations run until infected have been removed. An asynchronous updating scheme is used with $\Delta t = 1.0$ day equal to L^2 updates. Do the following to perform an update.

a: Select a random grid cell s_1. If s_1 is infected then proceed to (b). Else proceed to (c).

b: **1)** Select another site s_2. This site is chosen randomly on the lattice with probability p. Else with probability $1 - p$, select s_2 with a probability that decays exponentially with distance from s_1. To be explicit, select a distance d with probability $\propto \exp(-d/\lambda)$ and choose a random point s_2 at this distance.
2) If s_2 is susceptible, it is infected with probability $\beta\Delta t$. Else if s_2 is aware, it is infected with probability $\delta\Delta t$.
3) Select another cell s_3 as above. If s_3 is susceptible, is becomes aware with probability $\alpha\Delta t$.

c: s_1 is removed with probability $\gamma\Delta t$.

The extended model contains two spatial parameters, p, and λ in addition to the rate parameters α, β and γ. There is a probability of selecting identical targets during an update i.e., $s_2 = s_3$. Since the reactions $S \xrightarrow{\beta} I$ and $S \xrightarrow{\alpha}$ A are mutually exclusive, it

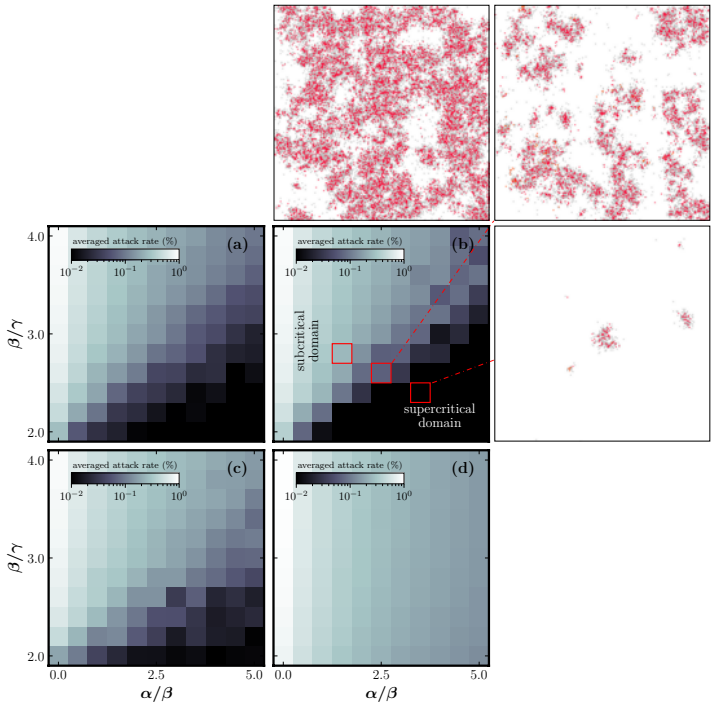

Fig 4. Phase diagram of the spatial model. The color shows the final attack rate (%). Outbreaks are controlled in the dark domain but spread unhindered in the light domain. (a) shows the spatial model on a 100×100 grid with $\delta = 0$, $p = 0.01$ and $\lambda = 2.0$. (b) is simulated on a 200×200 grid, but otherwise identical to (a). Representative spatial configurations are shown for selected parameters, where all infected have been removed. White grid cells are susceptible; grey cells are aware; red cells are removed. (c) Explores the effect of some susceptibility in the aware state, using $\delta/\gamma = \frac{1}{2}$ with other parameters as in (a). (d) Homogeneous mixing with $p = 1$, and otherwise identical to (a)

should be specified what happens in this event. Here we allow the reaction $S \xrightarrow{\beta} I$ to happen first. It is also possible to pick randomly between the two reactions, but the effect is completely negligible unless α and β are large. Global and local transmission allow for dispersal on different length scales. The effect of global transmission events is to seed spatially disassociated transmission clusters, which made up the epidemic in West Africa 2014-16 [22]. The previous known Ebola outbreaks have generally been localized, so this is a novelty. The effect of long-distance dispersal on epidemics has been studied by Shaw et al. [23,24]. For $p \sim 1$ or $\lambda \sim L$ we recover homogeneous mixing equivalent to the mean-field model.

3 Analysis

Fig. 4 explores the effect of awareness transmission and idealized reproductive number. Successful spreading is a stochastic phenomenon, and many outbreaks die out early by chance [25]. The extinction probability is large when $I(0) = 1$ so we initiate our simulations with a cluster of $I(0) = 16$ infected sites placed in the center. To estimate the attack rate in Fig. 4 we average over many simulations.

Outbreak size measured by the final attack rate increases with β/γ and decreases with α/β. The subcritical domain is carved out by the space of parameters where the

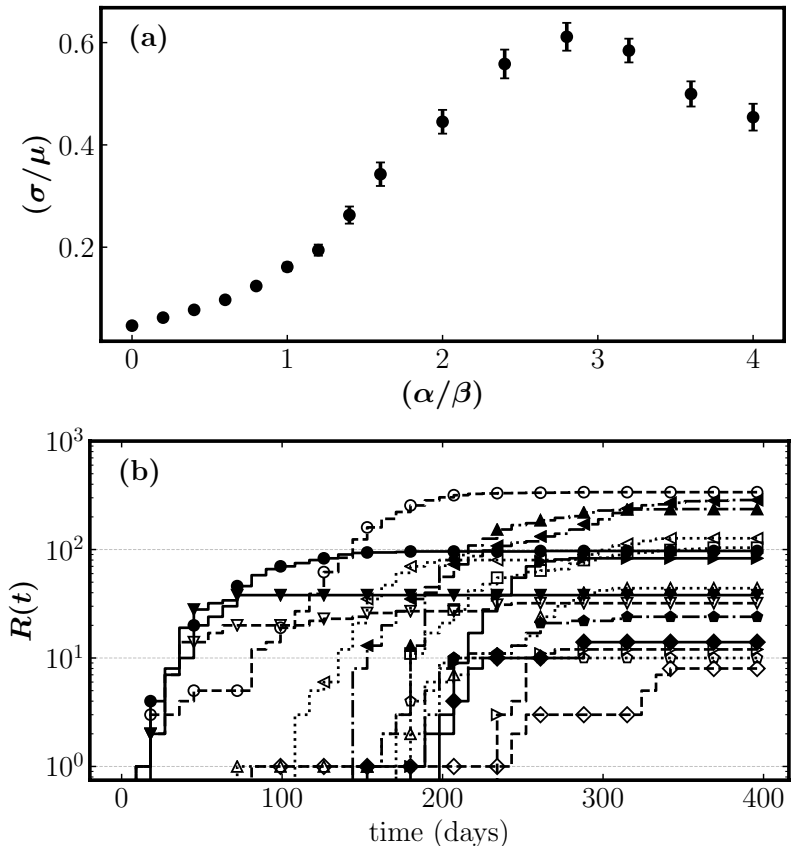

Fig 5. (a) shows the coefficient of variation c_v between the subgrids for increasing α. Model parameters: $\beta = 0.25$, $\gamma = 0.10$, $\delta = 0$, and $p = 0.01$. The scale parameter in the exponential distribution was 2.0. (b) shows cumulative cases $R(t)$ for each subgrid in a simulation around criticality $\alpha = 0.70$ with parameters as above.

disease is not contained. Outbreaks are rapidly enclosed by awareness in the supercritical domain. Fig. 4 (a) and (b) suggest that system size has a negligible effect. The attack rate is scale-invariant in the subcritical domain because the cluster is spanning the whole lattice. Scale-invariance is broken in the supercritical domain as the cluster grows to a finite size before it is enclosed by awareness. Here it is possible to reduce the attack rate by scaling the system.

Panel (c) shows the effect of $\delta > 0$, which is moderate provided that δ is not increased above the critical value where transmission is sustainable in a fully aware population.

Panel (d) reveals the absence of a supercritical state in a well-mixed system. It is no longer possible for awareness to spread around and enclose a cluster of infected cells; therefore, it does not affect the epidemic threshold [21]. The effect of susceptible depletion is also decreased as infected grid cells face much less intraspecific competition.

3.1 Heterogeneity measures

The fuzzy boundary between the sub and supercritical domain is particularly interesting. The epidemic can often seed multiple spatially dissociated transmission

clusters before containment, resulting in a high degree of spatial heterogeneity. The size variation among the clusters can range from a few infected to clusters spanning the whole system. We explore this by dividing a 200×200 lattice into subgrids of 50×50 grid cells. Variations between the subgrids can be used to measure spatial heterogeneity. Fig 5 (a) shows the coefficient of variation c_v between the 16 subgrids. The dispersion is low before criticality; the cluster will span the whole lattice producing only minor variations between the subgrids. Spatial heterogeneity is maximized around criticality where some regions have massive outbreaks and others none at all. The region-to-region variability drops in the supercritical state where transmission is rapidly contained.

Fig 5 (b) shows the number of cases over time in each subgrid. Features are comparable to Fig 1 distinguished by subexponential growth and outbreaks of varying sizes that saturate rapidly before susceptible depletion.

4 Discussion

The model can explain the spatial patterns observed during the 2014-16 epidemic in Guinea. However, many assumptions have been made throughout the paper. The rate of behavior change α and its effect δ is not derived from data. More data is needed to understand the dynamic interplay between infection and human behavior. Evidence from the ongoing Sars-CoV-2 pandemic suggests that behavior changes have a significant effect on disease transmission. However, the risk of Ebola infection is likely to induce more drastic behavior changes than Sars-CoV-2, given the vast discrepancy in the case fatality ratio. Data concerning Ebola-related behavior change is limited. It is known that participation in risky funerals declined over time in Guinea, Liberia, and Sierra Leone. The International Ebola Response Team further found that this decline was positively correlated with the within-district transmission intensity, supporting the proposition that local prevalence drives behavior changes [9]. Awareness is more likely to be present in communities with either ongoing transmission or past exposure. However, awareness is expected to fade over time as the perceived risk of infection decreases. Our model does not contain a fading term, but adding one is not difficult. Glaubitz et al. found that this could cause oscillatory behavior in a homogeneous mixing model [26]. The presence of spatial structure should have a dampening effect on such oscillations because different regions quickly come out of phase. If a localized outbreak ends and the remaining A states are returned to S states, there are no infected to spread the disease. It is, therefore, necessary to introduce the disease again, either through a global transmission event or by encroachment from another growing transmission cluster.

Precise estimates of the susceptibility of aware people δ are unnecessary; it suffices to show that the disease cannot survive in a fully aware population. Estimating δ is difficult because humans can exhibit a range of behaviors that produces a spectrum of A states with corresponding contact rates. However, it is possible to identify specific behaviors with a significant effect. Lagrand's model breaks the reproduction number down into components that can be ascribed to various settings, including community R_c, hospitals R_h, and funerals R_F [5]. The R_F component is driven by behavior and gives a lower bound on the effect of awareness. The weight carried by each of these terms can vary significantly between Ebola outbreaks, suggesting that δ is very outbreak-specific.

The spatial model is simulated on a grid with one idealized person in each grid cell. While this is not realistic, the effect of population density is unlikely to be profound. Hu et al. has estimated how contact rates scales with population density [27, 28]. However, symptomatic Ebola patients are likely to be bedridden during infection. Those most likely of exposure are caring family members, health care personal, or those attending funerals. Accordingly, the rates could be largely independent of population density.

The ongoing Sars-Cov-2 pandemic has shown us that variations in behavior explain

many differences between countries. Many factors influence how people respond, including the risk of infection, age, and compliance with public health guidelines. Nonetheless, the latter will carry more weight in countries with high trust in government. Ebola outbreaks have so far happened in countries where trust in government is low. Here the behavior response is more likely to be a local effect because people respond to community transmission more than recommendations from public health officials. We have shown how such a local behavior response can explain the abrupt termination of local outbreaks, as was observed during the 2014-2016 Ebola epidemic.

References

1. WHO Ebola Response Team. "Ebola virus disease in West Africa—the first 9 months of the epidemic and forward projections." New England Journal of Medicine 371.16 (2014): 1481-1495.

2. Piot, Peter. "Ebola's perfect storm." (2014): 1221-1221.

3. Lewnard, Joseph A., et al. "Dynamics and control of Ebola virus transmission in Montserrado, Liberia: a mathematical modelling analysis." The Lancet Infectious Diseases 14.12 (2014): 1189-1195.

4. Merler, Stefano, et al. "Spatiotemporal spread of the 2014 outbreak of Ebola virus disease in Liberia and the effectiveness of non-pharmaceutical interventions: a computational modelling analysis." The Lancet Infectious Diseases 15.2 (2015): 204-211.

5. Legrand, Judith, et al. "Understanding the dynamics of Ebola epidemics." Epidemiology & Infection 135.4 (2007): 610-621.

6. Rewar, Suresh, and Dashrath Mirdha. "Transmission of Ebola virus disease: an overview." Annals of global health 80.6 (2014): 444-451.

7. Glynn, Judith R., et al. "Asymptomatic infection and unrecognised Ebola virus disease in Ebola-affected households in Sierra Leone: a cross-sectional study using a new non-invasive assay for antibodies to Ebola virus." The Lancet infectious diseases 17.6 (2017): 645-653.

8. Whitty, Christopher JM, et al. "Infectious disease: tough choices to reduce Ebola transmission." Nature News 515.7526 (2014): 192.

9. International Ebola Response Team, et al. "Exposure patterns driving Ebola transmission in West Africa: a retrospective observational study." PLoS medicine 13.11 (2016): e1002170.

10. Butler, Declan. "Models overestimate Ebola cases." Nature News 515.7525 (2014): 18.

11. Funk, Sebastian, Gwenan M. Knight, and Vincent AA Jansen. "Ebola: the power of behaviour change." Nature 515.7528 (2014): 492-492.

12. Drake, John M., et al. "Ebola cases and health system demand in Liberia." PLoS Biol 13.1 (2015): e1002056.

13. Funk, Sebastian, et al. "The impact of control strategies and behavioural changes on the elimination of Ebola from Lofa County, Liberia." Philosophical Transactions of the Royal Society B: Biological Sciences 372.1721 (2017): 20160302.

14. Viboud, Cécile, et al. "The RAPIDD ebola forecasting challenge: Synthesis and lessons learnt." Epidemics 22 (2018): 13-21.

15. Kermack, William Ogilvy, and Anderson G. McKendrick. "A contribution to the mathematical theory of epidemics." Proceedings of the royal society of london. Series A, Containing papers of a mathematical and physical character 115.772 (1927): 700-721.

16. Lau, Max SY, et al. "Spatial and temporal dynamics of superspreading events in the 2014–2015 West Africa Ebola epidemic." Proceedings of the National Academy of Sciences 114.9 (2017): 2337-2342.

17. Kramer, Andrew M., et al. "Spatial spread of the West Africa Ebola epidemic." Royal Society open science 3.8 (2016): 160294.

18. Balcan, Duygu, et al. "Multiscale mobility networks and the spatial spreading of infectious diseases." Proceedings of the National Academy of Sciences 106.51 (2009): 21484-21489.

19. Kiskowski, Maria, and Gerardo Chowell. "Modeling household and community transmission of Ebola virus disease: epidemic growth, spatial dynamics and insights for epidemic control." Virulence 7.2 (2016): 163-173.

20. D'Silva, Jeremy P., and Marisa C. Eisenberg. "Modeling spatial invasion of Ebola in West Africa." Journal of theoretical biology 428 (2017): 65-75.

21. Funk, Sebastian, et al. "The spread of awareness and its impact on epidemic outbreaks." Proceedings of the National Academy of Sciences 106.16 (2009): 6872-6877.

22. Dudas, Gytis, et al. "Virus genomes reveal factors that spread and sustained the Ebola epidemic." Nature 544.7650 (2017): 309-315.

23. Shaw, M. W. "Simulation of population expansion and spatial pattern when individual dispersal distributions do not decline exponentially with distance." Proceedings of the Royal Society of London. Series B: Biological Sciences 259.1356 (1995): 243-248.

24. Wingen, Luzie U., James KM Brown, and Michael W. Shaw. "The population genetic structure of clonal organisms generated by exponentially bounded and fat-tailed dispersal." Genetics 177.1 (2007): 435-448.

25. Keeling, Matthew J., et al. "The effects of local spatial structure on epidemiological invasions." The Structure and Dynamics of Networks. Princeton University Press, 2011. 480-488.

26. Glaubitz, Alina, and Feng Fu. "Oscillatory dynamics in the dilemma of social distancing." Proceedings of the Royal Society A 476.2243 (2020): 20200686.

27. Hu, Hao, Karima Nigmatulina, and Philip Eckhoff. "The scaling of contact rates with population density for the infectious disease models." Mathematical biosciences 244.2 (2013): 125-134.

28. Borremans, Benny, et al. "The shape of the contact–density function matters when modelling parasite transmission in fluctuating populations." Royal Society open science 4.11 (2017): 171308.

Social contagion in a world with asymmetric influence

G. S. Halvorsen,* B. N. Pedersen, and K. Sneppen
Copenhagen University, Niels Bohr Institute, Blegdamsvej 17, 2100 Copenhagen, Denmark

(Received 8 July 2020; accepted 12 November 2020; published 3 February 2021)

Social media has blurred the distinction between news outlets and social networks by giving everyone access to mass communication. We simulate how influencers compete for attention on a social network by spreading information. The network structure occupies an ordered metastable state where one influencer maintains dominance for a sustained period or a fragmented state that divides attention between influencers. Numerical simulations are performed to map the domain of the ordered regime on various network topologies. Mutual coexistence between a few dominating influencers occurs on a scale-free social network. Our findings suggest the perception of fake news as a pervasive problem is endemic to a society where everyone can become a news outlet.

DOI: 10.1103/PhysRevE.103.022303

Social contagion processes have been simulated with local and reciprocal interactions between neighbors in a connected graph [1–5]. González-Avella *et al.* modeled the effect of mass media on the dissemination of culture [6–8]. Social media has disaggregated media influence by facilitating information sharing. Ordinary people can now communicate with unlimited subscribers, something previously reserved for news corporations. Members of a global social network can have as many subscribers as local newspapers or even large news corporations. We argue that users in a social network are now effectively news outlets, varying in size and impact. The capacity to interact with many is a defining property of the information age. The nature of this interaction is not reciprocal but directed; a collection of subscribers can receive information from a news outlet or an influencer, but there is no mutual exchange of information. Below, we simulate the emerging dynamics of a social network where any node can become an influencer and collect followers by sharing information. Our model integrates local reciprocal interactions between neighbors in a social network and global directed interactions between influencers and subscribers.

Before giving a formal description of the model, it is useful to describe its core mechanics in words. Consider a static undirected social network where nodes can be either followers or influencers. The topology of the social network has to be specified. A lattice is used to model the social network during the preliminary analysis, but other network topologies are considered toward the end. The basic idea is that influencers can build up a network of followers by sharing newsworthy information. Each follower is allowed to maintain only one directed link to an influencer at any point in time because attention is a finite resource [9]. Unlike the static links in the social network, these directed links can change ownership when a follower node decides to follow another influencer. Each node is assigned a news value τ, gauging its knowledge of current affairs. The network is updated in discrete steps. For each update, a random node a communicates with a random neighbor b in its social network. If b has a lower news value than a, then b unfollows its own influencer to follow a's influencer. If the neighbor b being attacked is an influencer, b will instead copy a's news value onto itself and its own followers.

Each node has a probability p_i of discovering a news event with every update. Galtung and Ruge [11] proposed a set of criteria known collectively as news values that influence the selection of published news. We quantify newsworthiness by assigning a news value of $\tau = t$ to a node that discovers a news event. Followers that discover news events are promoted to influencers. Influencers also update the news value of their subscribers to t upon discovering a news event. Recent news events are thus assigned a higher news value to ensure that new information takes precedence. The emergence and decay of novelty have been the subject of empirical and theoretical modeling studies [12–15].

Figure 1 shows the possible interactions on a simple lattice. Figure 1(a) shows the discovery of a news event followed by the capture of a node, and Fig. 1(b) shows how an influencer can immunize its followers by appropriating information.

I. MODEL

We consider N nodes connected by fixed links representing person to person communication in a static social network. A node can be either a follower f or an influencer S. Each node has a current information state τ that is equal to the time of origin of the last news update it has received. Furthermore, each node is assigned an index, $i, j, \ldots, n$, that shows which influencer it belongs to. This is just a way to keep track of different subcultures. For example, if an influencer $a_i \in S$ has index i, then all of its followers will inherit this index. The

*gustavhalvorsen@nbi.ku.dk

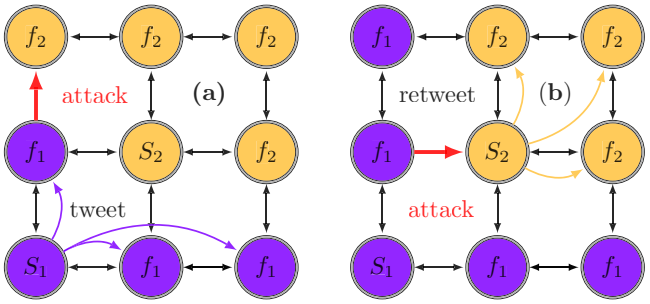

FIG. 1. Diagram of the model on a quadratic lattice. Each node represents a user on an undirected social network. Color and subscript indicate the follower's adherence to a news outlet. Panel (a) shows the discovery of a news event followed by the capture of a node. Panel (b) shows how an influencer (S_2) can immunize its followers by copying information.

probability that a node generates a news event is given by

$$p_i = \begin{cases} p_0(1+\eta k_i), & \text{influencer,} \\ p_0, & \text{otherwise,} \end{cases} \tag{1}$$

where k_i is the number of followers the influencer with index i presides over. Note that we define p_0 to be sufficiently small such that p_i never exceeds unity, i.e., $p_i = p_0(1+\eta k_i) \leqslant 1$. Here η is a positive feedback parameter between news generation and the number of subscribers [16]. Keep in mind that an influencer itself is a node and can therefore have no more than $N-1$ followers. Therefore, if $p_0 = 1/N$ and $\eta = 1.0$ then $p_i = \frac{1+(N-1)}{N} = 1$. To avoid p_i exceeding 1, we impose the following bounds, $\eta \leqslant 1$ and $p_0 \leqslant \frac{1}{N}$, on the model's parameters.

Time t is advanced by one increment $t \to t+1$ for each N updates performed on the system. To perform an update, do the following.

(i) Select a random node a. The chosen node discovers a news event with probability p_i if it is an influencer or p_0 otherwise. If a follower discovers a news event, it is promoted to an influencer, i.e., its state is changed from f to S, and it gains the news value $\tau = t$. If an influencer discovers a news event, it updates the news value of itself and its followers to $\tau = t$.

(ii) Proceed by selecting a random neighbor b to the node a. Let $\tau(a)$ and $\tau(b)$ be the news values of a and b, respectively. If b is not an influencer and $\tau(a) > \tau(b)$, then b adopts the news value $\tau(a)$ and begins to follow the same influencer as a. If b is an influencer and $\tau(a) > \tau(b)$, then b sets the news value of itself and its followers to $\tau(a)$.

The system is initialized at time $t = 0$ with all nodes occupying the follower state. These unclaimed followers have not been assigned a news value τ and can be captured as soon as a node discovers the first news event. News events that occur later on are assigned a higher news value because t increases as we perform more updates on the system. This mechanism is necessary to ensure that recent news events overwrite outdated ones. To prevent the system from freezing up with influencer nodes impervious to capture, we also demote influencers without any subscribers to the follower state. This is done whenever a full iteration of N updates has been performed. These demoted influencers are not following anything but can be absorbed by another subculture. As a result of this removal process, the number of influencers will eventually saturate around some steady-state value that depends on p_0 and N and on whether the system is ordered or fragmented.

II. RESULTS

Figure 2 show a simulation on a small system with a lattice topology and parameters $p_0 = 2.5 \times 10^{-4}$ and $\eta = 0.0$ over 1100 time step iterations. Figure 2(a) shows the size of each subculture. The system occupies a perpetually fragmented state in the absence of feedback. Heterogeneity in the distribution of newsworthy information drives the conflict between influencers. To quote William Gibson, "The future is already here—it's just not evenly distributed." An influencer must discover new information to stay relevant and hold on to its followers. A newspaper that printed the same stories every day would presumably also lose its subscribers. Figures 2(b) and 2(c) show snapshots of the simulation. The system has self-organized into a configuration where influencers (white

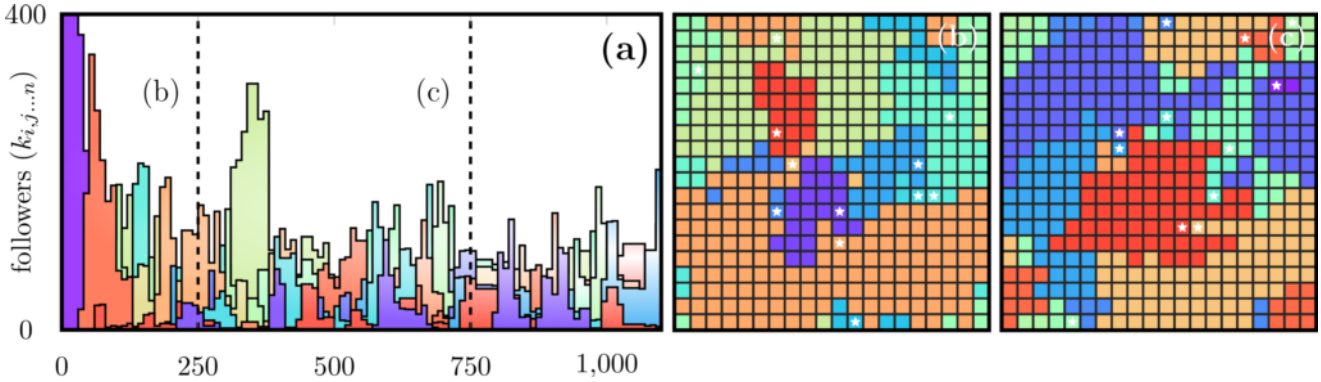

FIG. 2. Simulation on a quadratic lattice. Panel (a) shows the size of each subculture over 1100 time steps. Panels (b) and (c) each show a snapshot of the simulation at the labeled points in time. Each color defines a subculture, and the white stars represent influencers. The system occupies a perpetually fragmented state where no subculture dominates for an extended period. The simulation was carried out with periodic boundary conditions and parameters: $N = 20 \times 20$, $p_0 = 2.5 \times 10^{-4}$, and $\eta = 0.0$. Note that stars are only updated each time a full iteration of 400 updates has been performed. A full animation of the simulation is included as Supplemental Material [10].

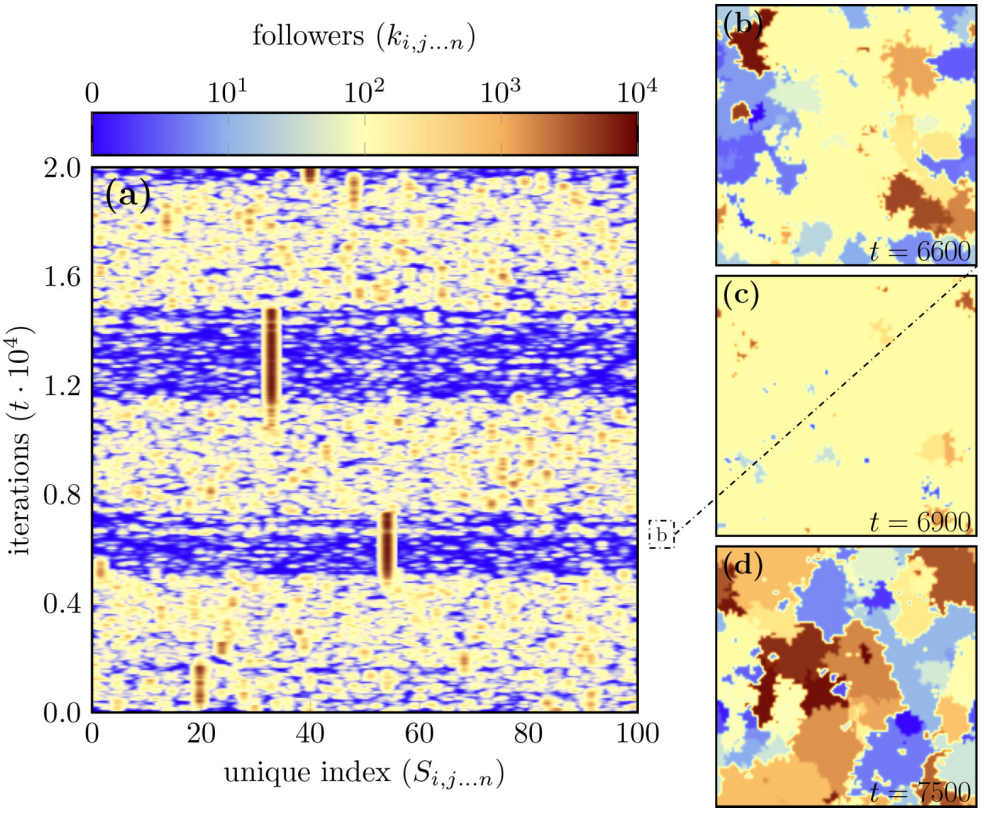

FIG. 3. Simulation with positive feedback on a quadratic lattice. Panel (a) shows the size of each subculture. Each vertical line represents the time evolution of a subculture. The solid lines are metastable states where the vast majority of followers belong to the same influencer. The diffuse blankets are fragmented states encompassing many subcultures of varying sizes. Panel (a) shows the first ordered metastable state emerges around $t = 5 \times 10^3$. Panels (b)–(d) show static snapshots of the simulation at different points in time. Panel (b) shows the monoculture on the verge of collapse as many emerging subcultures capture followers from the dominating influencer. The largest subculture makes a speedy recovery in panel (c) before collapsing in panel (d) into a fragmented state. Simulation was carried out with periodic boundary conditions and the following set of parameters: $N = 100 \times 100$, $\eta = 0.30$, and $p_0 = 4.0 \times 10^{-5}$. The color scheme in panel (a) displays a subculture's size, but in the remaining panels, it displays affiliation with identical color nodes belonging to the same subculture.

stars) are located on the boundary between subcultures. An influencer must be attacked directly before it can copy information from its attacker. Following the appropriation of a news event, the two influencers and their followers will have the same news value. This immediately suspends the conflict until another news or appropriation event induces a discrepancy in news value between them.

Figure 3 shows a simulation on a larger system with parameters $p_0 = 4.0 \times 10^{-5}$ and $\eta = 0.30$ over 20 000 time-step iterations. Figure 3(a) shows the size of each subculture over the simulation. An influencer can now increase its probability of discovering a news event by capturing more followers. This positive feedback loop induces metastable states where one influencer maintains dominance for a sustained period.

Figures 3(b)–3(d) show snapshots of the simulation. Figure 3(a) shows that the first ordered metastable state emerges around $t = 5 \times 10^3$. Figure 3(b) reveals that the ordered state is about to collapse as many emerging subcultures capture followers from the dominating influencer. The monoculture makes a swift recovery in Figure 3(c) before it finally collapses into a fragmented state in Fig. 3(d). The transitions between the ordered and the fragmented regime are short-lived compared to the particular state's lifetime. These shifts occur over a few hundred iterations for the chosen parameters, whereas the fragmented or ordered states tend to persist for thousands of iterations. Increasing η above a critical threshold eliminates the fragmented regime, but the system can still jump between different metastable states. The lifetime of a metastable state also increases with η. We also performed simulations on a one-dimensional system where no value of feedback was sufficient to induce ordered metastable states. This is consistent with van Hove's nonexistence theorem [17].

We use a linear feedback loop that increases p_i with the number of subscribers k_i, but other functional dependencies were also considered. Sublinear growth is usually insufficient to support an ordered regime unless η is increased to compensate. Let us assume that $N = 10^4$, $p_0 = 1/N$, and $\eta = 1.0$. So if p_i, as an example, increases with the square root of k_i, an influencer with $N - 1$ followers will have a p_i value of 0.1 instead of 1.0 obtained with the linear model. However, faster than linear growth does not necessarily support an ordered regime either. If p_i increases with the square of k_i, each influencer with 100 or more followers obtains a p_i value greater than 1.0. This caps the advantage of followers above a critical threshold, as there is no benefit to a p_i value greater than 1.

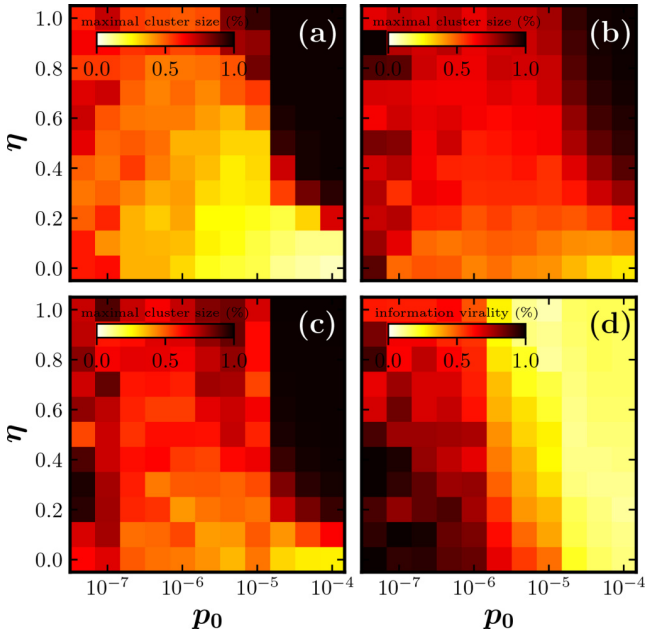

FIG. 4. Semilogarithmic phase diagrams. Panels (a)–(c) shows the time-averaged fraction of nodes belonging to the largest subculture for different network substrates. The followers in the largest subculture are counted for each time step and averaged over the full simulation. The subculture being sampled is not necessarily the same over the entire simulation. Panel (a) shows the quadratic lattice. Panel (b) shows a complete graph with interactions between random nodes. Panel (c) shows a small-world graph constructed by a Watts-Strogatz process: Each node is initially assigned four neighbors, and the links are randomly rewired between nodes with a probability of $\beta = 0.1$. Dark regions represent the ordered domain in each diagram, and the system becomes increasingly disordered with brightness. The quadratic lattice becomes fully disordered in the lower-right corner, whereas the other network substrates become fragmented. The ordered domain is smaller for random mixing than for local interactions. Panel (d) shows the percentage of viral news events that spread to half or more of the nodes on a quadratic lattice. Each simulation was carried out with $N = 10^4$ nodes and averaged over 10 000 time steps.

Figure 4 shows a collection of phase diagrams. Figures 4(a)–4(c) show the time-averaged size of the largest subculture for different network topologies. Figure 4(a) shows the familiar quadratic lattice with local interactions. Figure 4(b) shows a complete graph with interactions between random nodes, i.e., mean-field behavior. Figure 4(c) shows a small-world graph constructed by a Watts-Strogatz model where each node is initially assigned four neighbors. The links are then randomly rewired with a probability of $\beta = 0.1$. Social networks have small-world properties [18]. However, findings by Newman and Park suggest that real-world social networks differ from other networks in important ways [19]. All the network substates have an ordered regime for high values of η and p_0. Both variables contribute because p_i is increased by an increment of ηp_0 for each follower gained. Dark regions represent the ordered domain in Figs. 4(a) to 4(c). This region is larger on the lattice than on the complete graph. Emerging subcultures can grow exponentially on a complete graph, whereas local interactions permit only polynomial growth. Simulations on the lattice thus give the influencer of the largest subculture more time to discover a news event before losing a critical number of followers. News events become less frequent as we decrease p_0, which permits an emerging influencer to capture a large number of followers before the next news event occurs, explaining why the maximal cluster size increases for very low p_0. This effect is also more pronounced on the complete and small-world graph than on the lattice, where news events take longer to spread.

Figure 4(d) shows the fraction of viral news events that spread to at least half of the system on a quadratic lattice. A news event has a good chance of capturing the attention of a broad audience when p_0 is small. However, competition intensifies as p_0 is increased, and more recent news events often overwrite news events before they can spread to a large fraction of the system. For large p_0 only a small fraction of events go viral [20]. So if almost nothing happens, the few exciting events that occur are very likely to receive widespread attention. But in a world exposed to a vast flux of news events, only a tiny fraction of these events get viral coverage. Figures 4(a) and 4(d) show that information diversity is suppressed in the ordered regime, as only news events propagated by the dominating influencer receive a broad audience.

We also performed a preliminary analysis on a scale-free network [21]. The Barabási-Albert model was used to grow a scale-free network of $N = 10\,000$ nodes [21]. Each node is initially assigned four links that are preferentially attached to existing nodes with high degrees. As a result, a few nodes end up with disproportionately many links. Our analysis shows that mutual coexistence between a handful of dominating influencers emerges over time in the absence of positive feedback. The appropriation of news events was primarily a defensive mechanism on the lattice network. However, this mechanism can also be used offensively on a scale-free network. A node with many static links can easily pick up news events and use the information to attack other nodes together with its followers. Attacking these influencers' followers is difficult because their many links ensure that their news value is almost always up to date. We deemed a comprehensive analysis of the scale-free network to be prohibitively time-consuming. Simulations must be averaged over a long time because the nodes with many links have only a small probability of being promoted to influencers.

III. DISCUSSION

Our work concerns competition between news outlets in an information supply economy with finite attention. We have shown that a benefit to size can lead to a metastable state where one news outlet dominates. Shifts between stable states are often interspersed with periods of fragmentation. The collapse of the ordered state occurs when many new subcultures emerge and capture followers from the dominant influencer, decreasing its probability of discovering news. If it fails to update its news value, it will also continue to bleed subscribers, and the system collapses into a fragmented state. This represents a transformation from a centralized form of media influence to a disaggregated collection of independent

news outlets. We argue that ubiquitous information sharing has brought about a similar change in our society. Three news networks used to dominate mass media in the United States [22]. Easy access to communication has driven down the cost of becoming a news outlet or influencer, dramatically increasing p_0. The monetary benefit of being a news outlet has also diminished, meaning that η assumes lower values in a world where mass communication is available to everyone. For example, the rise of digital media explains the decline of local newspapers [23].

There is growing concern that the internet has brought about an epidemic of fake news by lowering the cost of entry to new competitors, many of whom reject journalistic norms [24]. Vosoughi *et al.* [25] showed that fake news stories spread more than the truth. Fake news outlets can fabricate stories of greater newsworthiness, so it should not be surprising that false news spreads more than the truth. However, some studies dispute the prevalence of fake news. Findings by Allen *et al.* [26] suggests that fake news only makes up a small percentage of Americans' daily media diets. True or false, the perception of fake news as being a huge issue is widespread. The advent of social media can explain this phenomenon. Residents of a polarized society may think that fake news is pervasive because information diversity is high. The inhabitants of a monoculture may be less inclined to share the perception of fake news as a problem—even if the dominating influence is passing on false information. Mass media in autocratic societies fits this description particularly well; a single news outlet effectively controls the flow of information, and the information is, we assume, overwhelmingly false. If so, it is information diversity that precipitates the perception of fake news.

The information content of news events was not modeled explicitly in this work, nor did we differentiate between real and fake news outlets or influencers. An extension of the model could assign a higher p value to fake news outlets. Introducing a measure of credibility would be necessary to penalize outlets that disseminate fake news. Respectable news outlets would then find themselves in a delicate situation when deciding whether or not to pass on information from another source. The risk of passing on false information entails a loss of reputation. However, journalists often face this dilemma because the race to report on a breaking news event first can drive even respectable news outlets to publish information before adequately vetting it.

To summarize, we model a network that exhibits transitions between a dominating media influence and a decentralized collection of independent news outlets. Our findings suggest the perception of fake news as a widespread problem is endemic to a society where everyone can become a media outlet.

ACKNOWLEDGMENTS

This project has received funding from the European Research Council (ERC) under the European Union's Horizon 2020 Research and Innovation Program, Grant Agreement No. 740704.

[1] P. Clifford and A. Sudbury, Biometrika **60**, 581 (1973).
[2] K. Sznajd-Weron and J. Sznajd, Int. J. Mod. Phys. C **11**, 1157 (2000).
[3] R. Hegselmann, U. Krause *et al.*, J. Artif. Soc. Soc. Stimul. **5** (2002).
[4] R. A. Holley and T. M. Liggett, The annals of probability **3**, 643 (1975).
[5] R. Axelrod, J. Conflict Resolut. **41**, 203 (1997).
[6] J. C. González-Avella, M. G. Cosenza, and K. Tucci, Phys. Rev. E **72**, 065102(R) (2005).
[7] J. C. González-Avella, V. M. Eguíluz, M. G. Cosenza, K. Klemm, J. L. Herrera, and M. San Miguel, Phys. Rev. E **73**, 046119 (2006).
[8] K. I. Mazzitello, J. Candia, and V. Dossetti, Int. J. Mod. Phys. C **18**, 1475 (2007).
[9] L. Weng, A. Flammini, A. Vespignani, and F. Menczer, Sci. Rep. **2**, 335 (2012).
[10] See Supplemental Material at http://link.aps.org/supplemental/10.1103/PhysRevE.103.022303 for full animation of Fig. 2 displayed at 8 frames per second.
[11] J. Galtung and M. H. Ruge, J. Peace Res. **2**, 64 (1965).
[12] F. Wu and B. A. Huberman, Proc. Natl. Acad. Sci. USA **104**, 17599 (2007).
[13] L. Lizana, M. Rosvall, and K. Sneppen, Phys. Rev. Lett. **104**, 040603 (2010).
[14] L. Lizana, N. Mitarai, K. Sneppen, and H. Nakanishi, Phys. Rev. E **83**, 066116 (2011).
[15] S. Bornholdt, M. H. Jensen, and K. Sneppen, Phys. Rev. Lett. **106**, 058701 (2011).
[16] W. B. Arthur, Sci. Am. **262**, 92 (1990).
[17] L. Van Hove, Physica (Amsterdam) **16**, 137 (1950).
[18] D. J. Watts and S. H. Strogatz, Nature (London) **393**, 440 (1998).
[19] M. E. J. Newman and J. Park, Phys. Rev. E **68**, 036122 (2003).
[20] S. Asur, B. A. Huberman, G. Szabo, and C. Wang, in *Proceedings of the Fifth International AAAI Conference on Weblogs and Social Media* (AAAI, Palo Alto, California, 2011).
[21] R. Albert and A.-L. Barabási, Rev. Mod. Phys. **74**, 47 (2002).
[22] D. B. Hindman and K. Wiegand, J. Broadcast. Electron. Media **52**, 119 (2008).
[23] R. K. Nielsen, *Local Journalism: The Decline of Newspapers and the Rise of Digital Media* (Bloomsbury, London, 2015).
[24] D. M. Lazer, M. A. Baum, Y. Benkler, A. J. Berinsky, K. M. Greenhill, F. Menczer, M. J. Metzger, B. Nyhan, G. Pennycook, D. Rothschild *et al.*, Science **359**, 1094 (2018).
[25] S. Vosoughi, D. Roy, and S. Aral, Science **359**, 1146 (2018).
[26] J. Allen, B. Howland, M. Mobius, D. Rothschild, and D. J. Watts, Sci. Adv. **6**, eaay3539 (2020).